A STUDY ON ENHANCING THERMAL STABILITY OF ALUMINA

by

Gülten Çelebi

B.S. Chemical Engineering, Boğaziçi University, 2017

Submitted to the Institute for Graduate Studies in
Science and Engineering in partial fulfillment of
the requirements for the degree of
Master of Science

Graduate Program in Chemical Engineering

Boğaziçi University

2021

to my family

ACKNOWLEDGEMENTS

First of all, I would like to express my sincere appreciation and gratitude to my thesis supervisor Prof. Ahmet Erhan Aksoylu for his guidance, valuable support, immense knowledge and vision, and above all, his belief and trust in me throughout my master. It was a great privilege and honor to study under his supervision.

I would like to express my deep thanks to Dr. Burcu Selen Çağlayan for her guidance and support all the time and sharing her knowledge during my research and writing of this thesis.

I would like to thank my thesis committee members, Prof. Ramazan Yıldırım and Prof. Hüsnü Atakül for devoting their valuable time and effort to my thesis and providing guidance and recommendations.

I consider it an honor to work with Dr. Belkız Merve Eropak and Ali Uzun for their endless help, mentorship, but above all, for their kindness and friendship. Because of you, I enjoyed every moment of my work, I was never afraid of trying things because I always had your support, and I learned too much. I would also like to show my gratitude to Cihat Öztepe for his great help and friendship. I cannot thank the three of you enough.

I would also like to thank to Serhat Özşahin for advising me to work with Professor Aksoylu for ChE 492, for his helps and friendship; Hasretnur Özata for being kind, friendly, and helpful all the time; Enes Emre Taş for sharing his great knowledge of chemistry with us; Olcay Türkmen for his cooperation all the time; Burcu Acar for her nice chats and helps; and Özgü Özer for her contributions to my thesis with her pre-studies and her helps. I do/will feel lucky always for being a part this research group and KB 411/A because of you. I would also like to thank to Murat Düzgünoğlu, Yakup Bal, and Dilek Kırkoç for their helps and kindness.

This thesis is dedicated to my lovely family, to my parents Rahime & Mustafa Çelebi, to my brother Muhammet Çelebi, to Aysel & Kenan Çevik, Sinan & Rüveyda Çelebi, and to my cousin Ece Demir for their unquestioned support, love, caring, and encouragement in everything I do; and to my nephews for bringing inspiration and lots of fun to my life.

I would like to express my deep thanks to Kadriye Deniz Köse and Ekin Yurdakul for being the greatest source of joy and trouble at the same time during my B.S. and M.S. years. Dear Deniz, I am grateful that I had such a thoughtful, devoted, wise, sleepy (only in Rhodes), and angry friend. Dear Ekin, I am thankful to your sensitive and gentle heart, our weird common understanding of buying, and your valuable support. Dear Onur Can Boy, I am thankful to you for standing by me against these two, for your valuable accompaniment, and for being worthy perspective for me all the time. I always feel lucky to know you guys. We shared too much, and we will. To less interventions and to more coffees, chats, the firsts, and memories.

I must express my gratitude to Rabia Akkuş, for her endless support, recipes for everything, her standards, friendship, being always sharing, and chats. I'm thankful to the silly coincidence that brought us together. I am deeply grateful to Semra Tuncay for her never-ending support, consultancy, friendship, and encouragement in my life. We have many things to do together. I'm also grateful to have Pınar Alp, Deniz Demiryürek Kurt, Nur Zengin and Hilal Demir Karaköse for being in my life, even though you are away from me, your existence, all by itself is a source of support and motivation for me. I am also thankful to my best friend Sema Ayten, you are, and you will be always with me in everything I do.

Finally, I would like to express my deep thanks to Nicolas Mendez Asbach for opening a new world to me. There are some strong women in my life that I take as role models. I must express my very profound gratitude primarily to my mother Rahime Çelebi and to Zehra Ayten, Çiğdem Gürses, Çiğdem Dalay, and Funda Gayretoğlu,

Financial support provided by Presidency of Republic of Turkey Department of Strategy and Budget (Ministry of Development) through project 2016K12-2828 (2016K121160) is gratefully acknowledged.

ABSTRACT

A STUDY ON ENHANCING THERMAL STABILITY OF ALUMINA

The use of temperature resistant support is a prerequisite for successful catalysts prepared to be used in reactions which need high temperature, like Dry and Mixed Reforming of Methane, catalytic oxidation, and combustion reactions. Alumina is a common and cheap catalyst support for achieving high metal dispersion, e.g., γ-Al_2O_3 has a surface area of 220 m^2/g. However, as high temperature leads to phase change from high- to low-SA alumina phases, i.e. $\gamma \rightarrow \delta \rightarrow \theta \rightarrow \alpha$, preventing surface area loss requires to shift the phase change temperatures up to higher levels. In the current study, the thermal stability of commercial γ-Al_2O_3 samples was enhanced via doping with stabilizers La, Ba and Pt through application of various preparation and pre-treatment parameters such as; pre-doping temperature, vacuum pressure, drying temperature, pH of the precursor solution, and heat treatment applied upon doping. Total of 142 samples were prepared in 19 sets of samples, and all samples were characterized by their surface area, pore volume and pore size distribution. Selected samples chosen to represent each set were furtherly tested by XRD and Raman spectroscopy. Reference γ-Al_2O_3 calcined at the highest temperature applied, 1150 ^oC, for 2 hours had BET surface area of 8.81 m^2/g. Under the same conditions, thermally resistant 1%La/Al_2O_3 and 1%Ba/Al_2O_3 samples prepared by incipient-to-wetness impregnation have BET surface areas of 61.74 m^2/g and 38.26 m^2/g, respectively. Results indicated that the effect of vacuum pressure and drying temperature applied during preparation were ambiguous. Changing only the pH of impregnation solution from pH_1(acidic) to pH_2(basic) led to decreased surface area values. While combination of pH regulation and post heat treatment significantly have a stabilizing effect leading 68.27 m^2/g surface area for 1%La/Al_2O_3 upon calcination at 1150 ^oC for 2 hours, further elaboration of pre-doping temperature applied led to the highest BET surface area of 70 m^2/g. XRD analysis confirmed the effect of pre-doping temperature on shifting the phase transfer temperature of alumina.

ÖZET

ALÜMİNANIN ISIL KARARLILIĞININ ARTIRILMASI ÇALIŞMASI

Sıcaklığa dirençli destek malzemenin kullanılması, Metanın Kuru ve Karışık Reformasyonu, katalitik oksidasyon ve yanma reaksiyonları gibi yüksek sıcaklık gerektiren reaksiyonlarda kullanılmak üzere hazırlanan başarılı katalizörlerin ön şartıdır. Alümina, yüksek metal dağılımı elde etmek için kullanılan yaygın ve ucuz bir katalizör desteğidir, γ-Al_2O_3'ün yüzey alanı 220 m^2/g'dır. Bununla birlikte, yüksek sıcaklık alümina fazlarının yüzey alanı yüksek fazlardan daha düşük fazlara kaymasına yol açtığından, $\gamma \rightarrow \delta \rightarrow \theta \rightarrow \alpha$ gibi, yüzey alanı kaybının önlenmesi faz değişim sıcaklıklarının daha yüksek seviyelere kaydırılmasını gerektirir. Mevcut çalışmada, ticari γ-Al_2O_3 numunelerinin ısıl kararlılığı La, Ba ve Pt metalleri eklenmesi yoluyla, çeşitli hazırlama ve ön işlem parametrelerin; metal ekleme öncesi sıcaklık, vakum basıncı, kurutma sıcaklığı, başlangıç çözeltisi pH'ı ve metal eklemesi üzerine uygulanan ısıl işlem vs. gibi uygulanmasıyla artırıldı. 19 sette toplam 142 numune hazırlandı; tüm numuneler yüzey alanı, gözenek hacmi ve gözenek boyutu dağılımı ile karakterize edildi. Setleri temsil etmek için seçilen seçilmiş numuneler ayrıca XRD ve Raman spektroskopisi ile test edildi. Uygulanan en yüksek sıcaklıkta, 1150 ^oC'de 2 saat, kalsine edilen γ-Al_2O_3'ın BET yüzey alanı 8.81 m^2/g olarak belirlendi. Aynı koşullar altında, ısıl dayanıklılığı artırılmış %1La/Al_2O_3 ve %1Ba/Al_2O_3 alümina numuneleri ıslak emdirme yöntemi ile elde edildi ve BET yüzey alanları sırasıyla 61.74 m^2/g ve 38.26 m^2/g olarak belirlendi. Sonuçlar, hazırlık sırasında uygulanan vakum basıncı ve kurutma sıcaklığının etkisinin belirsiz olduğunu gösterdi. pH etkisi, başlangıç çözeltisi pH'ı pH_1'den (asidik) pH_2'ye (bazik) değiştirerek araştırıldı; sonuçlar, bu numunelerin BET yüzey alanının azaldığını gösterdi. Bununla birlikte, pH ve kalsinasyon öncesi ısıl işlemin kombinasyonu, 1150 ^oC'de 2 saat kalsine edilmiş %1 La/Al_2O_3 üzerinde 68.27 m^2/g BET yüzey alanına yol açan önemli ölçüde kararlılık arttırıcı etkiye sahip olduğunu gösterdi. Uygulanan metal ekleme öncesi sıcaklık uygulamasının detaylandırılması, aynı koşullar altında 70 m^2/g'lık en yüksek BET yüzey alanının elde edilmesini sağladı. XRD analizi, alüminanın faz transfer sıcaklığının kayması üzerindeki ön sıcaklığın etkisini gösterdi.

TABLE OF CONTENTS

ACKNOWLEDGEMENTS……iv

ABSTRACT..... vi

ÖZET vii

LIST OF FIGURES xi

LIST OF TABLES..... xvi

LIST OF SYMBOLS xx

LIST OF ACRONYMS/ABBREVIATIONS xxi

1. INTRODUCTION..... 1

2. LITERATURE SURVEY 5

2.1. Catalysts and Catalyst Deactivation Mechanisms..... 6

2.2. Catalyst Support..... 8

2.2.1. Alumina as a Support Material 8

2.2.2. Phase Transition of Alumina 10

2.3. Support Preparation..... 12

2.3.1. Chemical preparation..... 12

2.3.2. Thermal treatment..... 13

2.4. Design of Heat-Resistant Alumina 13

2.4.1. Use of additives 14

2.4.2. Alternative Alumina Compounds 16

2.4.3. Preparation Process 17

2.4.4. Drying Process 18

3. EXPERIMENTAL WORK 20

3.1. Materials 20

3.1.1. Chemicals 20

3.1.2. Gases and Liquids 20

3.2. Experimental Systems 22

3.2.1. Support Preparation Systems 22

3.2.2. Support Characterization Systems 23

3.2.2.1. Brunauer-Emmett-Teller (BET) Surface Area Analysis 23

3.2.2.2. Raman Spectroscopy 24

3.2.2.1. X-Ray Diffraction (XRD) 24

3.3. Support Preparation and Pre-treatment 24

4. RESULTS AND DISCUSSION 30

4.1. Effect of Thermal Treatment on Alumina 31

4.2. Effect of Doping Metal Type 35

4.3. Effect of Pre-Doping Temperature 37

4.4. Effect of Impregnation Strategy 45

4.4.1. Effect of pH 45

4.4.2. Effect of Vacuum Pressure 48

4.4.3. Effect of Drying Conditions 49

4.5. Effect of Post Heat Treatments Upon Doping 56

4.6. Thermal Resistance of The Supports Prepared 65

4.7. Design Parameters of a Temperature Resistant Support 69

5. CONCLUSIONS 78

5.1. Conclusions 78

5.2. Recommendations 80

REFERENCES 81

APPENDIX A: RESULTS OF BET SURFACE AREAS FOR ALL SAMPLES 87

APPEDIX B: MATLAB CODE 94

APPEDIX C: DATA SHEET OF MATLAB CODE 96

LIST OF FIGURES

Figure 2.1.	The Catalyst Deactivation Mechanisms (Disdale W., 2007)	7
Figure 2.2.	Alumina Nomenclature in Literature (Wefers and Misra, 1987).....	9
Figure 2.3.	The Phase Change and Surface Area Change of Alumina with Respect to Temperature (Arai et al., 1996).....	10
Figure 2.4.	The Phase Change of Aluminum Hydroxides with Respect to Calcination Temperature and Starting Mineral.....	11
Figure 2.5.	The Thermal Treatment of Aluminum Hydroxides for the Phase Change	11
Figure 2.6.	The Phase Change Temperatures for Boehmite.....	13
Figure 3.1.	Schematic representation of the impregnation system and 1. Precursor solution beaker, 2. MasterFlex peristaltic pump, 3. Silicone tubing, 4. 250ml Büchner flask, 5. Retsch UR1 ultrasonic mixer, 6. KNF Neuberger vacuum pump (Baranak, 2014)	22
Figure 4.1.	XRD Profiles of Alumina Samples After Final Calcination at FCT_900, FCT_1000, FCT_1100, and FCT_1150	33
Figure 4.2.	BJH Pore Size Distribution for Alumina Samples After Final Calcination at FCT_900, FCT_1000, FCT_1100, and FCT_1150.....	34

Figure 4.3. BJH Pore Area Distribution for Alumina Samples After Final Calcination at FCT_900, FCT_1000, FCT_1100, and FCT_1150..... 35

Figure 4.4. BET Surface Areas of Ba-doped vs. La-doped Alumina. FCT_900, FCT_1000, FCT_1100, and FCT_1150..... 36

Figure 4.5. BET Surface Areas vs. Calcination Temperatures of the 1%La/Al_2O_3 Samples with Different PDT..... 39

Figure 4.6. The Effect of Various Pre-Doping Temperature on 1%La/Al_2O_3 Samples Calcined at FCT_1150..... 40

Figure 4.7. The Effect of Various Pre-Doping Temperature on 1%La/Al_2O_3 Samples..... 41

Figure 4.8. Temperature Treated (PDT) 1%La/Al_2O_3 Samples Calcined at FCT_1150 vs. Al_2O_3 Samples Calcined at FCT_1150..... 42

Figure 4.9. BJH Pore Size Distribution for 1%La/Al_2O_3 Samples at PDT_T_1, PDT_T_4, and PDT_T_6 and Al_2O_3 at FCT_1150..... 43

Figure 4.10. BJH Pore Area Distribution for 1%La/Al_2O_3 Samples at PDT_T_1, PDT_T_4, and PDT_T_6 and Al_2O_3 at FCT_1150..... 44

Figure 4.11. BET Surface Areas of 1%La/Al_2O_3 samples with respect to pH_1 vs. pH_2 and Calcination Temperatures; FCT_900, FCT_1000, FCT_1100, and FCT_1150..... 47

Figure 4.12. XRD Pattern of the Water-Alumina Treatment Samples..... 53

Figure 4.13. Raman Spectra of Water-Alumina Treatment Sample, S0 54

Figure 4.14. Raman Spectra of Water-Alumina Treatment Sample, S1 54

Figure 4.15. Raman Spectra of Water-Alumina Treatment Sample, S2 55

Figure 4.16. Incremental Pore Size Distribution of the Water – Alumina Treatment Samples 56

Figure 4.17. BET Surface Areas of Post-Heat Treatment Samples of Stages PHT_0 and PHT_1 for The Samples with Calcination Temperature of FCT_1000 58

Figure 4.18. Post Heat Treatment for Stages PHT_0 and PHT_1 for The Samples with Calcination Temperature of FCT_1100 59

Figure 4.19. Post Heat Treatment Upon Doping for Stages PHT_0, PHT_1, and PHT_2 for The Samples with Final Calcination Temperature of FCT_1150 61

Figure 4.20. Post Heat Treatment for Stages PHT_0, PHT_1, PHT_2, and PHT_3 for The Samples with Final Calcination Temperature of FCT_1150 ... 64

Figure 4.21. X-Ray Diffraction Results for 1%La/Al_2O_3 with Various Temperature and pH Treatments 66

Figure 4.22. X-Ray Diffraction Results for 1%La/Al_2O_3 with Various Temperature and pH Treatments 67

Figure 4.23. BJH Pore Size Distribution for 1%La/Al_2O_3 Samples for Different pH and Post-Heat Treatment (PHT) Cycles 68

Figure 4.24. BJH Pore Area Distribution For 1%La/Al_2O_3 Samples for Different pH and Post-Heat Treatment (PHT) Cycles..... 68

Figure 4.25. BET Surface Areas (m^2/g) of pH_2 Samples with Respect to Stage Number, Final Calcination Temperature (°C) and PDT (°C) 70

Figure 4.26. BET Surface Areas (m^2/g) of pH_1 Samples with Respect to Stage Number, Final Calcination Temperature (°C) and PDT (°C) 71

Figure 4.27. Circle Size Represent BET Surface Areas (m^2/g) of pH_1 Samples with Respect to Stage Number, Final Calcination Temperature (°C) and PDT (°C) 72

Figure 4.28. Circle Size Represent BET Surface Areas (m^2/g) of pH_1 Samples with Respect to Final Calcination Temperature (°C) and PDT (°C)..... 73

Figure 4.29. Circle Size Represent BET Surface Areas (m^2/g) of pH_1 Samples with Respect to Stage Number and PDT (°C)..... 74

Figure 4.30. Circle Size Represent BET Surface Areas (m^2/g) of pH_2 Samples with Respect to Stage Number, Final Calcination Temperature (°C) and PDT (°C) 75

Figure 4.31. Circle Size Represent BET Surface Areas (m^2/g) of pH_2 Samples with Respect to Final Calcination Temperature (°C) and PDT (°C)..... 76

Figure 4.32. The Circle Size Represent BET Surface Areas (m^2/g) of pH_2 Samples with Respect to Stage Number and PDT (°C) 77

LIST OF TABLES

Table 3.1.	The Properties of the Chemicals Used in Support Preparation	20
Table 3.2.	Specifications and Applications of the Gases Used	21
Table 3.3.	Specifications and Applications of the Liquid Used	21
Table 3.4.	Comparatively Analyzed Sets, Main Experimental Parameters and Parameter Ranges and Levels Used	27
Table 3.5.	Sample Numbers (Codes), Sample Sets Formed (I-X) and Parameter Levels.	28
Table 3.6.	Sample Numbers (Codes), Sample Sets Formed (X-XIX) and Parameter Levels	29
Table 4.1.	BET Surface Areas of Different Alumina Types	31
Table 4.2.	BET Surface Areas of Gamma-Alumina After Thermal Treatment at FCT_900, FCT_1000, FCT_1100 and FCT_1150	32
Table 4.3.	BET Surface Areas of La-doped and Ba-doped Alumina Samples	36
Table 4.4.	BET Surface Areas of Pre-Calcined and γ-Al_2O_3 Samples with Respect to Final Calcination Temperatures.....	37
Table 4.5.	BET Surface Areas of 1%La/Al_2O_3 Samples with Respect to Different PDT and Calcination Temperatures	38

Table 4.6. BET Surface Areas of 1%La/Al_2O_3 Samples with Respect to pH of pH_1 vs. pH_2 and Calcination Temperatures 46

Table 4.7. BET Surface Areas of 2%Pt/Al_2O_3 Samples with Respect to Vacuum Pressures 48

Table 4.8. BET Surface Areas of 2%Pt/Al_2O_3 Samples with Respect to Vacuum Pressures and Drying Conditions 49

Table 4.9. Temperature Increase in The Ultrasound Mixing Tank by Time..... 51

Table 4.10. BET Surface Areas of Alumina Samples with Respect to Drying Methods 52

Table 4.11. Post Heat Treatment Upon Doping Temperatures Corresponding to Stages..... 57

Table 4.12. Post Heat Treatment Applied Upon Doping for Stages PHT_0 and PHT_1 for The Samples with Calcination Temperature of FCT_1000 58

Table 4.13. Post Heat Treatment Upon Doping for Stages PHT_0 and PHT_1 for The Samples with Calcination Temperature of FCT_1100..... 60

Table 4.14. Post Heat Treatment Upon Doping for Stages PHT_0, PHT_1, and PHT_2 for The Samples with Final Calcination Temperature of FCT_1150..... 62

Table 4.15. Post Heat Treatment for Stages PHT_0, PHT_1, PHT_2, and PHT_3 for The Samples with Final Calcination Temperature of FCT_1150... 63

Table 4.16. Effect of Calcination Duration for PHT_0 1%La/Al_2O_3 with Final Calcination Temperature of 1100 ^oC 65

Table A.1. Data of BET Surface Areas of Alumina Types 87

Table A.2. Data of BET Surface Areas of Alumina Phases Calcinated at Different Temperatures 87

Table A.3. Data of BET Surface Areas for the Samples with PDT of PDT _T_5 and PDT_T_2 for Lanthanum Doping and PDT _T_5 for Barium Doping 88

Table A.4. Data of BET Surface Areas for the Samples with PDT of PDT _T_3, PDT _T_4 and PDT _T_1 89

Table A.5. Data of BET Surface Areas for the Samples with PDT of PDT_T_6 and PDT_T_7 90

Table A.6. Data of BET Surface Areas of for the Samples with PDT of PDT_T_5, PDT_T_6, and PDT_T_3 for pH_2 91

Table A.7. Data of BET Surface Areas of for 2%Pt/Al_2O_3 Calcinated at 1000 for 2 hours with Respect to Drying Temperatures (^oC) and Vacuum Pressures (bar) During Impregnation 92

Table A.8. Data of BET Surface Areas of for Alumina with Respect to Different Drying Methods 93

Table C.1. Data Sheet of MATLAB Code for pH_2 96

Table C.2. Data Sheet of MATLAB Code for pH_1 for PDT of PDT_T_5, PDT_T_2, and PDT_T_3 97

Table C.3. Data Sheet of MATLAB Code for pH1 for PDT of PDT_T_4, PDT_T_1, PDT_T_6, and PDT_T_7 98

LIST OF SYMBOLS

A	Surface area
A_m	Cross-sectional area of one molecule
c	BET constant
E_1	Heat of adsorption for the first layer
E_L	Heat of adsorption for the second and higher layers
P	Equilibrium pressure of adsorbates
P_0	Saturation pressure of adsorbates
R	Universal gas constant
S_g	Total surface area per unit weight of catalyst
Δt_n	Decrease in thickness
T	Adsorption temperature
υ	Adsorbed gas quantity
υ_m	Monolayer adsorbed gas quantity
V	Volume
ΔV	Volume of liquid adsorbate removed
w_{cat}	Catalyst weight
γ	Gamma phase
δ	Delta phase
θ	Theta phase
α	Alpha phase

LIST OF ACRONYMS/ABBREVIATIONS

3D	Three dimensional
BET	Brunauer–Emmett–Teller
BJH	Barrett-Joyner-Halenda
DI	Deionized
DRM	Dry Reforming of Methane
FCT_T	Final Calcination Temperature from 900 to 1150 ^{o}C
MSA	Metal Surface Area
MRM	Mixed Reforming of Methane
PDT_T_{1-7}	Pre-doping Temperatures from PDT_T_1 to PDT_T_7
PHT_0-3	Stage Levels of Post Heat Treatment Upon Doping from PHT_0 to PHT_3
PSD	Pore Size Distribution
S0	Sample 0
S1	Sample 1
S2	Sample 2
S3	Sample 3
S4	Sample 4
S5	Sample 5
S6	Sample 6
SA	Surface Area
SAPT	Standard Ambient Temperature and Pressure
TPV	Total Pore Volume
TSA	Total Surface Area
TT	Thermal Treatment
XRD	X Ray Diffraction
Vac_$_{1-3}$	Vacuum Levels from Vac_$_1$ to Vac_$_3$

1. INTRODUCTION

Greenhouse gases, mainly CO_2 and CH_4, cause many environmental problems including global warming, which is widely accepted as one of the most important problem in the human history. Capturing and utilization of industry's side products as carbon sources for economically viable chemicals and/or energy production is a far better way than their sequestration. Dry and mixed reforming of methane (DRM & MRM) are in the group of the most effective routes utilizing captured carbon (Guo et al., 2011; Zhang et al., 2018).

The most severe problems in such processes arise from high temperature. Heterogeneous catalysts prepared in research laboratories and tested for being used in high-temperature processes widely suffers from sintering, i.e., the loss of active surface due to structural modification of the catalyst. The thermal stability of a catalyst with the lowest possible loss of metal surface area and total surface area under harsh conditions requires the resistance of both the support and active phase(s) of the catalysts against deactivation, significantly against sintering (Arai and Machida, 1996; Forzatti and Lietti, 1999; Mizushima and Hori, 1993).

Catalyst support, which dominantly determines the physical structure of a solid catalyst, is a material with high surface area (Total Surface Area, TSA), porosity (Total Pore Volume, TPV) and Pore Size Distribution (PSD) as well as suitable surface chemistry, which are essential for obtaining well dispersed and stabilized active sites formed on its surface, resulting in high active metal surface area (MSA), and low mass transfer resistance of the catalyst (Rahmani et al., 2018).

Metal oxides, zeolites and activated carbon are common support materials used in industry and for research purposes. Even though zeolite-based catalysts are known to be highly active among solid catalysts in various reactions, they have poor stability under severe thermal conditions. Therefore, in plenty of energy and environmental applications, metal oxide-supported heterogeneous catalysts are widely used due to their satisfying thermal, chemical, mechanical, and hydrothermal stability under pretreatment (like calcination,

reduction) and reaction conditions. Alumina and ceria are market-dominant oxide supports due to their accessibility and cheapness (Guo et al., 2011).

In the reactions requiring high temperatures for considerable activity, alumina is widely used as support material of catalysts in both academic and industrial purposes owing to its high chemical inertness, high surface area, good thermal stability and mechanical strength under high temperature and severe reaction conditions. Alumina has various forms with wide range of surface area. For instance, TSA of α- Al_2O_3, which is the most stable and lowest surface area form, may have surface area as low as 1 m^2/g, while that of γ - Al_2O_3, which is the mostly employed alumina form in catalysis and adsorption applications owing to its good porosity/PSD characteristics, is normally ca. 220 m^2/g. However, with the rise in temperature, γ - Al_2O_3 turns into lower surface area Al_2O_3 forms, with the sequence of γ→δ→θ→α (Paranjpe, 2017; Simon et al., 1995).

In order to obtain well dispersed metal, especially for high metal loadings, a high-total surface area support, like γ - Al_2O_3, is an excellent material to be used as the catalyst support. On the other hand, in case of reactions that require high temperature, prevention of support sintering, which leads losses in surface area and porosity, through enhancing the thermal stability is compulsory. In practical terms, in order to achieve thermal stability, the phase change of Al_2O_3 to its lower-TSA forms should be shifted to higher temperatures by the modification on the surface of the support material without changing its physical structure (Paranjpe, 2017).

Modification of γ - Al_2O_3 to a thermally more stable form is possible with various methods, like use of additives. Even transformation to another mineral form from a different starting mineral is possible. Hydration is a promising hypothesis. Recent studies indicated that hydration of γ - Al_2O_3 with resource mineral of boehmite for more than 10h treatment time and environment with pH > 4 may lead to shift of boehmite to gibbsite. It is also possible to form bayerite by hydration from pH > 5 to pH 11 (Carrier et al., 2007).

One of the most convenient way of inhibiting sintering is the use of additives. The addition of Si, Ti, Ce, B, but particularly Ba, La occupies the surface sites, prevents surface diffusion, bulk diffusion, and therefore the phase transformation. As a result, large surface area and higher pore volume of alumina, i.e. suitable surface chemistry, is preserved by the addition of Ba, La, Si etc. (Arai et al., 1996).

In the current work, thermal stability of commercial γ-Al_2O_3 samples was enhanced via doping with stabilizers La, Ba and Pt through application of various preparation and pre-treatment parameters such as; pre-doping temperature, vacuum pressure, drying temperature, pH of the precursor solution, and heat treatment applied upon doping. Total of 142 samples were prepared in 19 sets; all samples were characterized by their surface area, pore volume and pore size distribution. Selected samples chosen to represent sets were furtherly tested by XRD and Raman spectroscopy. The optimal set of serial preparation conditions of thermally stabilized alumina yielded 70 m^2/g surface area upon 2 hours final calcination at 1150 ^oC, which was 8.81 m^2/g for the original γ - Al_2O_3. It should be noted that as the support(s) prepared in this work has potential to be a proprietary material, the experimental parameters that were determined as main parameters affecting the temperature resistance of the material, like pre-doping calcination temperature, are given as levels (or ranges) rather than absolute values.

In this thesis, Chapter 2 comprises a comprehensive literature survey on theoretical background of catalysts and catalyst deactivation mechanisms, catalyst support, alumina as a support material and phase transition of it, support preparation process including chemical preparation and thermal treatment, and design of heat-resistant alumina including use of additives, alternative alumina compounds, preparation process, and drying process. In Chapter 3, the experimental work done is briefly explained in terms of materials, support preparation systems, and support characterization systems which includes BET surface area analysis, Raman Spectroscopy, and XRD. The results and findings of experimental work are represented Chapter 4 as, effect of thermal treatment on alumina, effect of doping metal type, effect of pre-doping temperature, effect of impregnation strategy, effect of post heat treatments upon doping, effect of calcination conditions, and design parameters of a

temperature resistant support. Finally, the conclusions obtained throughout this study and recommendations for further studies are summarized in Chapter 5.

2. LITERATURE SURVEY

Global warming is widely accepted as one of the most important environmental problems in the human history. Greenhouse gases, primarily CO_2 and CH_4, trap the in the atmosphere and cause many environmental problems, mainly global warming. Production and burning of fossil fuels, natural gas, coal, oil, etc., releases CO_2 and CH_4 and, capturing and utilization of industry's side products as carbon sources for economically viable chemical and/or energy production is a far better way than their sequestration (Guo et al., 2011; Zhang et al., 2018).

Dry reforming of methane and mixed reforming of methane (DRM & MRM) is one of the most effective routes of utilization of captured carbon. Mixed reforming of methane is the combination of steam reforming and dry reforming of methane. The captured methane can entirely be converted into syngas via dry and mixed reforming of methane. Water – gas shift reaction is used to convert undesired side product, carbon monoxide, of dry reforming to a reactant, carbon dioxide, of dry reforming. Dry reforming of methane, steam reforming, and water-gas shift reaction are presented in in equations 2.1, 2.2, and 2.3, respectively (Jokar et al., 2018; Sharma and Ghoshal, 2015).

$$CH_4 + \ CO_2 \ \leftrightarrow 2CO + 2H_2, \tag{2.1}$$

$$CH_4 + \ 2H_2O \ \leftrightarrow \ CO_2 + 4H_2, \tag{2.2}$$

$$CH_4 + \ CO_2 \ \leftrightarrow 2CO + 2H_2. \tag{2.3}$$

Hence, the main obstacle of these reactions is the fast deactivation of catalysts, as it is not so different in other reactions, the stability against deactivation and lifetime of the catalysts are required to be developed (Daza, et al., 2012; Shtyka et al., 2020).

2.1.Catalysts and Catalyst Deactivation Mechanisms

Catalytic technologies are essential in term of saving energy. Reactants and products in the same state, ordinarily liquid, in a catalysis is classified as homogeneous. Reactants and products in different state, generally catalyst is solid and the reactants and the products in gas or liquid, in a catalysis is classified as heterogeneous. Heterogeneous catalysts are commonly used in several types of reactions in industry (Nasrallah M., 2018).

An advanced catalyst has some properties such as higher chemical, thermal and mechanical stabilities, long lifetime, higher activity, higher selectivity etc. In order to preserve the durability of the catalytic performance, preventing the deactivation of heterogeneous catalysts is required. The deactivation of heterogeneous catalysts is generally divided into three (Nasrallah M., 2018; Daza, et al., 2012; Shtyka et al., 2020).

- Poisoning
- Fouling (Coke Formation)
- Sintering

Poisoning is blocking of catalytic sites by chemisorption of reactants and their poison-like effects on the reaction. Sulphur, for instance, has poison-like effect on steam reforming, hydrogenation, methanation, etc. Fouling or coke formation, on the other hand, is a mechanical alteration and it is a blocking of catalytic sites by physical deposition of species (Argyle and Bartholomew, 2015; Disdale W., 2007).

Dry reforming of methane and mixed reforming of methane are high temperature processes. Heterogeneous catalysts prepared in research laboratories and tested for being used in high-temperature processes widely suffers from sintering, i.e. the loss of active surface, support surface area, and active phase-support reactions due to structural modification of the catalyst, i.e. pore collapse in the active sites or crystallite growth on the active phase. The thermal stability of a catalyst with the lowest possible loss of metal and total surface areas under harsh conditions requires the resistance of both its support and

active phase(s) against sintering (Arai et al., 1996; Forzatti et al., 1999; Mizushima et al., 1993; Argyle and Bartholomew, 2015).

The catalyst deactivation mechanisms are represented in Figure 2.1 (Disdale W., 2007).

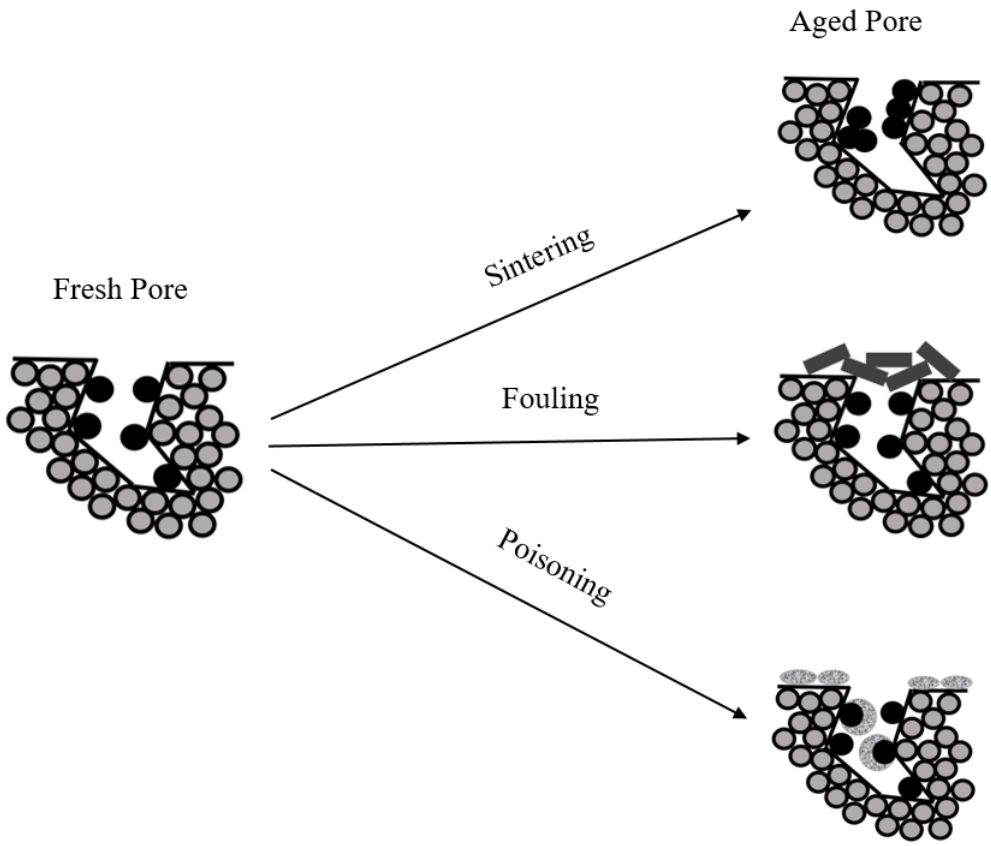

Figure 2.1. The Catalyst Deactivation Mechanisms.

: Support Material, : Metal, : Poison, : Carbon Deposition.

In all high temperature processes such as DRM, MRM, catalytic combustion, and oxidation, etc., the most severe problems in such reactions arise from high temperature and sintering is one of the sincerest problems in these reactions. In order to minimize loss of surface area of active sites during reaction, the total surface area and total pore volume of the catalyst support - possible active sites - should be increased. Consequently, catalyst support is determinative for a sintering-resistant catalyst, therefore, a reaction.

2.2. Catalyst Support

Catalyst support, which dominantly determines the physical structure of a solid catalyst, is a material with high surface area (Total Surface Area, TSA), porosity (Total Pore Volume, TPV) and Pore Size Distribution (PSD) as well as suitable surface chemistry, which are essential for obtaining well dispersed and stabilized active sites formed on its surface, resulting in high active metal surface area (MSA), and low mass transfer resistance of the catalyst (Rahmani et al., 2018).

Metal oxides, zeolites and activated carbon are common support materials. Even though zeolite-based catalysts are known to be highly active among solid catalysts in various reactions, they have poor stability under severe thermal conditions. Therefore, in plenty of energy and environmental applications, metal oxide-supported heterogeneous catalysts are widely used due to their satisfying thermal and hydrothermal stability under pretreatment (like calcination, reduction) and reaction conditions. Alumina and ceria are market-dominant oxide supports due to their accessibility and cheapness (Guo et al., 2011).

2.2.1. Alumina as a Support Material

Among all support types, alumina, Al_2O_3, is a common support material used both industrial and research purposes due to its lower price, textural properties and the controllability of its properties such as surface area, pore volume, pore-size distribution and acid/base characteristics. Above all, it is moderately stable under extreme conditions, therefore alumina can provide a wide range of surface areas and porosities for various catalytic applications. Alumina can be supplied in various mineral form given in Figure 2.2 and various phases (χ, θ, η, κ, ρ, γ, δ, α) for different purposes and have alternative forms such as activated alumina and hexaluminates. After all, alumina is a superior support for a catalyst (Rahmani et al., 2018; Trimm et al., 1986; Wefers and Misra, 1987; Trueba et al., 2005).

Mineral Name	Chemical Composition	Crystallographic Designation
Gibbsite	Aluminum trihydroxide	γ-$Al(OH)_3$
Bayerite	Aluminum trihydroxide	α-$Al(OH)_3$
Nordstrandite	Aluminum trihydroxide	$Al(OH)_3$
Corundum	Aluminum oxide	α-Al_2O_3
Boehmite	Aluminum oxide hydroxide	γ-AlOOH
Diaspore	Aluminum oxide hydroxide	α-AlOOH

Figure 2.2. Alumina Nomenclature in Literature.

The major problem in the usage of alumina is the sharp decrease in surface area with respect to increasing temperature. Some reactions require reasonably high temperatures and as a result, sintering cause the loss of active sites / surface area. In recent studies, the highest BET surface area for γ - Al_2O_3 is observed as 250 m^2/g for boehmite mineral. However, when temperature increases, the crystal phase structure of alumina changes to its other phases with lower surface area as in the sequence of γ→δ→θ→α. α - Al_2O_3 is the lowest surface area form of alumina and only has 66.2 m^2/g surface area. The phase change and surface area change of alumina according to temperature is given in Figure 2.3. Hence, it is essential to design a heat-resistant alumina catalyst with high surface (Arai et al., 1996; Häussermann et al., 2014; Trimm et al., 1986).

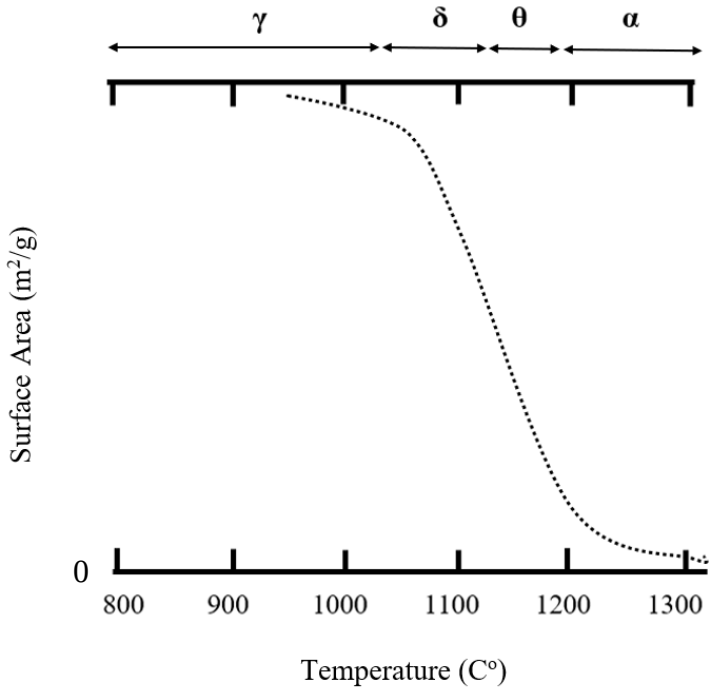

Figure 2.3. The Phase Change and Surface Area Change of Alumina with Respect to Temperature.

2.2.2. Phase Transition of Alumina

Wefers and Misra, illustrated the transformation sequence of aluminum hydroxides under thermal treatment with respect to starting mineral and calcination temperature. The scheme is represented in Figure 2.4 (Wefers and Misra, 1987).

Stumpf et al. illustrated the detailed stages of thermal treatment in order to observe transition of the phases of the aluminum hydroxides with respect to mineral types. The increase in temperature leads to the crystal phase structure of alumina changes to its other phases with lower surface area as in the sequence of $\gamma \rightarrow \delta \rightarrow \theta \rightarrow \alpha$. The scheme is represented in Figure 2.5. The recent studies showed that, transformation towards another mineral from a different starting mineral is possible by various modifications (Stumpf et al., 1950; Wefers and Misra, 1987; Lamouri et al., 2017; Cesteros, Y., 1999).

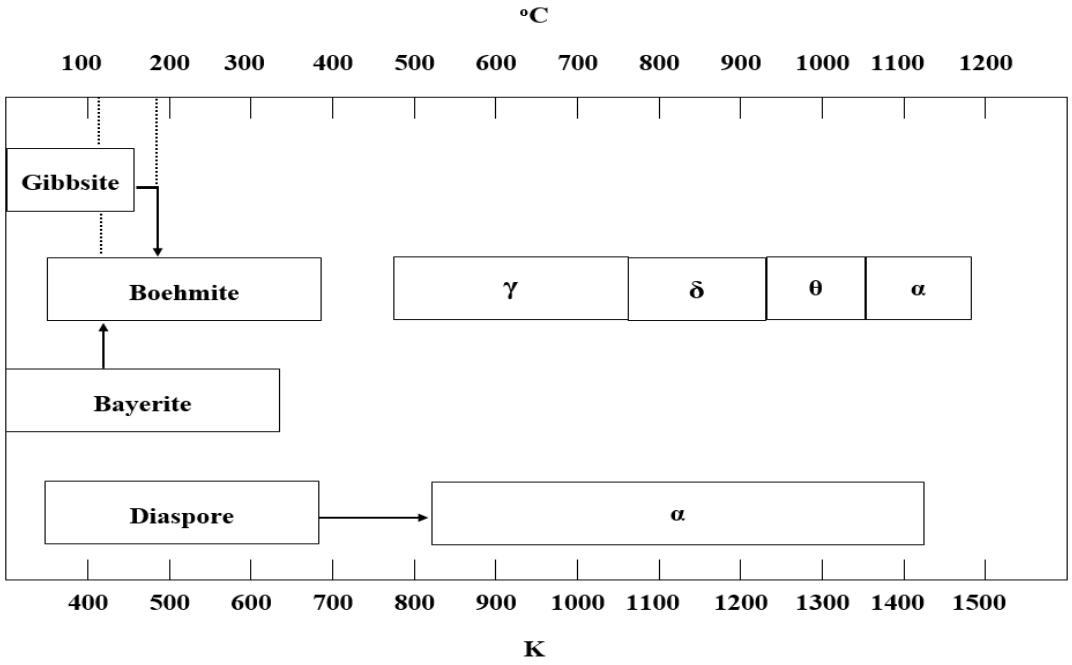

Figure 2.4. The Phase Change of Aluminum Hydroxides with Respect to Calcination Temperature and Starting Mineral.

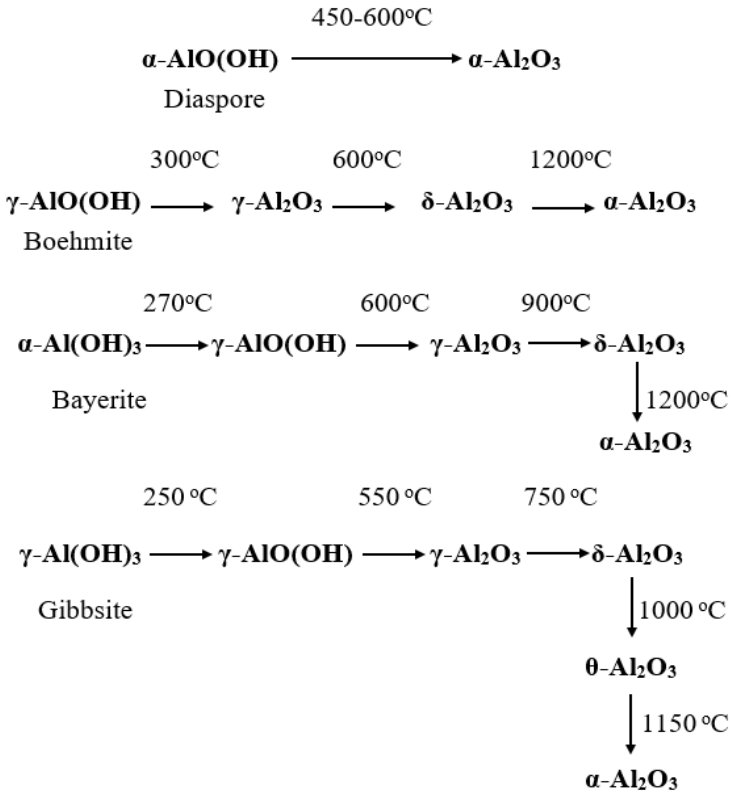

Figure 2.5. The Thermal Treatment of Aluminum Hydroxides for the Phase Change.

2.3. Support Preparation

The major development in stabilization of alumina is possible with adding dopants to support surface, in other words enhancing and modifying support surface in order to obtain higher surface area. Modification of the support surface by increasing active sites in order to provide doping metal to disperse better is possible with phase changes, i.e. pre doping thermal treatment. After adding the doping metals, the fixation of the metal particles requires thermal treatment as well.

2.3.1. Chemical preparation

There are various methods of preparation of catalysts/supports in literature, such as sol-gel method, deposition, precipitation, impregnation, etc. Each procedure serves for different goals. In the preparation of catalysts, impregnation is an advantageous method in terms of quickness, final configuration to be controllable, and ease of prepare a layer of actives sites (Yao et al., 2018; Deraz, N., 2018).

Impregnation usually consists of mixing of aqueous precursor solution of the metal to thermally treated porous support, drying, and calcination. There are 2 types of impregnation methods:

- Wet impregnation
- Dry Impregnation (Incipient to wetness)

In wet impregnation, excessive amount of solution is used. After the impregnation, solvent is dried and removed. In incipient to wetness impregnation, the volume of solution is as much as the volume of the total pore volume of the support. The procedure is followed by calcination (Deraz, N., 2018).

2.3.2. Thermal treatment

Thermal treatment is the most significant step of this research. Physical structure of the catalyst, particularly for the samples prepared with incipient to wetness as a doping method, depends almost totally on thermal stability of the support material. The form of Boehmite with the highest surface area is $\gamma - Al_2O_3$. The thermal treatment in the range of phase change regions leads the commercial γ-Al_2O_3 shift to its other forms with following order in Figure 2.6. In the direction of the shift the stability increases however, surface area decreases. Therefore, the optimum phase with respect to research purpose is required to determined and modifications to increase the surface area are required to be applied accordingly (Stumpf et al., 1950).

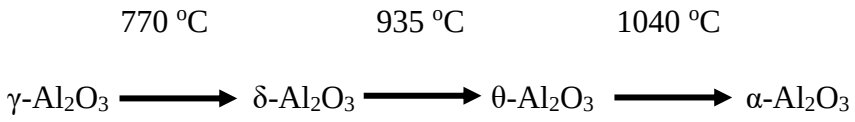

Figure 2.6. The Phase Change Temperatures for Boehmite.

Besides the thermal treatment before doping, thermal treatment upon doping, calcination, is essential for fixing the doped metal into the pores of the support. During the usage of support material, the doping material is required not to be moving or generating metal clusters with nearby metal particles. However, increase in calcination time causes remarkable decrease in surface area (İşli at al., 1997).

2.4. Design of Heat-Resistant Alumina

In order to design a heat-resistant alumina catalyst with high surface area, therefore higher thermal stability, there are three main modifications feasible.

- Use of additives
- Alternative alumina compounds
- Preparation process
- Drying process

2.4.1. Use of additives

Use of additives are one of the most suitable methods to obtain thermally stable alumina. The studies showed that most of the dopants attempted in previous investigations seem to retard the phase change from γ - alumina to α - alumina in the environments with increasing temperature. It is presumed that the delay is resulted from that the doped ions block diffusion and cause slowing in the transformation to the stable α – alumina phase and/or it leads to decrease in surface energy which is defined as the driving energy for sintering. La, Ba, Ce, Y, Si, Zr, B, and Th are some of the additives mentioned in the many studies used and claimed as modifiers of thermally resistant alumina, especially La and Ba addition (Andersson, 2005; Arai et al., 1996).

In one of the studies of Thevenin et al., Ba-modified alumina and La-modified alumina are prepared by incipient wetness method. The La and Ba added compounds are calcined at 1000 ^{o}C. Both the La-containing material and Ba-containing material maintain a large surface area and high resistance towards sintering and the BET surface areas are indicated as 107 and 94 m^2/g, respectively. Furthermore, Labalme et al., modified alumina with Barium and calcined at 1200 ^{o}C and stated that the generated catalyst is strongly heat resistant and inhibits α - Al_2O_3 transformation. Moreover, Shohaimi et al., reported in the article that BET surface area for Ba doped Al_2O_3 catalyst calcined at 1100°C is found as 39.65 m^2/g. Later, spent form of Ba doped Al_2O_3 is characterized by nitrogen adsorption analysis and its surface area is found as 44.05 m^2/g. The fresh catalyst has 11% lower surface area than the spent catalyst. With respect to this result, it is presumed that the surface area is increased during catalytic reaction due to generation of new active sites. The result also implies that the Ba doped catalyst have high reusability (Labalme et al., 1996; Shohaimi et al., 2012; Thevenin et al., 2001).

Arai et al., is stated that surface area decreases significantly with the increment in calcination temperature, given in Fig. 2.5. Calcination is obviously one of the most important steps in the manufacture of a catalyst. It is used in order to fix the features of the catalyst. Hence, calcination is a barrier required to reduce its effects to have thermally resistant alumina with relatively high surface areas. So as to overcome the effect of calcination temperature, use of additives is one of the excellent solutions (Arai et al., 1996; Labalme et al., 1996; Shohaimi et al., 2012; Thevenin et al., 2001).

Ozawa at al., studied thermal stability and characterization of gamma alumina modified with rare earths prepared by impregnation method and stated in the study that modification is highly effective to improve the thermal stability of γ - Al_2O_3. After the heat treatment under 1200 ^oC for 5 h, the surface area of pure alumina is 12 m^2/g while the surface area of Lanthanum doped alumina is 51 m^2/g and Cerium doped alumina is 40 m^2/g. The addition of lanthanum is stated as more promising than the addition of cerium to improve the thermal resistance of γ - Al_2O_3. Besides, Zou et al., investigated surface acidity and basicity of gamma alumina doped with K^+ and La^{3+} and calcined at elevated temperatures. Basic metal oxide of La_2O_3 is added to γ - Al_2O_3 to obtain high surface area support at high-temperature. At 1000 ^oC 10 wt.% La_2O_3/ γ - Al_2O_3 the surface area is indicated as 57 m^2/g, while 25 wt.% La_2O_3/ γ - Al_2O_3 the surface area is indicated as 36 m^2/g. Doping of Lanthanum does not seem to improve the loss of surface area in γ - Al_2O_3, however the transformation of it to other phases is inhibited (Ozawa at al., 1990; Zou et al., 2003; Huang et al., 2020).

In the line with thermally stable alumina study, it can be stated that use of additives has a strong stabilizing effect on alumina in terms of thermodynamical properties and surface structure (Andersson, 2005).

2.4.2. Alternative Alumina Compounds

Alumina can be found naturally or synthetically in various forms. The most promising ones to are activated alumina and hexaaluminate to improve the thermal stability of alumina (Rabia et al., 2018; Tian et al., 2016).

Hexaaluminates or hexagonal aluminate compounds are widely used as composite ceramics, catalysts and/or catalyst supports in high temperature reactions. The formula is presented as $AB_xAl_{12-x}O_{19}$. A is a large cation such as Na, Ba, La and resides in the mirror plane while B represents a transition-metal such as Mn, Fe, Co, Cu, Ni. or a noble metal Ir, Ru, Pd, Rh. $LaAl_{12}O_{19}$ is a common type of a hexaaluminate. Hexaaluminates can be synthesized by various methods such as sol–gel, co-precipitation, reverse microemulsion etc. All are based on dissolving precursors in liquid, then drying and calcination (Gao et al., 2012; Tian et al., 2016).

Zarur et al., investigated nanometer-sized barium hexaaluminate particles prepared by reverse microemulsion mediated sol-gel method. The produced complex oxide showed significant improvements both in thermal stability and increment in surface area compared to typical sol-gel method. Surface areas after calcination at 1300 °C of various barium hexaaluminate materials synthesized and processed in different ways reach to 136 ± 30 m^2/g. Moreover, in the study of Cho et al., surfactant-mediated synthesis of metal substituted hexaaluminate from alumina sol is investigated. Freeze–drying or sol–gel method is used to obtain highly stable manganese substituted hexaaluminate. Under 1200 °C for 6 h of heat treatment, γ - alumina transformed to highly pure θ – alumina while it is expected to transform to α – alumina at or greater than 1000 °C. Therefore, hexaaluminates synthesized by either method are highly attractive as catalytic supports for applications requiring high temperature applications (Cho et al., 2001; Zarur et al., 2000).

Another aluminum oxide product is activated alumina. It is produced from aluminum hydroxide by dehydroxylating and owed its high surface area, highly porous form and some unique properties to it. Its high adsorption capacity makes it suitable to be used as catalyst for wastewater treatment and as adsorbent in various applications. The chemical formula is represented by $Al_2O_{(3-x)}(OH)_{2x}$ where x ranges from 0 - 0.8. Activated alumina only has metastable form, γ – alumina. Nano sized γ -alumina is the primary material and porous solid structure is made by thermal treatment of aluminum hydroxide. Surface area of activated alumina is more than 200 m^2/g (Pearson, 2003; Rabia et al., 2018; Wei et al., 2001).

In a recent study, Beleka and Dhoble, highly porous alumina granules by a modified sol–gel method. SEM micrograph demonstrated homogeneous and highly porous structure of granule alumina. Due to high porosity average grain size is detected as 30 nm and BET surface area is detected as 447 m^2/g after treatment at 500 ^oC for 2 h which is very high compared to literature and commercial alumina in the market. Levy et al., investigated the effect of foreign ions on the stability of activated alumina and its function as a precursor material. Samples have heat treatment up to 1000°C for 5 h. K^+, Li^+ and Mg^{2+} are impregnated on alumina in order to determine the foreign ion effect. Initially, the received alumina has a surface area of 278 m^2/g. By the addition of MgO in 0.0 to 0.02 ion ratio, surface areas rise from 210 to 218 m^2/g. On the other hand, potassium ions are added in the form of K_2O with various ratios, and surface area rises from 210 to 235 m^2/g. As a result, Lithium ions give the least stabilization measured and Potassium ions give greater stabilization of all, while Magnesium ions give an intermediate stabilization. Hence, activated alumina is also a very promising material worth to be investigated (Beleka and Dhoble, 2018; Levy and Bauer, 1967).

2.4.3. Preparation Process

Another modification on alumina is the modification of preparation process. Preparation process has also an undeniable effect on the stability of Alumina. The major factors with the most direct effects in the literature are listed.

- Amount of dopant
- Preparation method

Alphonse and Faure investigated thermal stabilization of alumina for different amount of La dopants and calcination temperatures and indicated in the study that La dopant amount is required to be determined with respect to surface area of starting γ -alumina. Pijolat et al. was earlier observed higher BET surface area and pore volume around 1% La doping. (Alphonse and Faure, 2014; Pijolat et al., 1992)

Alphonse and Faure stated in the study that, La doping provides stabilization for the textural properties only valid for the temperature treatments under 1200°C. (Alphonse and Faure, 2014).

The poor textural properties due to high temperature can be improved for catalytic applications by the development of more efficient synthesis methods. Tian et al., investigated and compared the effect of the preparation method on the specific surface area of alumina compounds. By sol-gel method, Ba hexaaluminates obtains a surface area of 13 m^2/g at 1450 °C and after calcination at 1600 °C for h, the surface area remains 11 m^2/g. For co-precipitation, $BaAl_{12}O_{19}$ hexaaluminate has a surface area of 15 m^2/g calcined at 1300 °C. Ultimately, by reverse microemulsion, the particle size and specific surface area of Ba-hexaaluminate calcinated at 1300 °C is found respectively as 30 nm and 160 m^2/g which is the largest surface area obtained in the research (Tian et al., 2016).

2.4.4. Drying Process

The last modification can be applied to recovered catalysts. Zarur et al., indicated in the study of reverse microemulsion-mediated synthesis and structural evolution of barium hexaaluminate nanoparticles that drying technique are also affect the stability of alumina. In

the study in order to remove the residual surfactants in the recovered samples, the samples are subjected to drying which might be oven drying or supercritical drying. Oven drying led to average surface areas of 53-69 m^2/g while supercritical drying led to high average surface areas of 78-136 $m^{2/}$g, respectively, after the samples calcinated at 1300 °C. Hence, it is claimed that drying technique affects the particle size and morphology of the compound significantly. The drastic difference between two drying methods is related to that supercritical drying is specifically more effective in preventing from particle agglomeration and growth during the removal of organics than oven drying (Zarur et al., 2000).

Moreover, Fokin et al., investigated the effect of drying methods of Al_2O_3 powder mixture on the properties. In the study a spray dryer, spray dryer equipped with a nozzle in a vacuum drying oven, and a freeze-drying system are compared. The compounds operated with a spray drying method is obtained a homogeneous and agglomerate-free dispersion of alumina (Fokin et al., 2017; Zarur et al., 2000).

3. EXPERIMENTAL WORK

3.1. Materials

3.1.1. Chemicals

The chemical materials used for the support preparation in this research are research grade and tabulated in Table 3.1.

Table 3.1. The Properties of the Chemicals Used in Support Preparation.

Chemical	Formula	Specification	Source	MW (g/gmol)
Aluminum oxide	γ-Al_2O_3	100 %	Alfa Aesar	101.96
Barium nitrate	BaN_2O_6	<= 100 %	Merck	261.34
Lanthanum nitrate hexahydrate	LaN_3O_9*6 H_2O	<=100 %	Carlo Erba Reagents	433.02
Tetraammineplatinum(II) nitrate	$[Pt(NH_3)_4](NO_3)_2$	99.995%	Sigma-Aldrich	387.21

3.1.2. Gases and Liquids

The formulas, specifications, and applications of the gases and the liquids used in this study are tabulated in Table 3.2 and Table 3.3, respectively. Liquid nitrogen is supplied by

Advanced Technologies Research and Development Center of Boğaziçi University. All the gases in this research are supplied by the Linde Group, Gebze, Turkey, ammonium hydroxide is supplied by Merck KGaA Turkey.

Table 3.2. Specifications and Applications of the Gases Used.

Gas	**Formula**	**Specification**	**Application**
Dry air	-	99.998%	BET Degas Unit Pneumatic Valve
Helium	He	99.999%	Inert
Argon	Ar	99.995%	Inert

Table 3.3. Specifications and Applications of the Liquid Used.

Liquid	**Formula**	**Specification**	**Application**
Water	H_2O	Deionized (DI)	Aqueous solution
Ammonium hydroxide	NH_4OH	25%	pH manipulation
Liquid nitrogen	N_2	Refrigerated, liquid	BET analysis

3.2. Experimental Systems

In this research, two main groups of experimental systems are used.

- Support Preparation Systems: Support preparation is performed by using incipient-to-wetness impregnation.
- Support Characterization Systems: Support characterization systems are used to analyze the characterization of the structural and the surficial properties of the support samples prepared.

3.2.1. Support Preparation Systems

The system is used for support preparation by incipient-to-wetness impregnation method and it consists of a precursor aqueous solution beaker, a MasterFlex peristaltic pump, Silicone tubing, a 250ml Büchner flask, a Retsch UR1 ultrasonic mixer, and a KNF Neuberger vacuum pump respectively. The support preparation system is schematically represented in Figure 3.1 (Baranak, 2014).

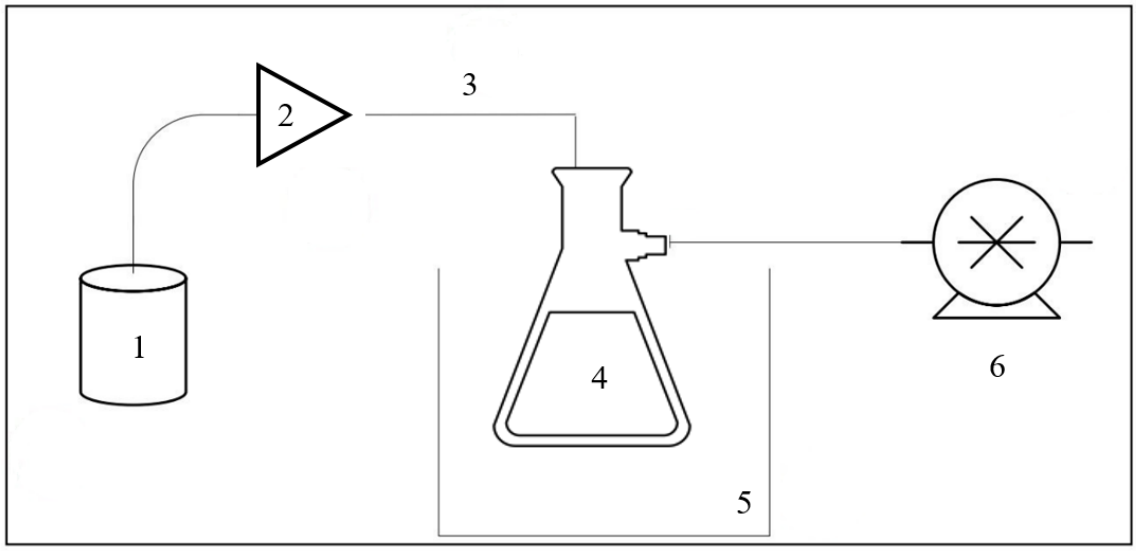

Figure 3.1. Schematic representation of the impregnation system and 1. Precursor solution beaker, 2. MasterFlex peristaltic pump, 3. Silicone tubing, 4. 250ml Büchner flask, 5. Retsch UR1 ultrasonic mixer, 6. KNF Neuberger vacuum pump.

3.2.2. Support Characterization Systems

3.2.2.1. Brunauer-Emmett-Teller (BET) Surface Area Analysis: The analyses were performed at Synthetic Natural Gas and Hydrogen Production Technologies Laboratory (SNG&HydTec Lab). Total surface area, pore size distribution, and pore volume distribution of the mesoporous support materials were measured by physisorption of N2 via Micromeritics 3Flex Surface Characterization Analyzer using Brunauer-Emmett-Teller (BET) equation and Barrett-Joyner-Halenda (BJH) pore size distribution method, respectively presented in equations 3.1, 3.2, 3.3, and 3.4,

$$\frac{1}{v\,[\,(P_0/P)-1\,]} = \frac{c-1}{v_m C}\left(\frac{P}{P_0}\right) + \frac{1}{v_m c}. \tag{3.1}$$

P and P_0 are the equilibrium and saturation pressure of adsorbates at the temperature of adsorption (mmHg), v is the adsorbed gas quantity (cm^3), v_m is the monolayer adsorbed gas quantity (cm^3), and c is the BET constant; expressed as,

$$c = exp\left(\frac{E_1 - E_L}{RT}\right). \tag{3.2}$$

E_1 is the heat of adsorption for the first layer and E_L is that for the second and higher layers, T is the adsorption temperature, and R is the universal gas constant. Total surface area (m^2/g_{cat}) is measured by equation 3.3 as,

$$S_g\left(\frac{m^2}{g}\right) = (V_m/22{,}414)(6.02 \times 10^{23})(A_m)\left(\frac{1}{w_{cat}}\right)(10^{-20}). \tag{3.3}$$

S_g is total surface area per unit weight of catalyst (m^2/g), w_{cat} is catalyst weight (g), and A_m is cross-sectional area of one molecule ($\dot{A}$).

Barrett-Joyner-Halenda (BJH) pore size distribution method is applicable only to the mesopore and small macropore size range. The pore size is classified by pore diameter into microporous (<2 nm), mesoporous (2 - 50 nm), and macroporous (>50 nm). The BJH equation is presented in equation 3.3 as (Valenzuela-Muñiz, 2012; Maraeva et al., 2018),

$$V_n = R_n(\Delta V)_n - R_n \Delta t_n \sum_{i=1}^{n-1} c_i A_i. \quad (3.4)$$

V_n is the volume of the set of pores emptied of their capillary condensate in the nth desorption step, R is the universal gas constant, $(\Delta V)_n$ is the volume of liquid adsorbate removed from the pores in the nth desorption step, c is the BET constant presented in equation 3.2, Δt_n being the decrease in thickness of the multilayer as a result of the nth desorption step, and A_i the surface area of the set of pores involved in the ith desorption step.

3.2.2.2. Raman Spectroscopy: The crystalline structures of treated alumina samples were analyzed by Raman spectroscopy, a Renishaw inVia Raman microscope with a 514nm Ar+ laser (20mW), approximately 2mW intensity, 10s acquisition time, and a total of 20 accumulations per spectrum. The analyses were performed at the Advanced Technologies Research and Development Center of Boğaziçi University.

3.2.2.1. X-Ray Diffraction (XRD): The crystalline phases of the support samples were analyzed by X-Ray diffraction, a Rigaku D/MAX-Ultima+/PC X-ray diffraction with an X-ray generator with Cu target and scan speed of 2°/min. The analyses were performed at the Advanced Technologies Research and Development Center of Boğaziçi University.

3.3. Support Preparation and Pre-treatment

All the samples, except the ones belong to Set-I in Table 3.5, were sieved to 10-18 mesh (1-2 mm). Total of 142 samples were prepared and tested for their thermal resistance -*in terms of the change observed in their Total Surface Area (TSA), Total Pore Volume (TPV) and Pore Size Distribution (PSD) upon heat treatment*- according to an experimental design having pre-doping heat treatment and its level (PDT_T_{level}), doping material, doping pH level, drying temperature and procedure, post heat treatment before final calcination and number of stages (PHT_{level}_#stage) applied, and final calcination temperature level and duration as the experimental parameters.

In this context, 7 temperature levels for pre-doping heat treatment (PDT_T_{1-7}), 3 doping materials (La, Ba, Pt), 2 doping pH level (pH_1&2), 1- 3 stages of post heat treatment (PHT_1-3) before final calcination, and 4 final calcination temperature (FCT_ T_{1-4} as 900, 1000, 1100 and 1150 ^{o}C, respectively) for 2 durations were used, as given in Table 3.4, Table 3.5, and Table 3.5. Drying was performed in an oven, and calcination and heat treatments were performed in a muffle furnace.

The samples were grouped into sets according to the main experimental variable tested through comparative analysis of the sets. It should be noted that as the support(s) prepared in this work has potential to be a proprietary material, the experimental parameters that were determined as main parameters affecting the temperature resistance of the material, like pre-doping calcination temperature, are given as levels (or ranges) rather than absolute values. The sets of the samples tested are as follows (see Tables 3.4, Table 3.5, and Table 3.6);

Sets I-III: These sets have 12 pristine samples, and the characterization results were used as reference bases. In Set-I, the materials tested were Al_2O_3 High SA 1-8 pellet (Gamma), Al_2O_3 High SA pellet (Gamma), Al_2O_3 Low Si pellet and Al_2O_3-SiO_2 13-Percent Low SA pellet.

Starting with Set-II and in all other sets, Aluminum Oxide (Alfa Aesar with CAS of 1344-28-1) ground to 10-18 mesh size was used as the starting material.

Sets IV-XI: These sets have total of 79 samples. The samples were grouped into those sets such as to elucidate the effect of pre-doping calcination temperature on thermal stability through comparative analysis of the physical properties of the samples between the sets. All the samples except those in set IX were doped with Lanthanum. Note that effect of Lanthanum and Barium addition was also studied through comparative analysis of the physical properties of the samples belongs to sets VIII and IX which were exposed to same pre-doping calcination temperature. For sets IV-XI, 7 pre-doping calcination temperature levels within range 450-1075 ^{o}C were applied as the main experimental parameter. Note that the pre-doping temperature increases as 450 ^{o}C<T_1<T_2<T_3<T_4<T_5<T_6<T_7<1075 ^{o}C.

Sets XII-XV: These sets have total of 32 samples. The samples were grouped into those sets such as to elucidate the effect of doping pH level used on thermal stability through comparative analysis of the physical properties of the samples belong to Sets V, VI, VIII, X and Sets XII-XV. Note that for example Set V and Set XII, Set VI and Set XIII, etc. have the same preparation methodology except the pH level used during doping. Two pH levels that were used during doping are within the range of 3.5-8.0. All the samples were doped with La.

Sets XVI-XVIII: These sets have total of 12 samples doped with Platinum. The samples were grouped into those sets such as to elucidate the effect of drying temperature and time used upon impregnation on thermal stability through comparative analysis of the physical properties of the samples belong to those sets.

Set XIX: This set has total of 7 undoped aluminum oxide samples only exposed to drying procedure. No final heat treatment was applied to those samples; thus, their physical properties were considered as a reference basis for the samples belongs to Sets XVI-XVIII.

Note that for all sets, except Set-I, post heat treatment before final calcination was applied in 0-3 stages (PHT_1-3) for temperature range of 500-1200 ºC.

Table 3.4. Comparatively Analyzed Sets, Main Experimental Parameters and Parameter Ranges and Levels Used.

Comparatively Analyzed Sets	**Main Experimental Parameter**	**Main Experimental Parameter_ Range & Levels**
IV, V, VI, VII, VIII, X, XI	Pre-doping heat treatment temperature level	450-1075 ^{o}C; 7 levels
VIII & IX	Doped Material (La vs. Ba)	0.25-3%; 1 level
V & XII; VI & XIII; VIII & XIV; X & XV	Doping pH level	3.5-8; 2 levels
XVI-XVIII	Drying T & time (for Pt doping)	(-195.79)-110 ^{o}C (5 levels) &16h or 16+16 h
XIX	Vacuum pressure applied (doping) & Drying T & time	Mixed (see the related section in Results and Discussion)

Table 3.5. Sample Numbers (Codes), Sample Sets Formed (I-X) and Parameter Levels.

Set No.	**Sample No.**	**PDT_T_{level}* T(ºC)***	**Doping Mat.**	**pH_{level}**	**Vac_{level}**	**Drying_T(ºC)**	**PHT_stage**	**FCTs (ºC)**	**t_{FC}** (h)**
I	1-4	-	-	-	-	-	-	-	-
II	5-8	-	-	-	-	-	0	900-1150	2
III	9-12	T_5	-	-	-	-	0	900-1150	2
IV	13-20	T_1	La	pH_1	1	110	0 &1	None-1150	2
V	21-33	T_2	La	pH_1	1	110	0-3	None-1150	1 or 2
VI	34-45	T_3	La	pH_1	1	110	0-3	None-1150	2
VII	46-54	T_4	La	pH_1	1	110	0-2	None-1150	2
VIII	55-64	T_5	La	pH_1	1	110	0-2	None-1150	2
IX	65-70	T_5	Ba	pH_1	1	110	0 & 1	None-1150	2
X	71-82	T_6	La	pH_1	1	110	0-3	None-1150	2

*: 450 $^{o}C<T_1<T_2<T_3<T_4<T_5<T_6<T_7<1075\ ^{o}C$

**: when applied

Table 3.6. Sample Numbers (Codes), Sample Sets Formed (X-XIX) and Parameter Levels

Set No.	**Sample No.**	**PDT_T_{level} * T(ºC)**	**Doping Mat.**	**pH_level**	**Vac_level**	**Drying_T(ºC)**	**PHT_stage**	**FCTs (ºC)**	**t_{FC}** (h)**
XI	83-91	T_7	La	pH_1	1	110	0-2	None-1150	2
XII	92-99	T_2	La	pH_2	1	110	0-2	None-1150	2
XIII	100-107	T_3	La	pH_2	1	110	0-2	None-1150	2
XIV	108-115	T_5	La	pH_2	1	110	0-2	None-1150	2
XV	116-123	T_6	La	pH_2	1	110	0-2	None-1150	2
XVI	124-127	T_5	Pt	pH_1	1	25,40,110	-	1000	2
XVII	128-131	T_5	Pt	pH_1	2	25, 40, 110	-	1000	2
XVIII	132-135	T_5	Pt	pH_1	3	25,40, 110	-	1000	2
XIX	136-142		-	-	1 or none	-195.79, -18, 25,40,110	-	-	-

*: 450 ºC<T_1<T_2<T_3<T_4<T_5<T_6<T_7<1075 ºC

**: when applied.

4. RESULTS AND DISCUSSION

In the current work, the aim is to enhance the thermal stability of various granular form commercial γ-Al_2O_3 samples via doping with stabilizers, La, Ba and Pt, through using various preparation and pretreatment methods/parameters. In this context, the results of parametric analysis on the temperature stability of supports are presented in five sections (4.1-4.5):

- Effect of Thermal Treatment on Reference Alumina Samples
- Effect of Doping Metal Type (metals: La, Ba, Pt)
- Effect of Pre-doping Heat Treatment on Alumina (levels: PDT_T_{1-7})
- Effect of Impregnation Strategy
- Effect of Post Heat Treatment Before Final Calcination (levels: PHT_1-3)

The thermal resistance of the supports prepared are determined on the basis of how limited is the loss in their surface area upon final calcination treatment conducted at temperatures of 900, 1000, 1100 and 1150 ^oC, which are indicated as final calcination temperature (FCT). As calcination duration may also affect the structure, two durations, 1h and 2h, were applied. The thermal of the support prepared is discussed in section 4.6.

In the final section, section 4.7 of Results and Discussion part, the optimum design parameters of a temperature resistant support for the tested parameters and parameter ranges are discussed.

The extent of loss in Total Surface Area (TSA), Total Pore Volume and Pore Size Distribution (PSA) of the support samples prepared compared to the reference sample, generic γ-alumina, upon treatment at Final Calcination Temperature is used as a measure of their temperature resistance, while the comparative analysis of the results obtained from characterization techniques, like XRD, are used in explaining the temperature resistance of the samples in terms of their crystal structure.

It should be noted that as the support(s) prepared in this work has potential to be a proprietary material, the experimental parameters that were determined as main parameters affecting the temperature resistance of the material, like pre-doping calcination temperature, are given as levels (or ranges) rather than absolute values.

4.1.Effect of Thermal Treatment on Reference Alumina Samples

BET surface area tests conducted over different alumina types and tabulated in Table 4.1.

Table 4.1. BET Surface Areas of Different Alumina Types.

Alumina Types	**BET Surface Area (m^2/g)**
Al_2O_3 High SA 1-8 pellet (Gamma)	217.05
Al_2O_3 High SA pellet (Gamma)	214.82
Al_2O_3 Low Si pellet	0.57
Al_2O_3-SiO_2 13-Percent Low SA pellet	~0

Since the aim is to obtain temperature resistant support, the alumina samples with high BET surface areas in Table 4.1 were exposed to final calcination (FCT) in ascending temperature order at 900, 1000, 1100, and 1150 ^oC for 2 hours and tested for BET surface areas. The results are presented in Table 4.2.

Table 4.2. BET Surface Areas of Gamma-Alumina After Thermal Treatment at FCT_900, FCT_1000, FCT_1100 and FCT_1150.

	Final Calcination Temperature - FCT (ºC)	**TT Duration (h)**	**BET Surface Area (m^2/g)**
γ-Al_2O_3 High SA pellet	900	2	159.70
	1000	2	116.71
	1100	2	42.81
	1150	2	8.81

The results show the low temperature-resistance of all reference alumina samples in the absence of pre-treatment/doping applied. The BET surface area of the samples decreases with the increase in final calcination temperature. The pores on the surface of the samples are closed up and the surface is flattened by temperature increment. To observe the effects of temperature on reference Alumina samples, the samples were further characterized by X-Ray Diffraction and presented in Figure 4.1.

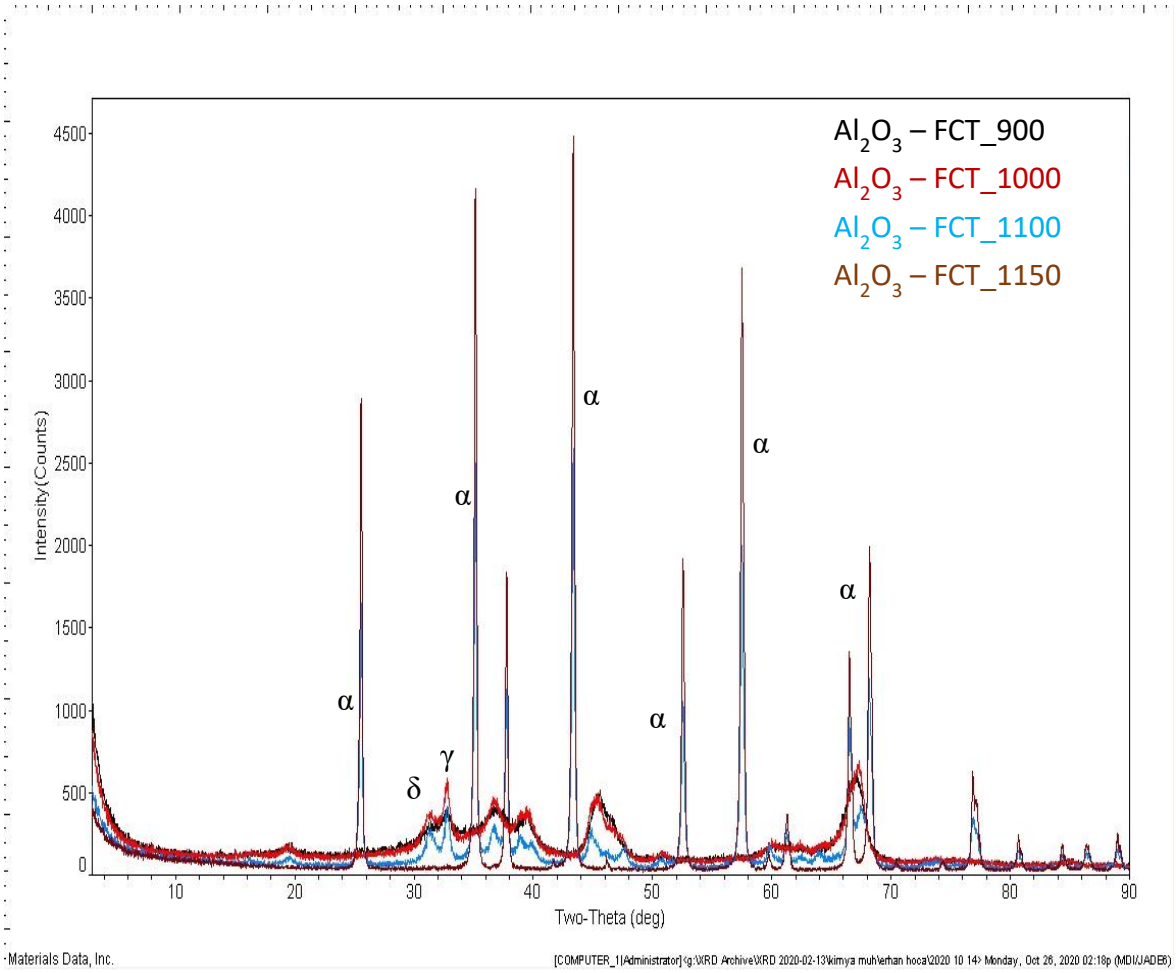

Figure 4.1 XRD Profiles of Alumina Samples After Final Calcination at FCT_900, FCT_1000, FCT_1100, and FCT_1150.

In Figure 4.1, the alumina sample exposed to final calcination temperature of 1150 ^{o}C has the highest intensity α peaks among all; the sample exposed to FCT_1100 has the second highest intensity α peaks. Since the higher intensity peak indicates the crystallinity in structure, clear α-Al_2O_3 formation is observed for the samples exposed to FCT_1150 and FCT_1100. Although FCT_1100 shows γ-Al_2O_3 and δ-Al_2O_3 formations as well; the samples exposed to FCT_900 and FCT_1000 show more distorted γ-Al_2O_3 and δ-Al_2O_3 formations with broad and low intensity peaks (Santos et al., 2000).

.

In Figure 4.2 and 4.3, BJH pore size distribution and pore area distribution of alumina samples after thermal treatment at FCT_900, FCT_1000, FCT_1100, and FCT_1150 are represented. The samples with FCT_1100 and FCT_1150 have wider pore sizes in terms of pore width and tend to have macroporous structure (pore width >50nm). The samples exposed to FCT_900 and FCT_1000 calcination temperature have mesoporous structure and most of their pores have 10-25 nm width.

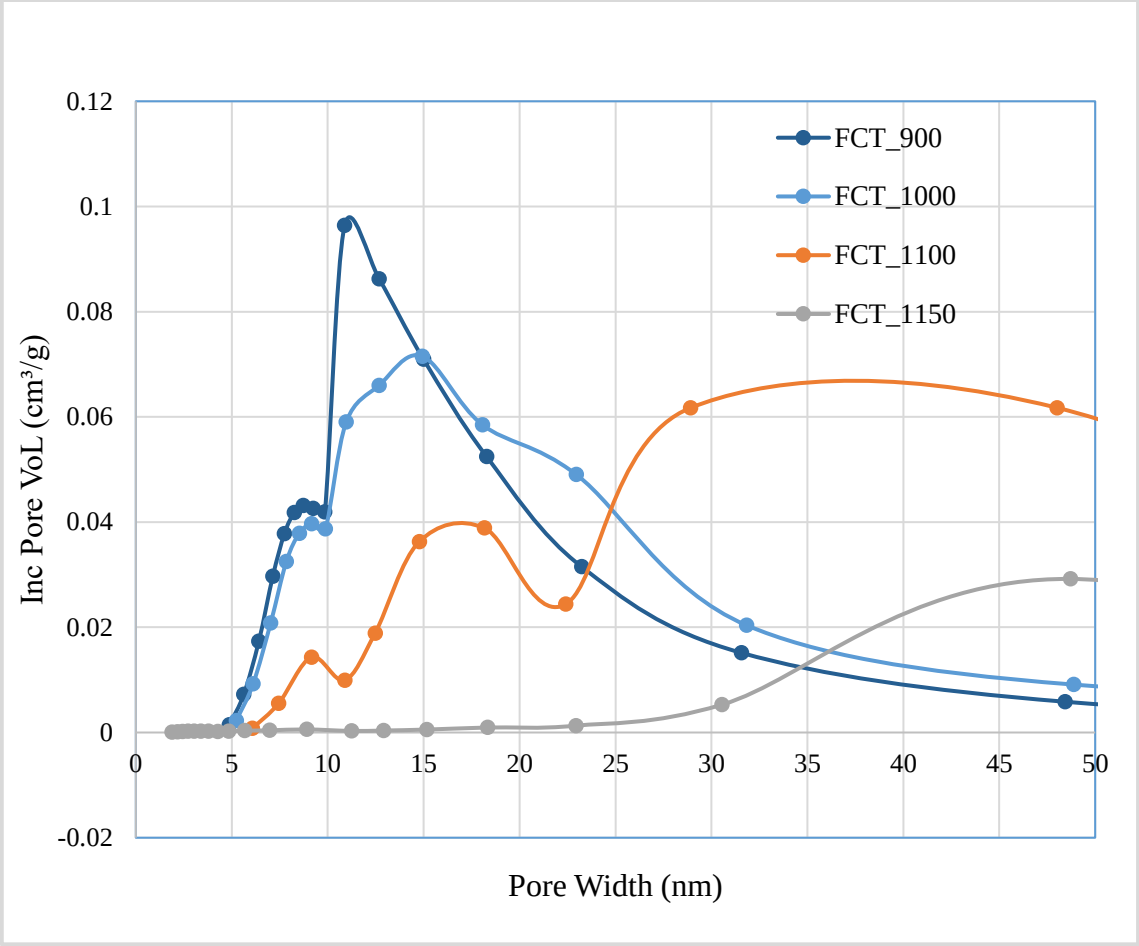

Figure 4.2 BJH Pore Size Distribution for Alumina Samples After Final Calcination at FCT_900, FCT_1000, FCT_1100, and FCT_1150.

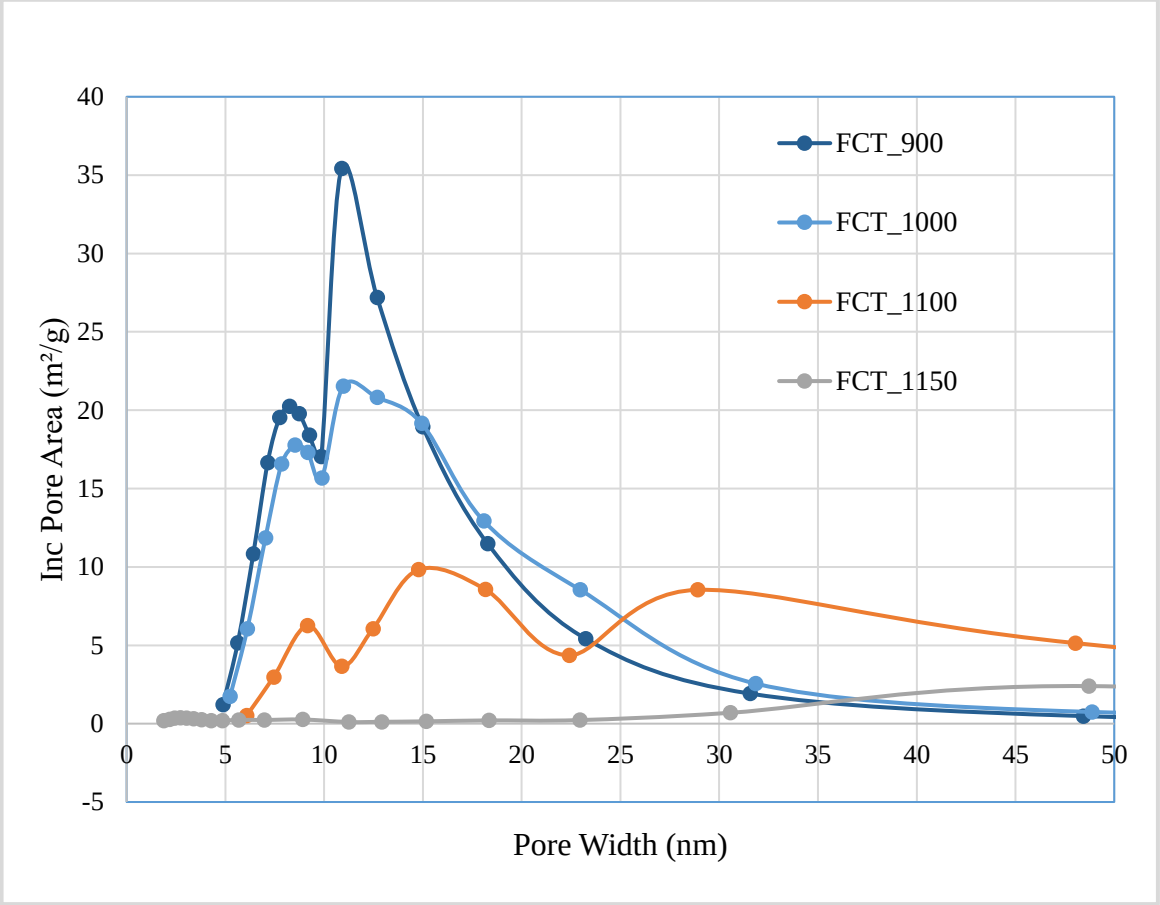

Figure 4.3 BJH Pore Area Distribution for Alumina Samples After Final Calcination at FCT_900 , FCT_1000, FCT_1100, and FCT_1150.

4.2.Effect of Doping Metal Type

In this section, aiming to make the support surface ready for metal loading, the γ-Al_2O_3 pellets were dehumidified at 150°C for 2 hours and were treated with pre-doping heat treatment at PDT_T_5 for 4 hours in a muffle furnace. Then, 1wt% of Lanthanum or 1 wt% Barium were doped on the pretreated sample by impregnation. The doped samples were dried overnight and calcined (FCT) at FCT_900, FCT_1000, FCT_1100, and FCT_1150 for 2 hours. All the samples were characterized by their BET surface area. The BET surface areas of La-doped and Ba-doped samples are tabulated in Table 4.3, and the decrease with increasing calcination temperature is presented Figure 4.4.

Table 4.3. BET Surface Areas of La-doped and Ba-doped Alumina Samples.

	BET Surface Area (m^2/g)	
Calcination T (°C)	**La doped Al_2O_3**	**Ba doped Al_2O_3**
FCT_900	134.17	145.09
FCT_1000	122.23	134.07
FCT_1100	87.24	83.04
FCT_1150	61.74	38.26

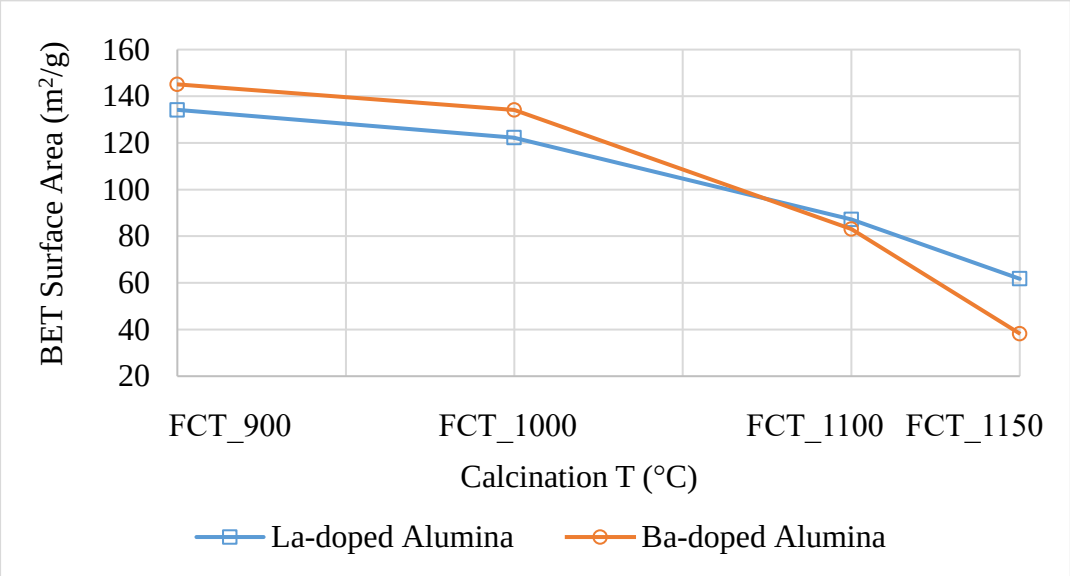

Figure 4.4 BET Surface Areas of Ba-doped vs. La-doped Alumina. FCT_900, FCT_1000, FCT_1100, and FCT_1150.

Even though Ba-doped samples have higher BET surface areas at FCT_900 and FCT_1000; at higher temperatures, FCT_1100 and FCT_1150, La-doped samples have higher BET surface area, and thus have better thermal stability. This is the reason why the subsequent studies were continued with La-doped samples.

4.3.Effect of Pre-Doping Temperature

γ-Al_2O_3 pellets that were presented in section 4.2 were heat treated via dehumidifying at 150°C for 2 hours, and calcining at PDT_T_5, a rather mid-level temperature, for 4 hours in a muffle furnace. In order to understand the effect of pre-doping treatment, the samples treated at PDT_T_5 without any metal doping, were calcined FCT_900, FCT_1000, FCT_1100, and FCT_1200 for 2 hours and characterized by their BET surface area. The results are compared to γ-Al_2O_3 calcined at the same temperatures for 2 hours; all results are presented in Table 4.4.

Table 4.4. BET Surface Areas of Pre-Calcined and γ-Al_2O_3 Samples with Respect to Final Calcination Temperatures.

	BET Surface Area (m^2/g)	
Calcination T (°C)	**Pre calcined-Al_2O_3**	**γ-Al_2O_3**
FCT_900	133.34	159.70
FCT_1000	97.42	116.71
FCT_1100	10.84	42.81
FCT_1150	9.79	8.81

Both for pre-calcined and reference γ-Al_2O_3 samples, decrease of BET surface area with respect to rising calcination temperature is inevitable. However, the pre-calcined samples affected remarkably compared to γ-Al_2O_3 samples exposed to final calcination conditions FCT_900, FCT_1000, and FCT_1100; at FCT_1150. The results clearly show that γ-Al_2O_3 has higher BET surface area than pre-calcined samples for the whole set except for the case upon calcination at 1150 ^oC.

In order to comprehensively analyze the effect of pre-doping temperature (PDT), the 7 set of pellets were treated at PDT_T_1, PDT_T_2, PDT_T_3, PDT_T_4, PDT_T_5, PDT_T_6, and PDT_T_7, in ascending temperature order, for 4 hours in the muffle furnace. The seven samples were impregnated with 1% of Lanthanum and each were calcined at FCT_900, FCT_1000, FCT_1100, and FCT_1150 for 2 hours. The BET surface area results are presented in Table 4.5 and Figure 4.5.

Table 4.5. BET Surface Areas of 1%La/Al_2O_3 Samples with Respect to Different PDT and Calcination Temperatures.

		BET Surface Area (m^2/g)						
		Pre-Doping Temperature (°C)						
		PDT_T_1	**PDT_T_2**	**PDT_T_3**	**PDT_T_4**	**PDT_T_5**	**PDT_T_6**	**PDT_T_7**
Calcination Temperature (°C)	**0**	204.59	201.33	187.49	174.62	177.87	158.53	135.19
	FCT_900	154.81	157.91	151.47	144.58	134.17	133.20	120.40
	FCT_1000	128.50	134.95	136.63	122.85	122.23	119.00	112.85
	FCT_1100	85.05	86.19	82.17	87.65	87.24	92.04	96.35
	FCT_1150	49.32	56.64	55.71	45.75	61.74	59.23	67.90

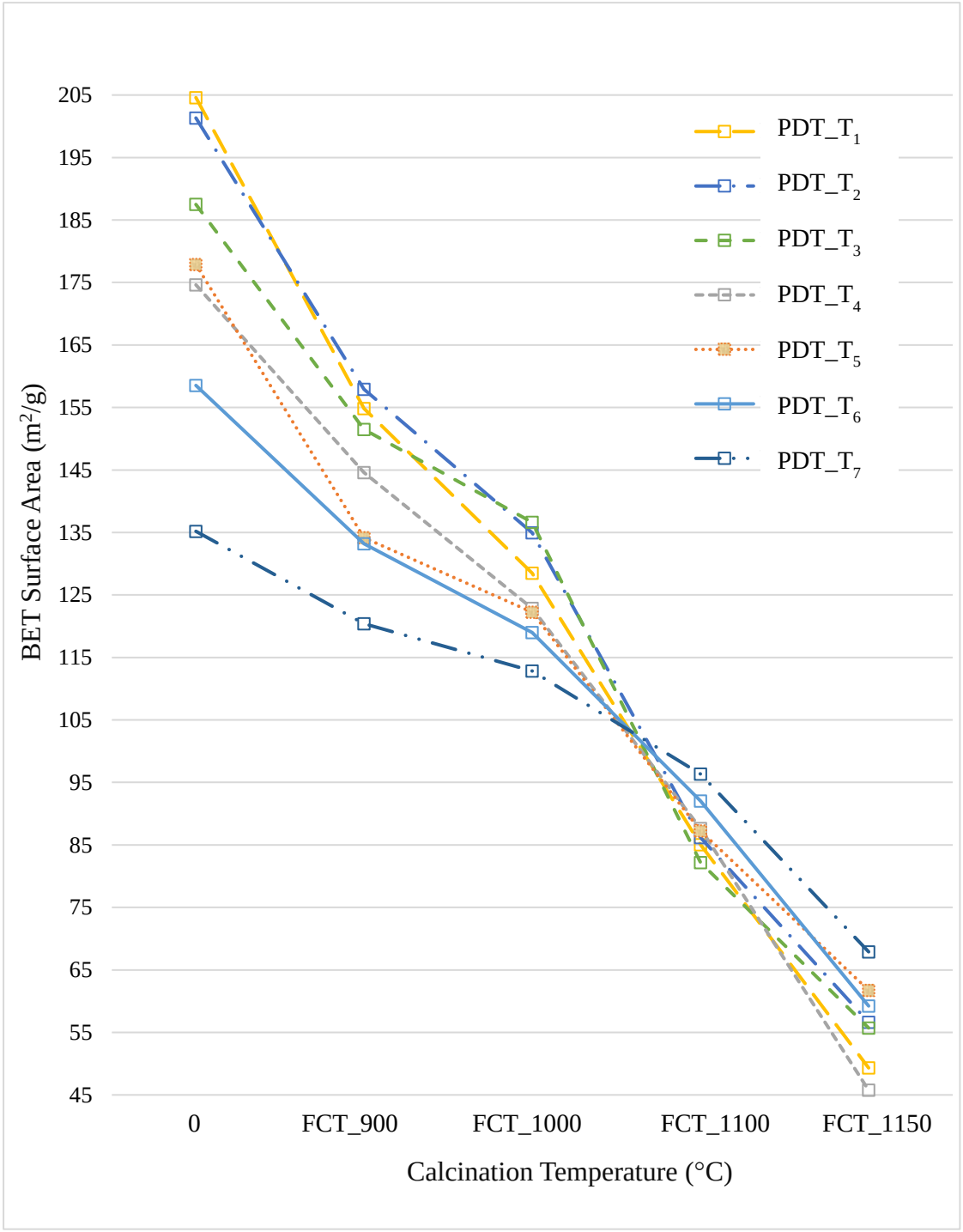

Figure 4.5 BET Surface Areas vs. Calcination Temperatures of the 1%La/Al_2O_3 Samples with Different PDT.

Table 4.5 and Figure 4.2 indicate that the surface areas of all samples are decreased with increase in final calcination temperature, yet the samples treated with pre-doping

temperatures of PDT_T_2, PDT_T_3, PDT_T_5, and PDT_T_6 shown slightly more stable BET surface areas than the samples with PDT of PDT_T_1 and PDT_T_4. The sample with pre-doping heat treatment temperatures of PDT_T_7 has the highest stability among others.

In order to observe the effect of pre-doping temperature on their crystalline phases, a group of samples treated with PDT_T_1, PDT_T_4, and PDT_T_6 prior to La doping was characterized by X-Ray Diffraction upon the application of the highest calcination temperature FCT_1150. The results are presented in Figure 4.6, 4.7, and 4.8.

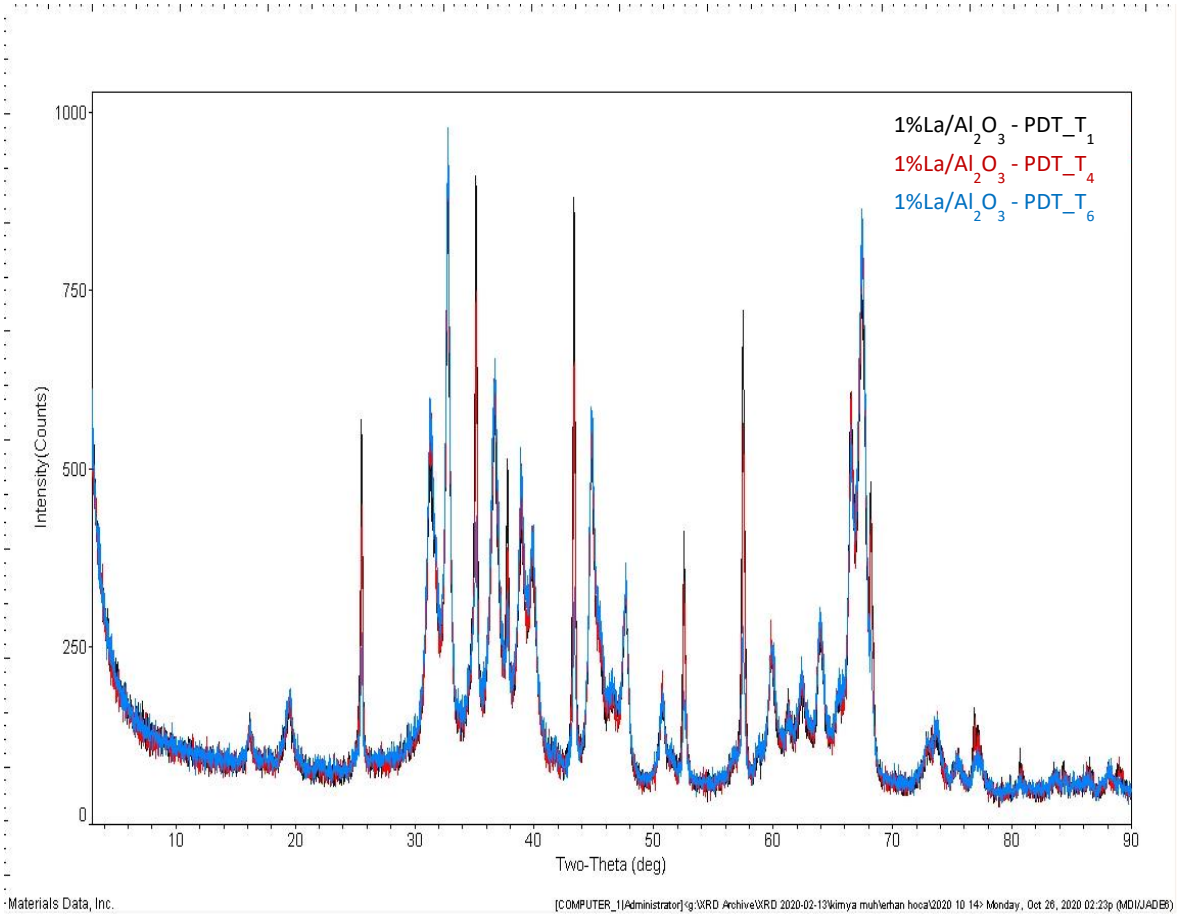

Figure 4.6 The Effect of Various Pre-Doping Temperature on 1%La/Al_2O_3 Samples Calcined at FCT_1150.

In Figure 4.7, the effect of pre-doping temperatures of PDT_T_1, PDT_T_4, and PDT_T_6 on 1%La/Al_2O_3 samples calcined at FCT_1150 is clearly shown. At 2θ=27.5º, 43.6º, and 57.8º the transition from γ- Al_2O_3 to α- Al_2O_3 is more significant for the sample treated with PDT_T_1, however the intensity is low for the sample treated with PDT_T_6. The crystal structure is more distinctive for lower pre-doping temperatures. High pre-doping temperatures coupled with doping may form a barrier for a transition from γ- Al_2O_3 to α-Al_2O_3, therefore can provide higher surface area, and consequently high temperature resistance, especially for high final calcination temperatures.

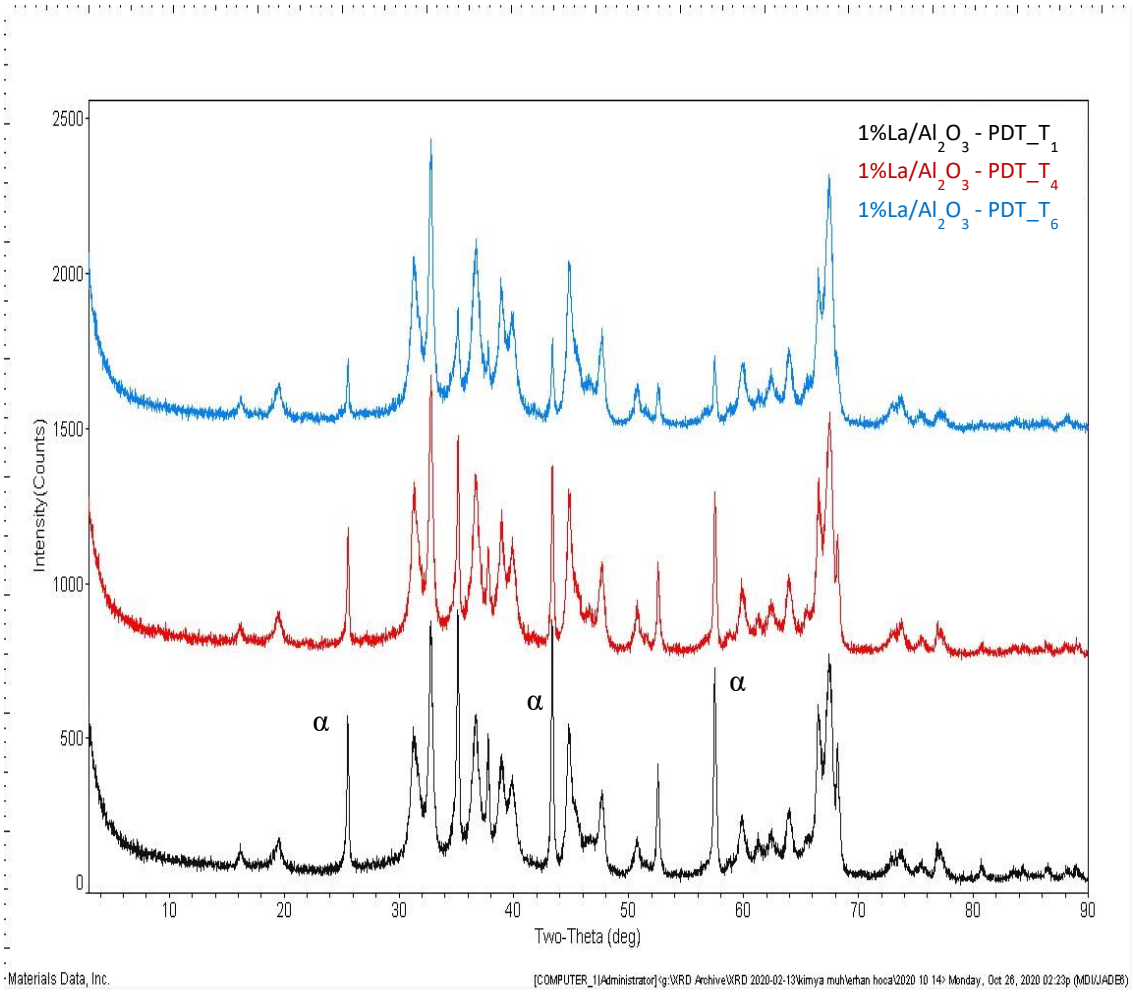

Figure 4.7 The Effect of Various Pre-Doping Temperature on 1%La/Al_2O_3 Samples.

In Figure 4.8, 1%La/Al_2O_3 samples treated with PDT_T_1, PDT_T_4, and PDT_T_6 and the reference γ- Al_2O_3 sample were comparatively analyzed upon calcination at FCT_1150. The XRD profile of reference γ- Al_2O_3 has many distinct characteristic Al_2O_3 peaks representing low surface area α phase. On the other hand, the amplitude of α peaks drastically decrease for 1%La/Al_2O_3 samples treated thermally prior to doping. The results indicate that for La impregnated samples, the increase in pre-doping temperature as well as La doping inhibit phase transition to low SA phases.

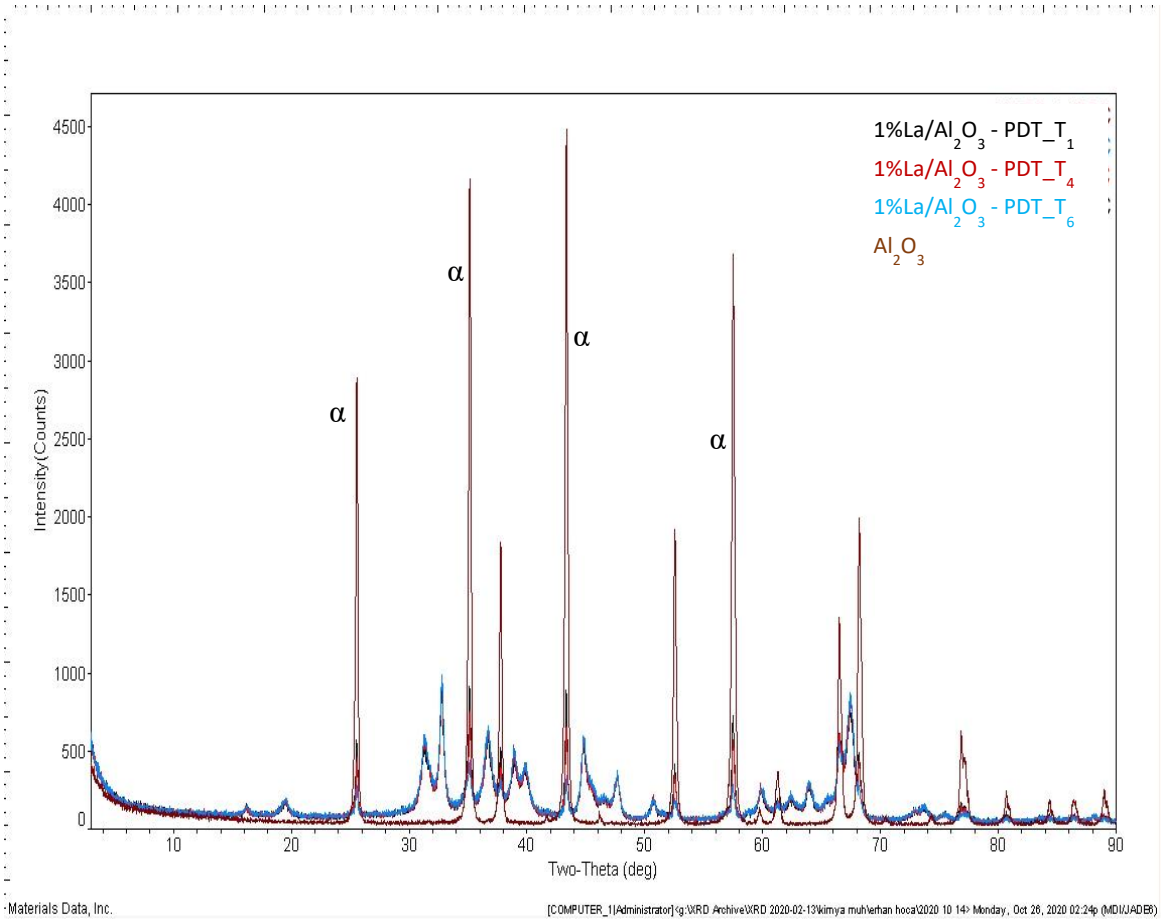

Figure 4.8 Temperature Treated (PDT) 1%La/Al_2O_3 Samples Calcined at FCT_1150 vs. Al_2O_3 Samples Calcined at FCT_1150.

In Figure 4.9 and 4.10, BJH pore size distribution and pore area distribution of 1%La/Al_2O_3 samples thermally treated at PDT_T_1, PDT_T_4, and PDT_T_6 before La doping and calcined at FCT_1150, and reference Al_2O_3 samples calcined at FCT_1150 are represented.

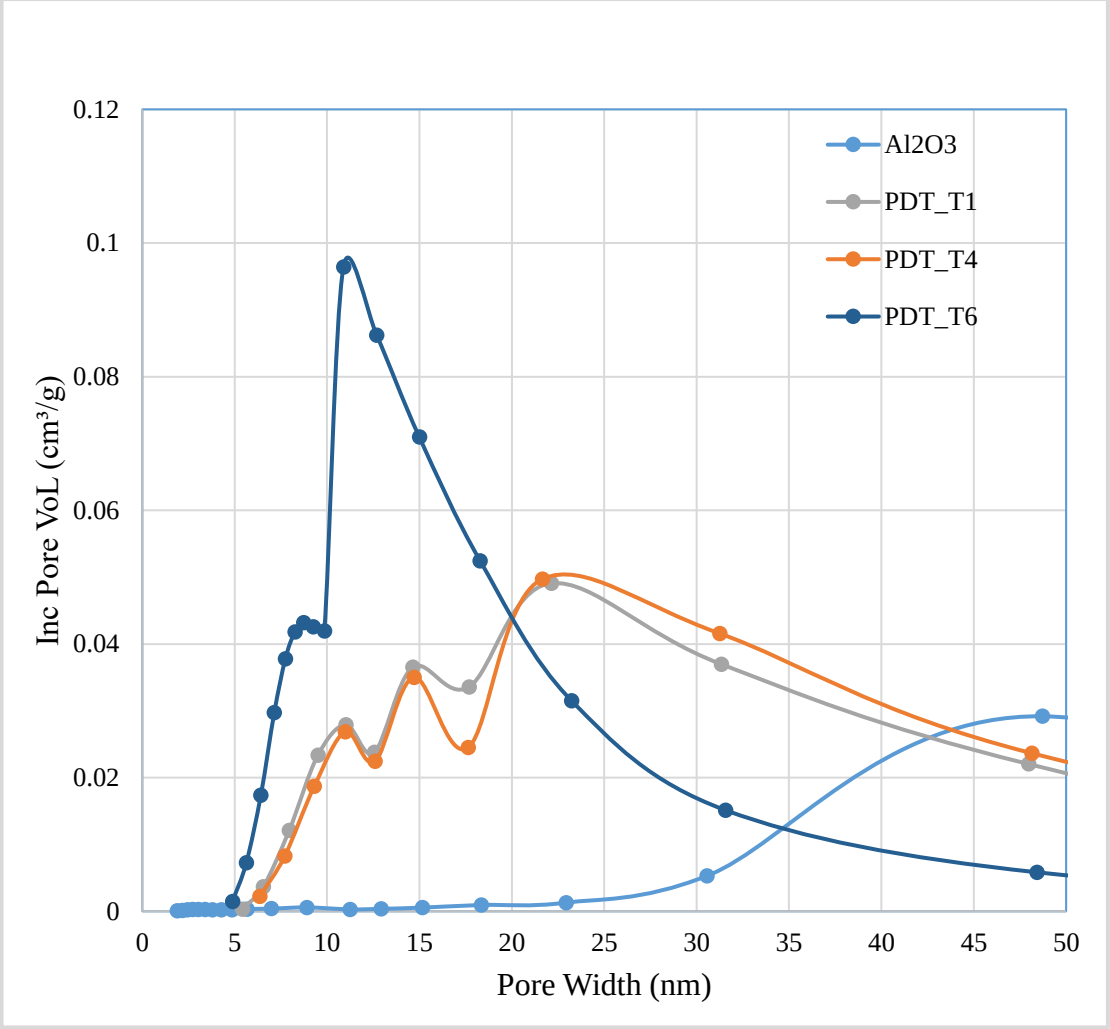

Figure 4.9 BJH Pore Size Distribution for 1%La/Al_2O_3 Samples at PDT_T_1, PDT_T_4, and PDT_T_6 and Al_2O_3 at FCT_1150.

The results presented in Figure 4.9 clearly show that reference Al_2O_3 sample calcined at FCT_1150 have lost almost all its pores having size less than 35 nm pore width. The pores with smaller diameters may have collapsed and have formed larger pores. In the case of

pores assumed as non-intersecting cylindrical capillaries, pores with smaller pore diameters provide higher total surface area (per volume) than macroscopic pores. On the other hand, the 1%La/Al_2O_3 samples with different pre-doping temperatures have 15-25 nm pore width. Between the 1%La/Al_2O_3 samples, the one pretreated with PDT_T4 has retained its porosity and most of its pores populated in 5-15 nm. region. However, the La-doped ones pretreated with PDT_T_1 and PDT_T_4 have similar BJH pore size distribution and pore area distribution, probably because they may have gone through similar phase transitions, as confirmed by Figures 4.7 and 4.8. Very low amplitude α peaks in XRD profile of PDT_T_6 treated sample is fully in accordance with its higher thermal stability in terms of physical properties.

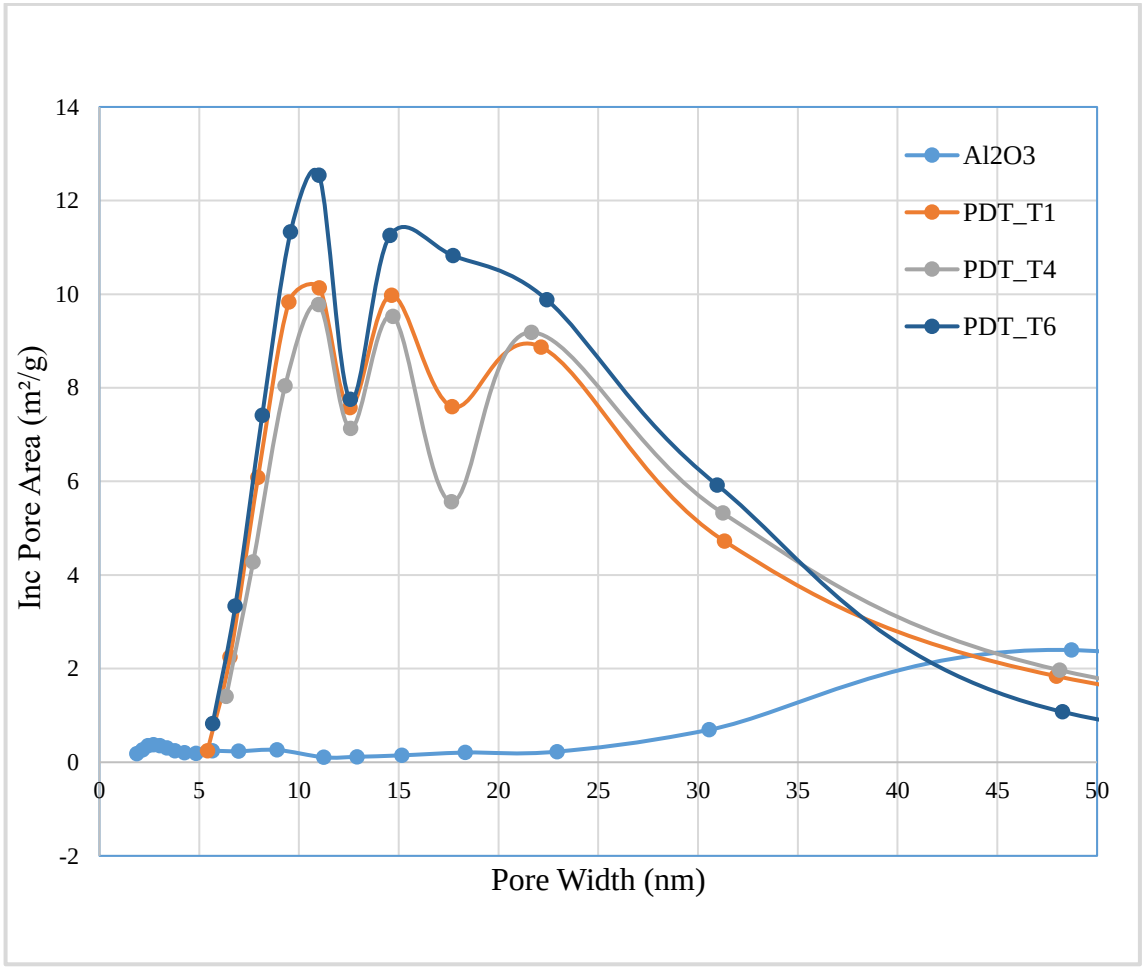

Figure 4.10 BJH Pore Area Distribution For 1%La/Al_2O_3 Samples at PDT_T_1, PDT_T_4, and PDT_T_6 and Al_2O_3 at FCT_1150.

4.4. Effect of Impregnation Strategy

In this section, the effects of parameters used in impregnation step of the procedure is investigated. There pH of precursor solution, effect of vacuum pressure during impregnation, and drying conditions after the impregnation were considered as impregnation parameters.

4.4.1. Effect of pH

The aqueous precursor solution consists of $La(NO_3)_3 * 6\ H_2O$ dissolved in deionized water. The pH of deionized water was measured as 6.19 at temperature of 26.6°C. When $La(NO_3)_3 * 6\ H_2O$ is dissolved in deionized water, the pH of the solution was pH_1 at 23.6°C. In order to test the effect of precursor solution pH, the precursor solution with an increased basicity, pH_2, by adding a certain amount of base were also used in doped samples. The impregnation procedure was applied with the modified precursor solution for 1% La doping on to the samples treated with pre-doping temperatures of PDT_T_2, PDT_T_3, PDT_T_5. The samples were calcined at FCT_900, FCT_1000, FCT_1100, and FCT_1150 for 2 hours prior to TSA, TPV and PSD tests. The BET surface area results of the samples are tabulated in Table 4.5.

Table 4.6. BET Surface Areas of 1%La/Al_2O_3 Samples with Respect to pH of pH_1 vs. pH_2 and Calcination Temperatures.

			BET Surface Area (m^2/g)				
			Calcination Temperature (°C)				
			0	**FCT_900**	**FCT_1000**	**FCT_1100**	**FCT_1150**
Pre-Doping Temperature (°C)	**pH_1**	**PDT_T_2**	201.33	157.91	134.95	86.19	56.64
		PDT_T_3	187.49	151.47	136.63	82.17	55.71
		PDT_T_5	177.87	134.17	122.23	87.24	61.74
		PDT_T_6	158.53	133.20	118.10	92.05	59.23
	pH_2	**PDT_T_2**	191.32	154.69	119.89	81.54	43.99
		PDT_T_3	192.35	127.01	119.28	80.85	30.13
		PDT_T_5	156.94	136.96	112.38	79.56	50.07
		PDT_T_6	170.92	147.35	116.16	84.14	54.60

In order to have a comparative analysis, BET surface areas of 1%La/Al_2O_3 samples prepared with precursor solutions having pH_2 versus pH_1 exposed to final calcination temperatures (FCTs) are shown in 3D bar graph in Figure 4.11.

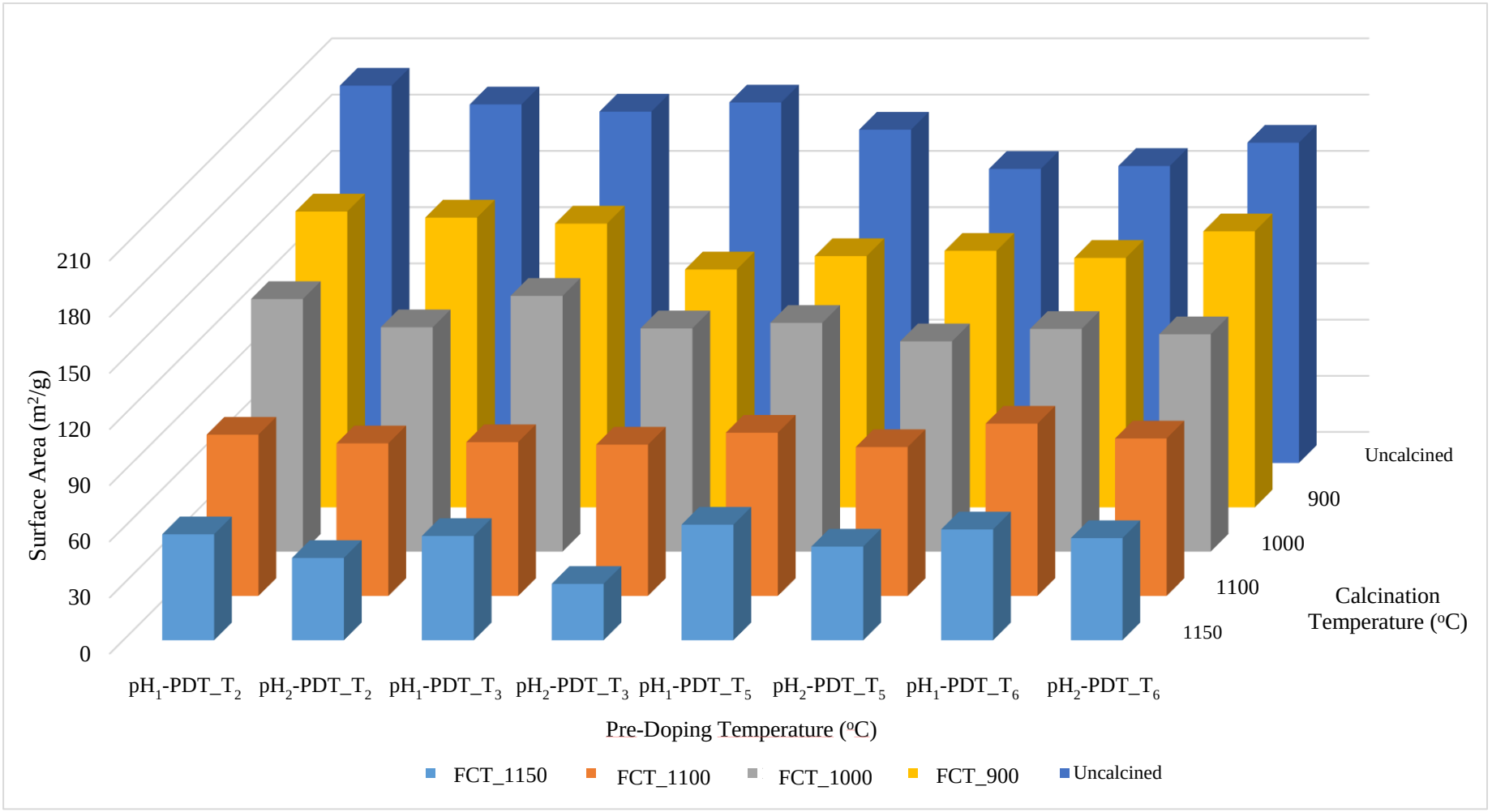

Figure 4.11 BET Surface Areas of 1%La/Al_2O_3 Samples with Respect to pH_1 vs. pH_2 and Calcination Temperatures; FCT_900, FCT_1000, FCT_1100, and FCT_1150.

The results indicate that the thermal stability of the doped samples is higher when they prepared with acidic precursor solution. It should be noted that the contribution of pH to stability is further investigated in section 4.5 by exposing the samples to additional heat treatment (cycles) prior to final calcination.

4.4.2. Effect of Vacuum Pressure

Vacuum pressure level used during impregnation is another experimental parameter tested. In standard procedure, the vacuum pressure in the suction flask is set to Vac_{1} bar. It should be noted that except from the samples in section 4.4.2, all the samples are exposed to Vac_{1} bar vacuum pressure in the suction flask. To investigate the effect of increase in the vacuum pressure on surface area, 2%Pt/Al_2O_3 samples with pre-doping temperature treatment of PDT_T_5 were prepared under vacuum pressure of Vac_{1}, Vac_{2} bar, and Vac_{3} bar, in descending order. The results are tabulated in Table 4.7.

Table 4.7. BET Surface Areas of 2%Pt/Al_2O_3 Samples with Respect to Vacuum Pressures.

	Vacuum Pressure (bar)		
	Vac_{1}	**Vac_{2}**	**Vac_{3}**
BET Surface Area (m^2/g)	116.02	123.27	121.27

The aim of the use of vacuum during impregnation is to empty the pores of the support for making them available for the penetration of precursor solution. However, as can be seen from the initial results in Table 4.7, there is no trendy effect observed for applied vacuum level on the surface area of the samples. Therefore, while investigating the effect of drying (see Section 4.4.3), all samples were prepared for vacuum pressure of all Vac_{1}, Vac_{2}, and Vac_{3} bar for cross-comparison.

4.4.3. Effect of Drying Conditions

In the standard procedure of thermally resistant support preparation, impregnation is followed by immediate drying at 110°C in the oven overnight. In this section, effect of drying on physical properties of the supports impregnated under different vacuum pressure levels is investigated.

Each of 2%Pt doped Al_2O_3 samples, which were exposed to pre-doping temperature treatment of PDT_T_5 and impregnated under the vacuum pressures of Vac_$_1$, Vac_$_2$, and Vac_$_3$ bar, were divided into two; one group were dried immediately after impregnation at 40°C (slow drying) and the other at 110°C (standard drying) in the oven overnight. Moreover, the samples prepared under the same conditions were filtered and dried at room temperature and pressure (SATP - 25℃ &1 bar) for 12 hours, then divided into two and dried at 40°C and at 110°C in the oven overnight. Then, in order to observe their thermal resistance, all the samples were calcined at FCT_1000 for 2 hours. The results of BET surface area measurements are presented in Table 4.8.

Table 4.8. BET Surface Areas of 2%Pt/Al_2O_3 Samples with Respect to Vacuum Pressures and Drying Conditions.

		BET Surface Area (m^2/g)		
		Vacuum Pressure (bar)		
		Vac_$_1$	**Vac_$_2$**	**Vac_$_3$**
Temperature °C	**40**	118.145	130.2135	114.1122
	110	116.0233	123.2708	121.2675
	25+40	116.6153	119.7588	121.8919
	25+110	127.9279	128.7101	115.4575

Even though for the samples prepared under Vac_{-1} and Vac_{-2}, the ones dried immediately after impregnation at 40 °C have higher surface areas than those dried at 110°C, the trend is just the opposite for the samples prepared under Vac_{-3}, which is the highest vacuum applied. For the samples prepared under Vac_{-1} and Vac_{-2}, SATP+100 ^{o}C drying yielded higher TSA, but when the vacuum level increased to Vac_{-3}, increase in final drying temperature to 110 ^{o}C led to a decrease in TSA. Consequently, no solid conclusion could be drawn from the data presented in Table 4.9.

Apart from drying temperature, different drying techniques were also investigated for unprocessed alumina samples in this section to understand the aging effects and/or structural change towards a Gibbsite through the interaction of alumina with water. It should be noted that Gibbsite, which is aluminum tri-hydroxide, can form on the surface when alumina is treated with water even at room temperature. In this part of the study, 2 grams γ-Al_2O_3 having 1-2 mm particle size were treated with 100ml deionized water for 12 hours, then exposed to extreme drying methods, as listed below, and characterized by BET surface area, Raman spectroscopy, and X-Ray diffraction. The drying methods applied on samples are listed below:

S0: γ-Al_2O_3 with 1-2 mm particle size.

S1: 2 grams of γ-Al_2O_3 / 100ml deionized water kept at ultrasonic mixing at Vac_{-1} bar vacuum pressure for 12 hours, filtered, and dried at 40°C for 21 hours in the oven.

S2: 2 grams of γ-Al_2O_3 / 100ml deionized water kept at SAPT for 12 hours, filtered, directly poured into liquid N_2 (melting point of -195.79), and dried at 40°C for 21 hours in the oven.

S3: 2 grams of γ-Al_2O_3 / 100ml deionized water kept at SAPT for 12 hours, filtered, placed into liquid N_2 with a flask, and dried at 40°C for 21 hours in the oven.

S4: 2 grams of γ-Al_2O_3 / 100ml deionized water kept at SAPT for 12 hours, filtered, kept at the freezing section of the refrigerator for 20 hours, and dried at 40°C for 21 hours in the oven.

S5: 2 grams of γ-Al_2O_3 / 100ml deionized water kept at SAPT for 12 hours, filtered, and dried at 40°C for 21 hours in the oven.

S6: 2 grams of γ-Al_2O_3 / 100ml deionized water kept at SAPT for 12 hours, filtered, kept at SAPT for 92 hours, and dried at 40°C for 21 hours in the oven.

During 12 hours of ultrasonic mixing of S1, temperature of water in the tank varied by time. The variation by time is a matter of parameter change and might be stabilized for further studies. As a reference, the change in temperature is presented in Table 4.9.

Table 4.9. Temperature Increase in The Ultrasound Mixing Tank by Time.

Time (h)	**Water Temperature in the Tank (ºC)**	**Ambient Temperature (ºC)**
t=0	29	20
t=1	34.5	22
t=2	41	25
t=3	42	27
t=4	46	27
t=5	47	27
t=6	48	25.5
t=7	47.5	25.5
t=8	47	26.5
t=9	48	26.5
t=10	48	26.5
t=11	47	26.5
t=12	47	26.5

The BET surface area results of samples S0, S1, S2, S3, S4, S5, and S6 are tabulated in Table 4.10.

Table 4.10. BET Surface Areas of Alumina Samples with Respect to Drying Methods.

Samples	**BET Surface Area (m^2/g)**
S0	216.63
S1	230.00
S2	232.71
S3	226.93
S4	212.86
S5	224.31
S6	220.51

BET surface area of S0, untreated γ-Al_2O_3, is 216.63 m^2/g, Since S5 is 224.31 m^2/g, water treatment and slow single-step drying may be effective in increasing surface area. Among all samples, S1 and S2 have the highest BET surface areas. S1 includes ultrasonic mixing, and ultrasonic mixing can lead to considerable changes in surface morphology. S2 includes direct liquid N_2 contact; there the water in the pores of alumina may be frozen too fast and caused more cracks due to the expansion of water when it freezes. S3 was placed into liquid N_2 with a flask and has slightly lower surface area, while S4 kept at the freezing section of the refrigerator for 20 hours; the results indicate that slow freezing has no effect on increasing surface area of alumina. Both methods in S1 and S2 can be identified as possibly promising as the yielded increase is 8.4%.

To further investigate the phase identification, the samples are analyzed via X-Ray diffraction (XRD). XRD patterns were recorded by continuous scan mode at 2^o min^{-1} and with an X-ray generator with Cu K_α target. XRD pattern is presented in Figure 4.12.

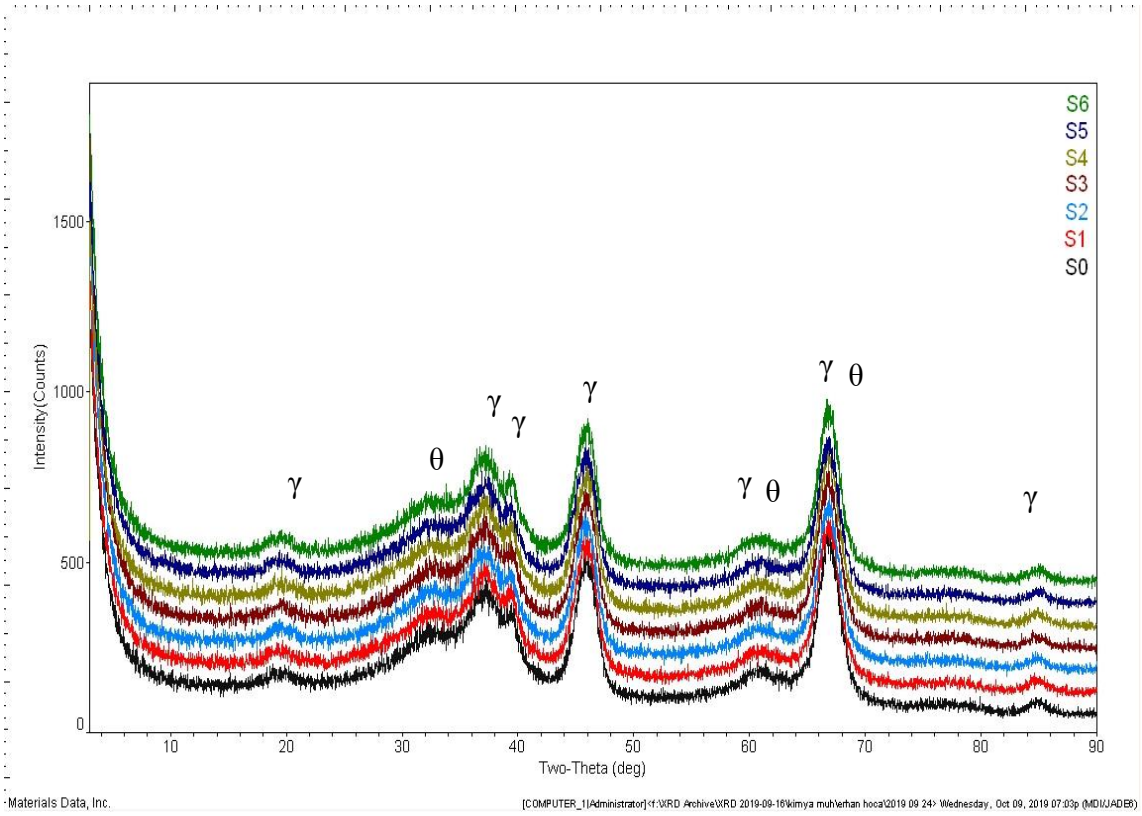

Figure 4.12 XRD Pattern of the Water-Alumina Treatment Samples.

The XRD profiles of all samples follow the same pattern, and only γ and θ phases are observed in the structure. Broad peaks may indicate more defects in the crystal structure, therefore high surface area.

The starting material was a Boehmite. In order to investigate any Gibbsite formation from Boehmite, the samples with the highest surface area, S1 and S2, and the untreated γ-Al_2O_3 with 1-2 mm particle size, S0, were analyzed by Raman spectroscopy. The results of the Raman analyses on S0, S1, and S2 are presented in Figure 4.13, Figure 4.14, and Figure 4.15, respectively.

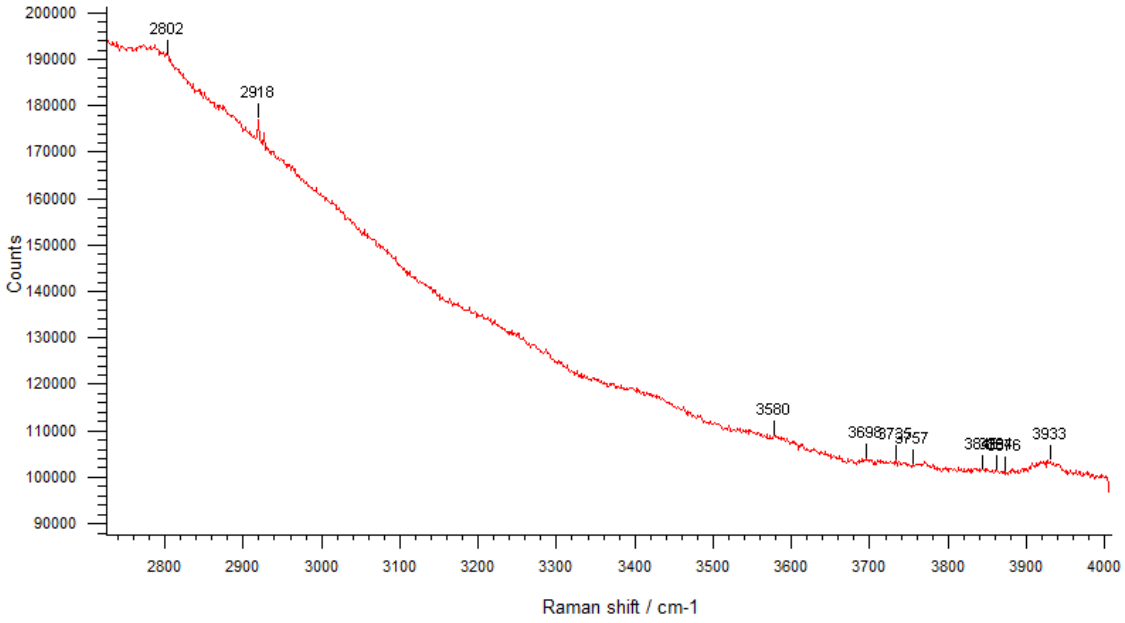

Figure 4.13 Raman Spectra of Water-Alumina Treatment Sample, S0.

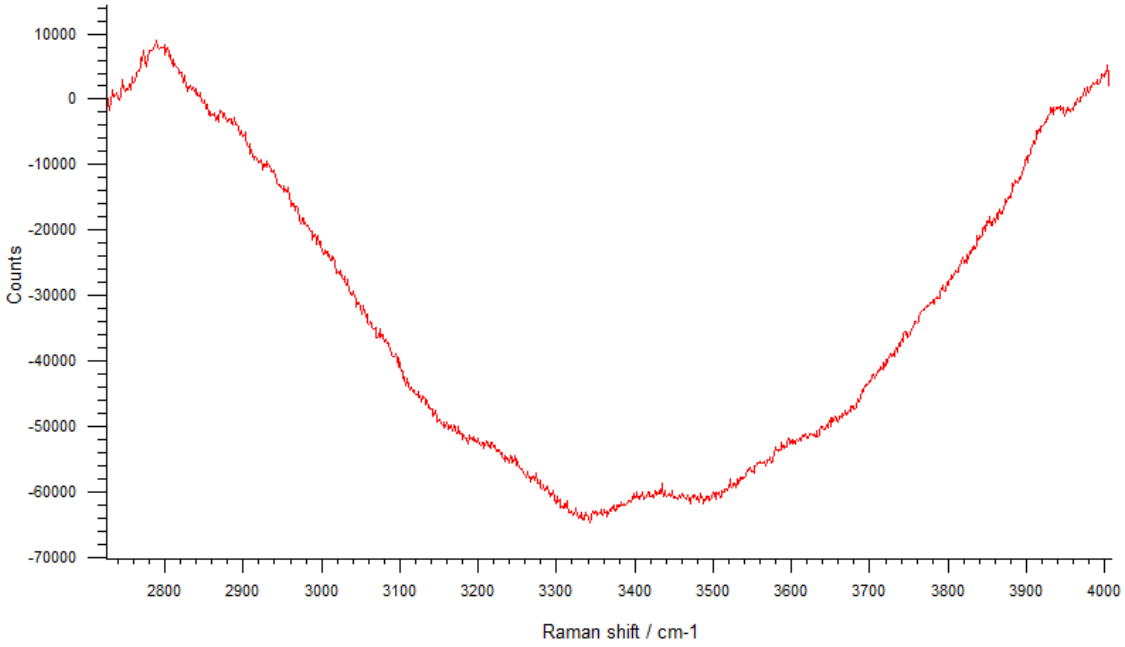

Figure 4.14 Raman Spectra of Water-Alumina Treatment Sample, S1.

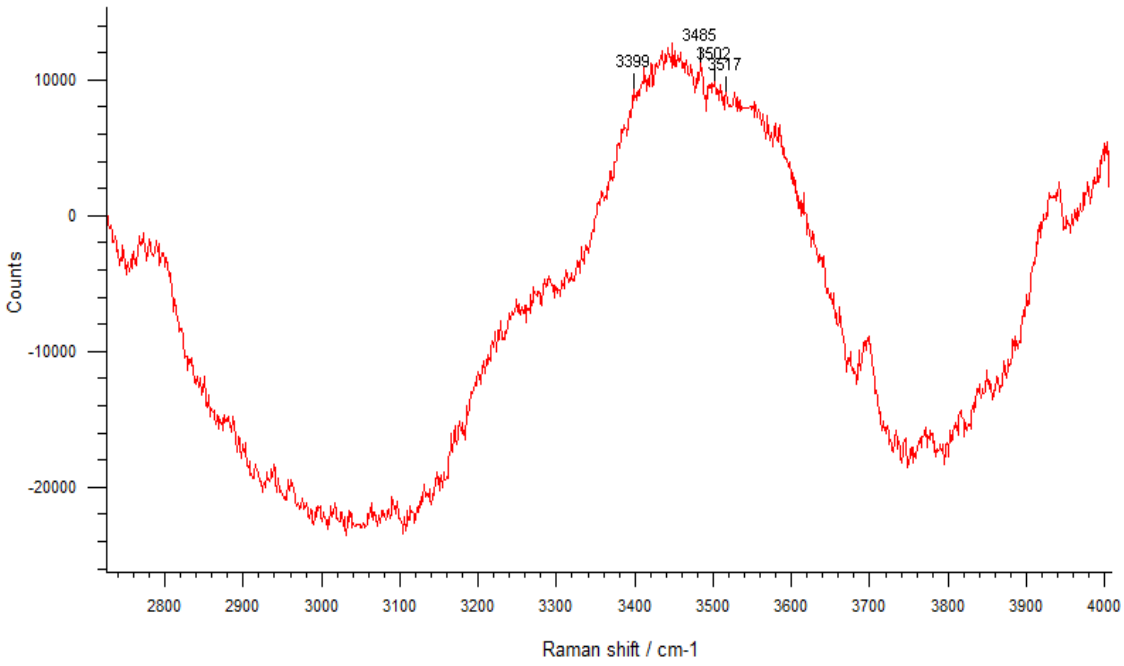

Figure 4.15 Raman Spectra of Water-Alumina Treatment Sample, S2.

The peaks are distinguishable at 3399 cm^{-1}, 3484 cm^{-1}, and around 3540 cm^{-1} and are compatible with Bayerite formation (Zhang *et al.*, 2015).

Incremental pore size distribution of the samples is also investigated via Barrett-Joyner-Halenda (BJH) pore size distribution method. BJH pore size distribution method is applicable only to the mesopore and small macropore size range. Pore volume of the samples corresponding to their pore width is observable in Figure 4.16.

As can be seen in Figure 4.16, the most common pore width is 5-20 nm range for all samples having a peak at ca. 12 nm, and the structure is mesoporous. The sample S1 has the broadest peak and the lowest incremental pore volume, while S4, has the narrowest peak size range, implying the lowest pore width variation, and the highest incremental pore volume at ca. 12 nm.

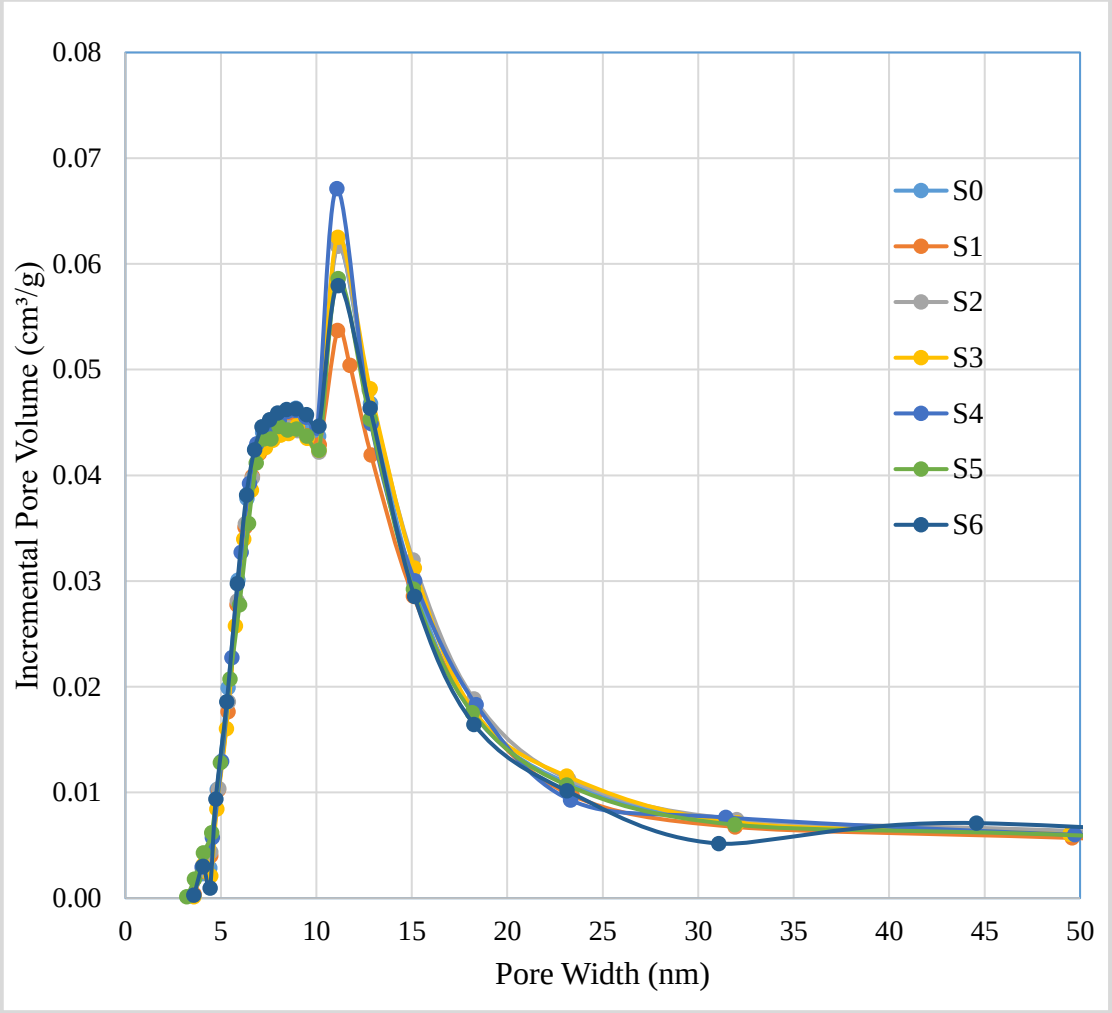

Figure 4.16 Incremental Pore Size Distribution of the Water – Alumina Treatment Samples.

4.5.Effect of Post Heat Treatments upon Doping

In this section, the cumulative effect of post-heat treatment applied upon doping on thermal stability of the alumina samples is analyzed. In the standard procedure, the samples were dried immediately at 110°C in the oven overnight after the impregnation step, and calcined at FCT_900, FCT_1000, FCT_1100, and FCT_1150 for 2 hours. Then, the samples were analyzed for their BET surface areas to observe the effects of high temperatures applied during final calcination on support materials. As exposure to sudden high temperature may cause drastic changes on physical structure of the support, such as breaking down/closing of

the pores, the effect of post heat treatment (PHT) before final calcination, which may limit the possible changes during FCT, was investigated.

The post heat treatment to La impregnated samples was applied in 0-3 stages (PHT_1-3) for temperature range of 500-1200 ^{o}C before final calcination. As can be seen from Table 4.11, single stage PHT was applied to samples prior to application of FCT_1000, 1100 and 1150, while two-stage PHT was applied prior to FCT_1100 and 1150, and three-stage was applied only prior to FCT_1150.

Table 4.11. Post Heat Treatment Upon Doping Temperatures Corresponding to Stages.

		Sample Calcination Temperature (°C)			
		FCT_900	**FCT_1000**	**FCT_1100**	**FCT_1150**
Post Heat Treatment Stages	**PHT_0**	-	-	-	-
	PHT_1	-	√	√	√
	PHT_2	-	-	√	√
	PHT_3	-	-	-	√

In order to observe the effects of no- and single-stage post-heat treatment applied on the samples treated at FCT_1000 for 2 hours, their BET surface areas were measured and comparatively analyzed in Table 4.12.

Table 4.12. Post Heat Treatment Applied Upon Doping for Stages PHT_0 and PHT_1 for The Samples with Calcination Temperature of FCT_1000.

		BET Surface Area (m^2/g)	
		Post-Heat Treatment Stages	
		PHT_0	**PHT_1**
Pre-Doping Temperature (°C)	**PDT_T_2**	134.95	124.69
	PDT_T_3	136.63	125.05
	PDT_T_6	118.99	117.73

The samples with calcination temperature of FCT_1000 was exposed to post-heat treatment for 2 hours and the BET surface areas are represented in Figure 4.17 to observe the effects of post-heat treatment applied upon doping for PHT_0 and PHT_1.

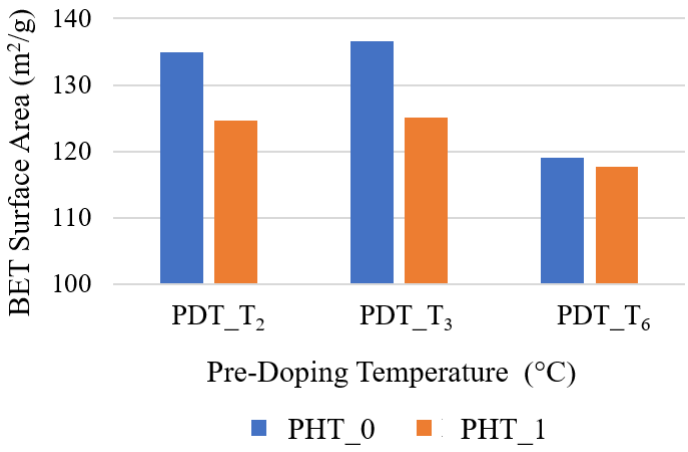

Figure 4.17 BET Surface Areas of Post-Heat Treatment Samples of Stages PHT_0 and PHT_1 for The Samples with Calcination Temperature of FCT_1000.

The BET surface areas of the samples, which had been exposed to non- and single stage post-heat treatment applied upon doping and calcined at FCT_1100 are represented in Figure 4.18 and Table 4.13 to observe the effects of post-heat treatment applied upon doping for stages PHT_0 and PHT_1.

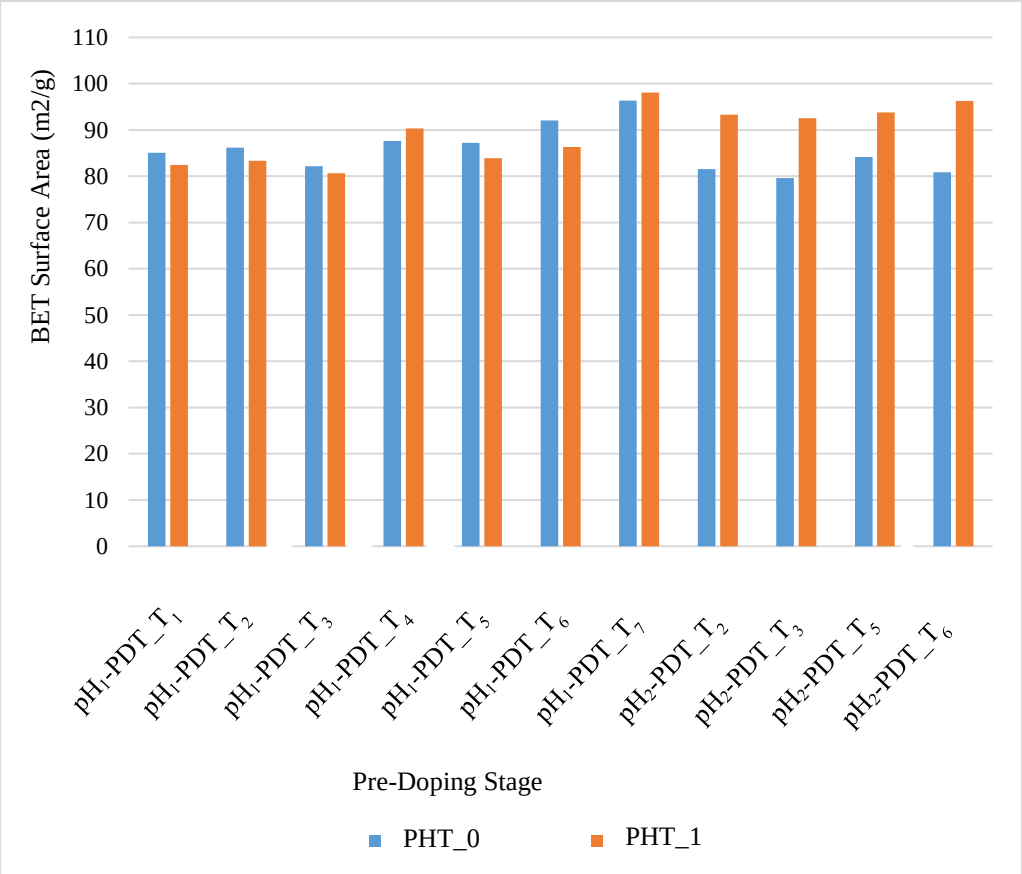

Figure 4.18 Post Heat Treatment for Stages PHT_0 and PHT_1 for The Samples with Calcination Temperature of FCT_1100.

Table 4.13. Post Heat Treatment Upon Doping for Stages PHT_0 and PHT_1 for The Samples with Calcination Temperature of FCT_1100.

			BET Surface Area (m^2/g)	
			PHT Stages	
			PHT_0	**PHT_1**
Pre-Doping Temperature (°C)	**pH_1**	**PDT_T_1**	85.05	82.44
	pH_1	**PDT_T_2**	86.19	83.32
	pH_1	**PDT_T_3**	82.17	80.61
	pH_1	**PDT_T_4**	87.65	90.31
	pH_1	**PDT_T_5**	87.24	83.87
	pH_1	**PDT_T_6**	92.05	86.32
	pH_1	**PDT_T_7**	96.35	98.09
	pH_2	**PDT_T_2**	81.54	93.27
	pH_2	**PDT_T_3**	79.56	92.55
	pH_2	**PDT_T_5**	84.14	93.80
	pH_2	**PDT_T_6**	80.85	96.26

The BET surface areas of the samples, which had been exposed to non-, single and two-stage post-heat treatment applied upon doping and calcined at FCT_1150 are represented in Figure 4.19 and Table 4.14 to observe the effects of post-heat treatment applied upon doping for stages PHT_0**,** PHT_1 and PHT_2.

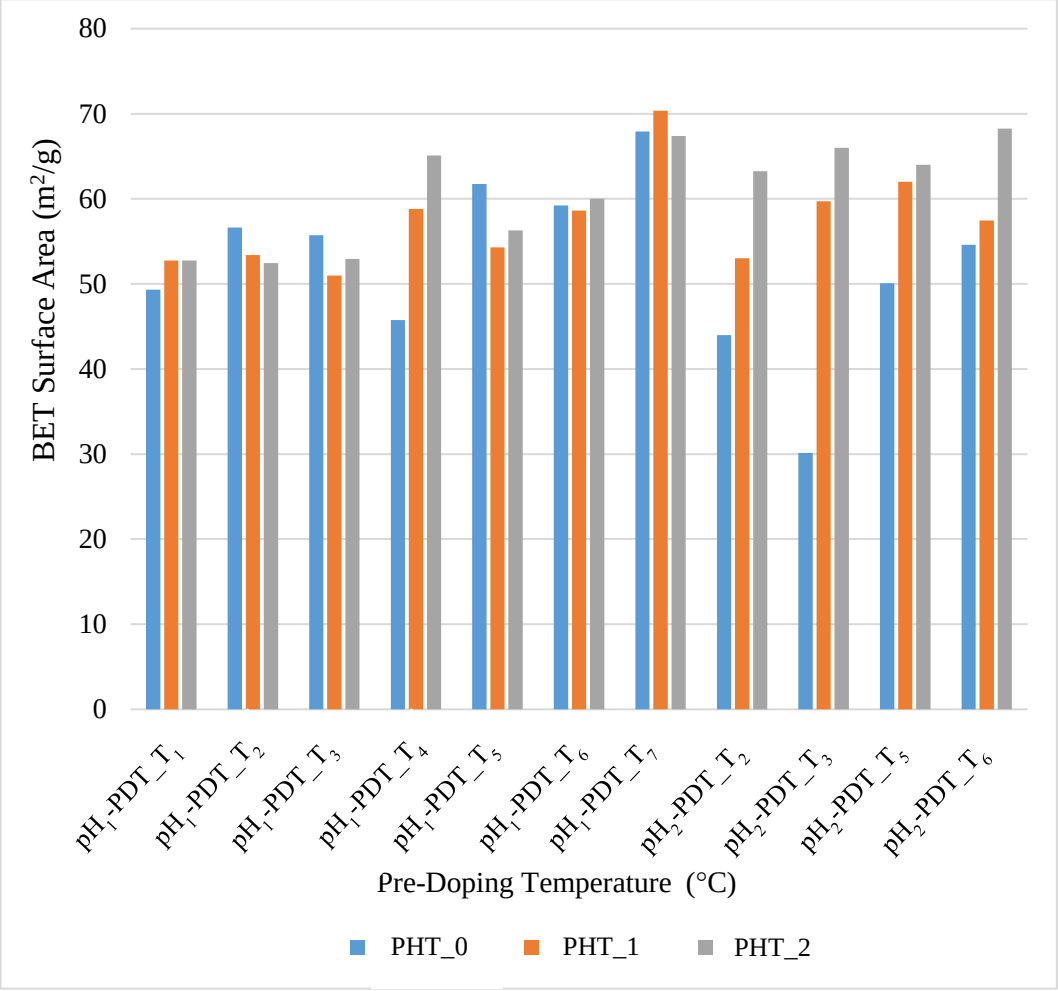

Figure 4.19 Post Heat Treatment Upon Doping for Stages PHT_0**,** PHT_1, and PHT_2 for The Samples with Final Calcination Temperature of FCT_1150.

Though the results show that the surface areas of the samples prepared with pH_1 are close to each other, the BET surface area of the samples prepared with pH_2 show an increasing trend.

Table 4.14. Post Heat Treatment Upon Doping for Stages PHT_0**,** PHT_1, and PHT_2 for The Samples with Final Calcination Temperature of FCT_1150.

			BET Surface Area (m^2/g)		
			Post Heat Treatment Stages		
			PHT_0	**PHT_1**	**PHT_2**
Pre-Doping Temperature (°C)	**pH_1**	**PDT_T_1**	49.32	52.74	52.74
	pH_1	**PDT_T_2**	56.64	53.39	52.44
	pH_1	**PDT_T_3**	55.71	50.97	52.93
	pH_1	**PDT_T_4**	45.75	58.80	65.10
	pH_1	**PDT_T_5**	61.74	54.31	56.30
	pH_1	**PDT_T_6**	59.23	58.61	60.01
	pH_1	**PDT_T_7**	67.90	70.36	67.39
	pH_2	**PDT_T_2**	43.99	53.01	63.24
	pH_2	**PDT_T_3**	30.13	59.72	65.98
	pH_2	**PDT_T_5**	50.07	62.02	64.01
	pH_2	**PDT_T_6**	54.59	57.45	68.27

The BET surface areas of the samples, which had been exposed to non-, single-, two- and three-stage post-heat treatment applied upon doping and calcined at FCT_1150 are represented in Figure 4.20 and Table 4.15 to observe the effects of post-heat treatment applied upon doping for stages PHT_0**,** PHT_1, PHT_2 and PHT_3.

Since the increment in BET surface area with the increasing stage number is demonstrated for the samples prepared with precursor solution with pH_2, 3-stage (PHT_3) study was performed only for the samples prepared with standard procedure having precursor solution acidity as pH_1. There the samples treated with pre-doping temperatures of PDT_T_2, PDT_T_3, and PDT_T_6 were analyzed.

Table 4.15. Post Heat Treatment for Stages PHT_0, PHT_1, PHT_2, and PHT_3 for The Samples with Final Calcination Temperature of FCT_1150.

		BET Surface Area (m^2/g)			
		Post-Heat treatment Stages			
		PHT_0	**PHT_1**	**PHT_2**	**PHT_3**
Pre-Doping Temperature (°C)	**PDT_T_2**	56.64	53.39	52.44	65.03
	PDT_T_3	55.71	50.97	47.13	52.93
	PDT_T_6	59.23	58.61	60.01	59.29

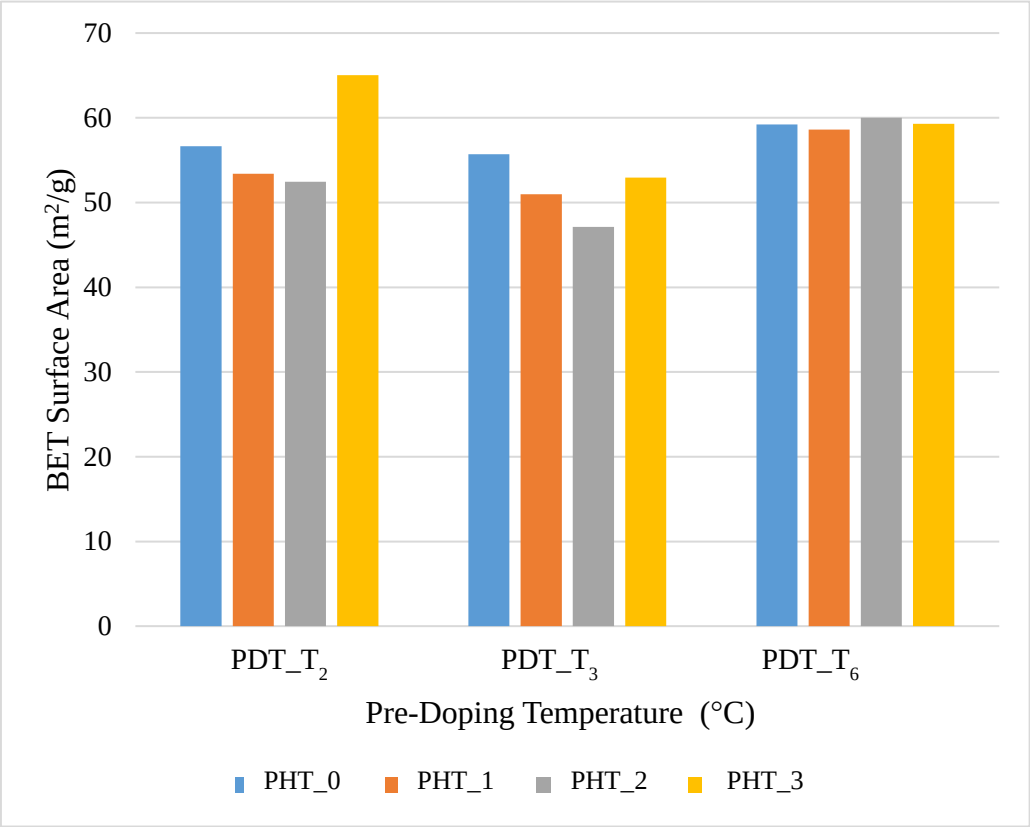

Figure 4.20 Post Heat Treatment for Stages PHT_0, PHT_1, PHT_2, and PHT_3 for The Samples with Final Calcination Temperature of FCT_1150.

For the samples prepared by standard procedure with precursor solution of pH_1, the effect of post heat treatment upon impregnation is ambiguous. For the samples with pre-doping temperatures of PDT_T_3, PDT_T_4, and PDT_T_6, the BET surface area increased with the post heat treatment upon doping however, for the samples with pre-doping temperatures of PDT_T_2 and PDT_T_5, the BET surface area decreased with the post heat treatment upon doping. For the rest of samples prepared by standard procedure with precursor solution of pH_1, the BET results are varying; thus, the results indicated that for the samples prepared with precursor solution acidity of pH_1, the post heat treatment upon doping has no significant effect on their thermal stability.

For the samples prepared with precursor solution having acidity of pH_2, the effect of post heat treatment upon doping is significant. The BET of the samples treated with pre-doping temperatures PDT_T_2, PDT_T_3, PDT_T_5 and PDT_T_6 showed increment along with

the increase in number of post heat treatment stages upon doping. In section 4.4.1, the stabilizing effect of pH on alumina is mentioned. The combination of pH and post heat treatment upon doping significantly have a stabilizing effect on the structure of alumina for high final calcination temperatures.

4.6. Thermal Resistance of the Supports Prepared

In this section, thermal resistance of the supports prepared in sections 4.1-4.5 were studied on the basis of their physical and crystal structure stability upon final calcination. The limited loss in TSA and TPV, and limited change(s) in PSD profile and crystal structure, analyzed by XRD, upon application of final calcination at temperatures 900, 1000, 1100 and 1150 ^{o}C were used as the stability measures. Through comparative analysis, the set of parameters used for yielding the highest thermal stability were determined. In the tests, calcination was conducted for 2 hr. duration which guarantees surface stabilization. In order to analyze the effect of shorter calcination, for 1 hour, the sample 1%La/Al_2O_3 prepared through PHT_0 with pre-doping temperature of PDT_T_2 and pH_1-precursor solution, was divided into two, and separately calcinated at FCT_1100 for 2 hours and for 1 hour, in a muffle furnace. The BET surface area results are presented in Table 4.16.

Table 4.16. Effect of Calcination Duration for PHT_0 1%La/Al_2O_3 with Final Calcination Temperature of 1100 ^{o}C.

Calcination Duration (h)	**BET Surface Area (m^2/g)**
2	83.32
1	97.89

The results clearly revealed that 2h as the calcination duration yields more reliable data to be used for understanding thermal stability.

In order to compare the combined effect of impregnation pH and post-heat treatment upon doping, 1%La/Al_2O_3 with pre-doping temperature of PDT_T_6 was prepared with both pH_1-precursor solution and pH_2-precursor solution were calcined and tested by their properties to observe the effect of pH. In this context, the sample prepared with pH_1 was calcined at FCT_900 and FCT_1150, and that prepared with pH_2 and 2-stage PHT were calcined at FCT_1150 ^oC, and and all were characterized by X-Ray Diffraction; the patterns are represented in Figure 4.21 and in Figure 4.22.

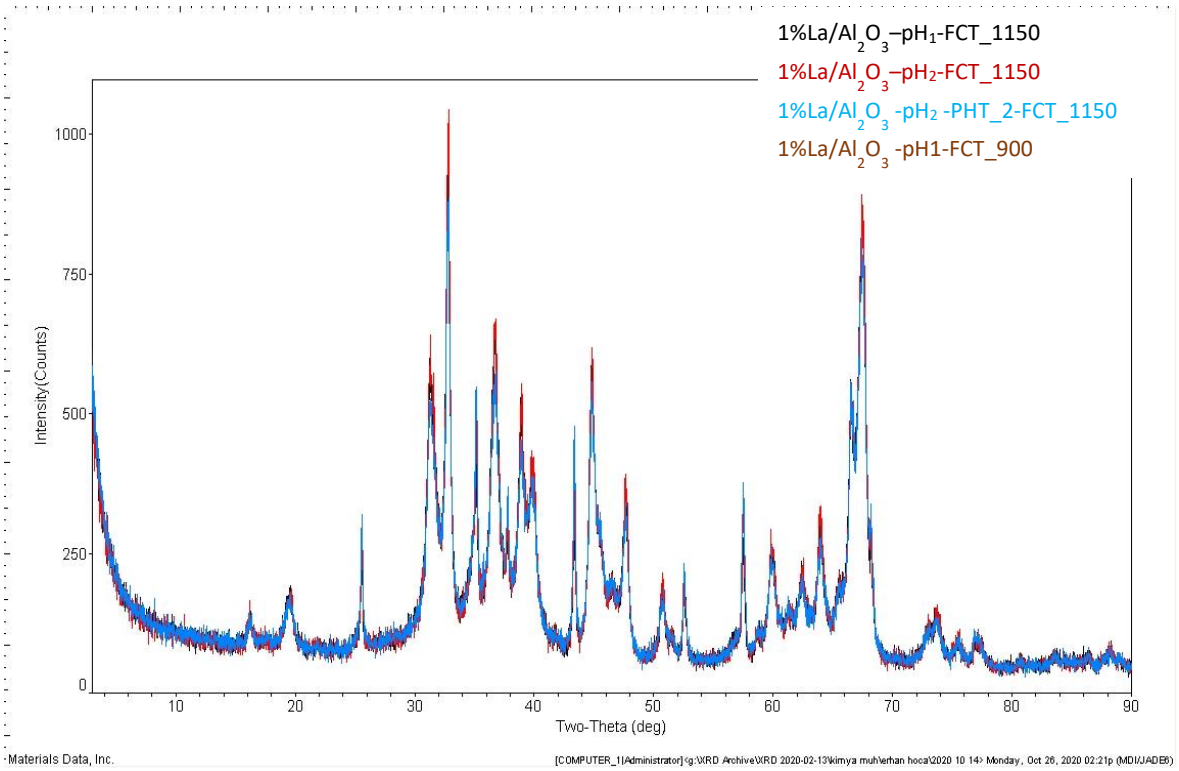

Figure 4.21 X-Ray Diffraction Results for 1%La/Al_2O_3 with Various Temperature and pH Treatments.

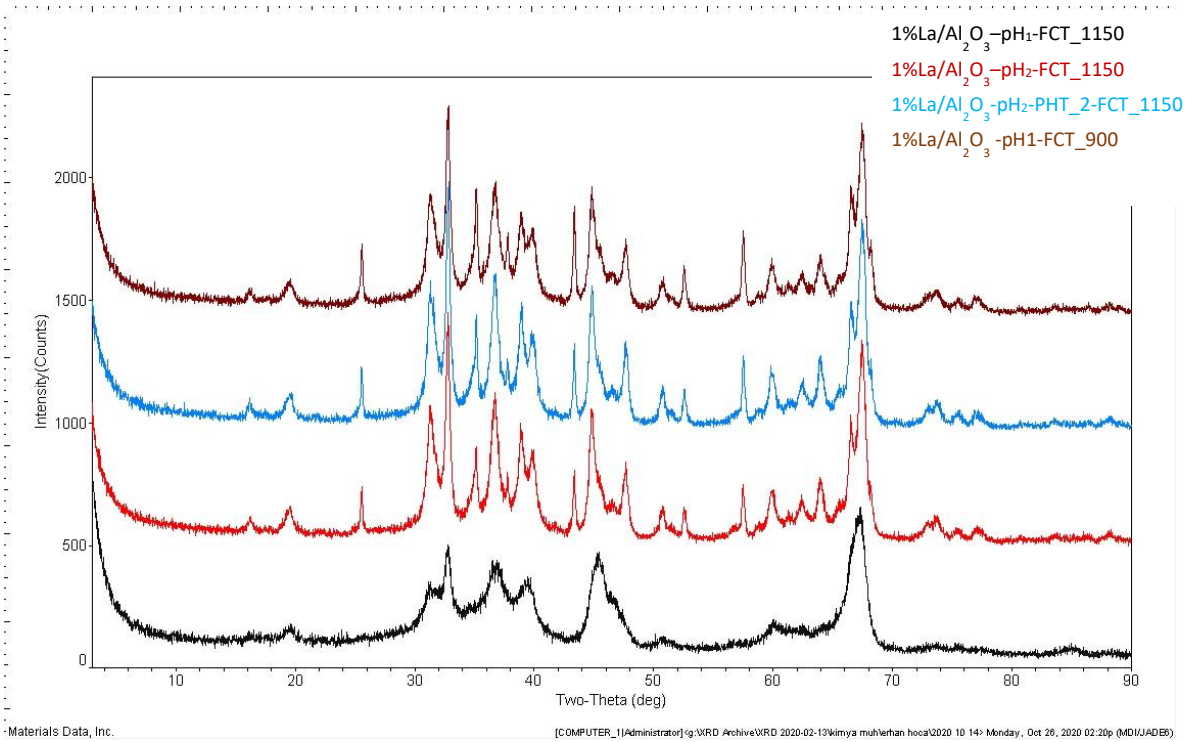

Figure 4.22 X-Ray Diffraction Results for 1%La/Al_2O_3 with Various Temperature and pH Treatments.

In Figure 4.22, all the XRD results have similar peaks, except for 1%La/Al_2O_3 exposed to final calcination at 900 ^oC, i.e., the lowest calcination temperature. Therefore, pH manipulation or post heat treatment upon doping do not have any remarkable effect on the phase change in terms of XRD results.

In Figure 4.23 and 4.24, 1%La/Al_2O_3 samples prepared with different pH and post-heat treatment (PHT) cycles were characterized by their BJH pore size distribution and pore area distribution upon calcination at FCT_900 and FCT_1150. Although the effect of pH and the effect of post-heat treatment upon doping are ambiguous, the effect of final calcination temperature on physical structure is clearly distinguishable.

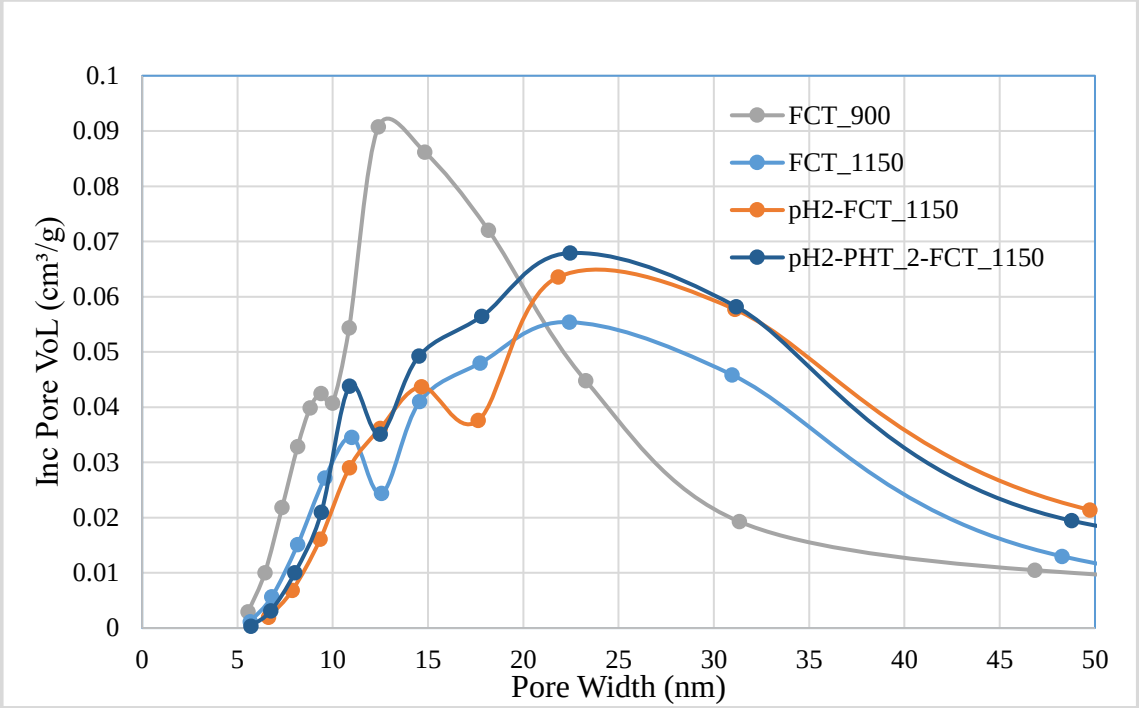

Figure 4.23 BJH Pore Size Distribution for 1%La/Al_2O_3 Samples for Different pH and Post-Heat Treatment (PHT) Cycles.

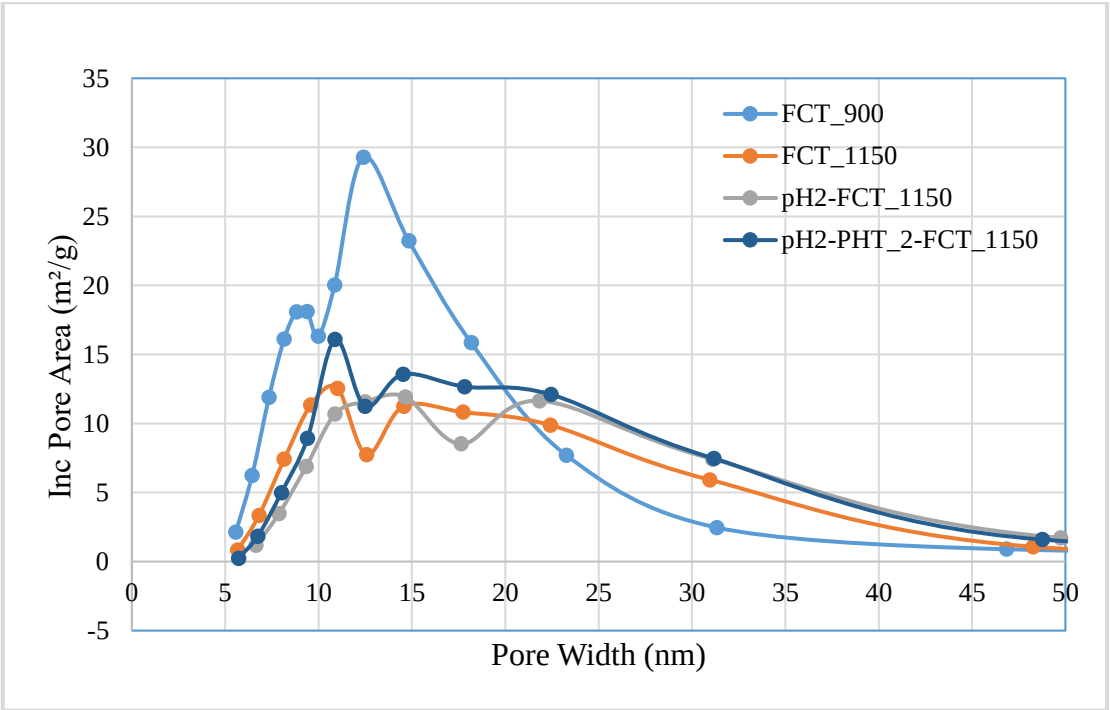

Figure 4.24 BJH Pore Area Distribution for 1%La/Al_2O_3 Samples for Different pH and Post-Heat Treatment (PHT) Cycles.

4.7. Design Parameters of a Temperature Resistant Support

In this section, the BET surface area results for most of the samples prepared throughout this thesis were analyzed for all parameters by 3-D figures obtained via Excel and MATLAB. The parameters are:

- Doping Metal Type

  Lanthanum, Barium

- Pre-Doping Temperature

  PDT_T_1, PDT_T_2, PDT_T_3, PDT_T_4, PDT_T_5, PDT_T_6 and PDT_T_7

- Impregnation Strategy

  pH_1, pH_2

- Post Heat Treatment Upon Doping Stages

  PHT_0, PHT_1, PHT_2, and PHT_3

In Figure 4.25, BET surface areas of pH_2 samples with respect to stage number (PHT), and PDT (°C) is analyzed. BET surface areas of the samples increase with increasing pre-calcination stage number, even though their final calcination temperatures are high, such as 1100 ^oC (FCT_T_3), and 1150 ^oC (FCT_T_4), showing the positive effect of heating stages on thermal stability of the supports for high temperatures. In Figure 4.26, BET surface areas of pH_1 samples with respect to stage number and PDT (°C) is analyzed. Though at the first look there is no clear correlation observed, a detailed analysis of the results showed the positive effect of high T pre-doping heat treatment with single stage pre-calcination treatment combination on thermal stability of the support samples.

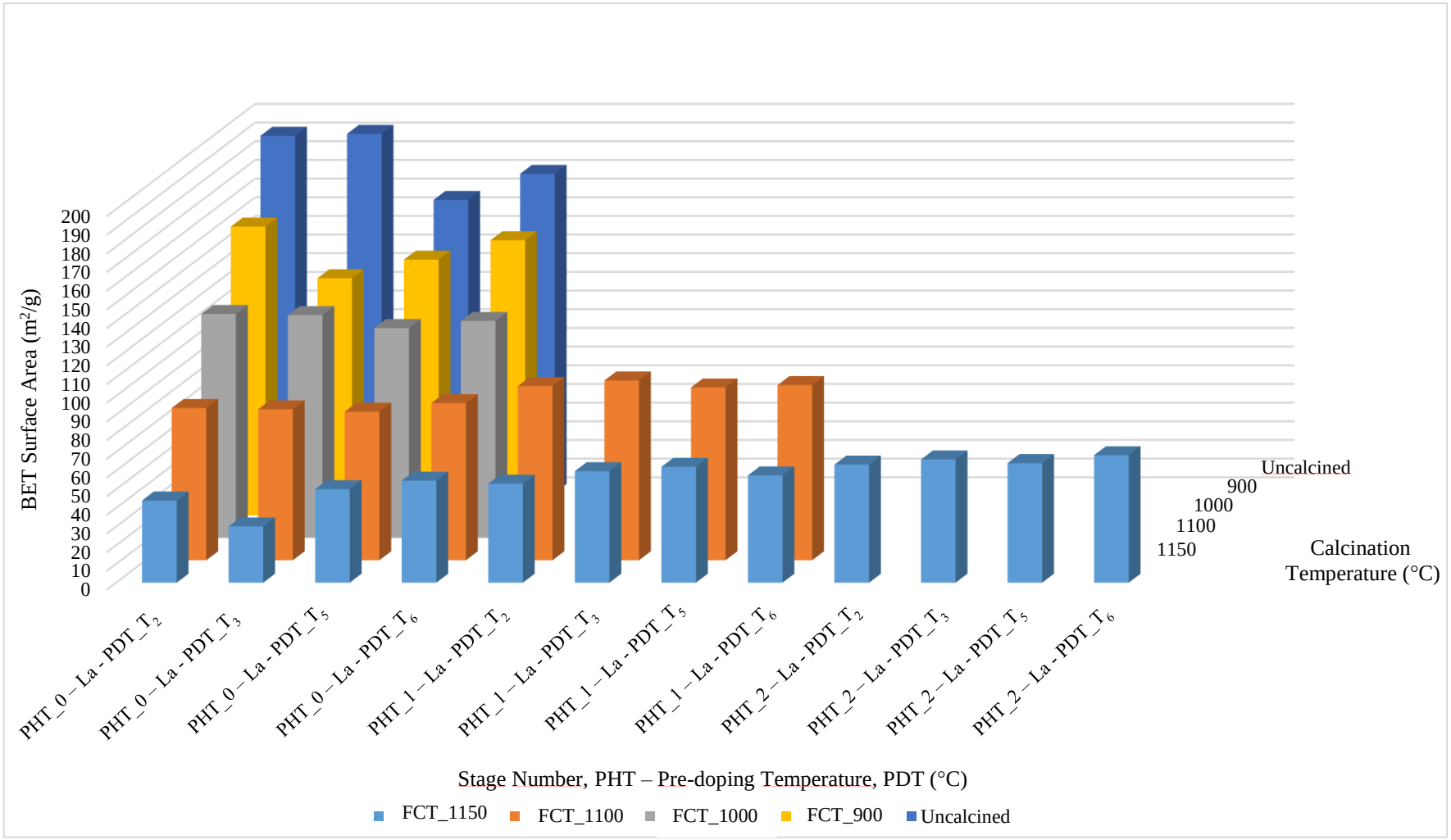

Figure 4.25 BET Surface Areas (m^2/g) of pH_2 Samples with Respect to Stage Number, Final Calcination Temperature (°C) and PDT (°C).

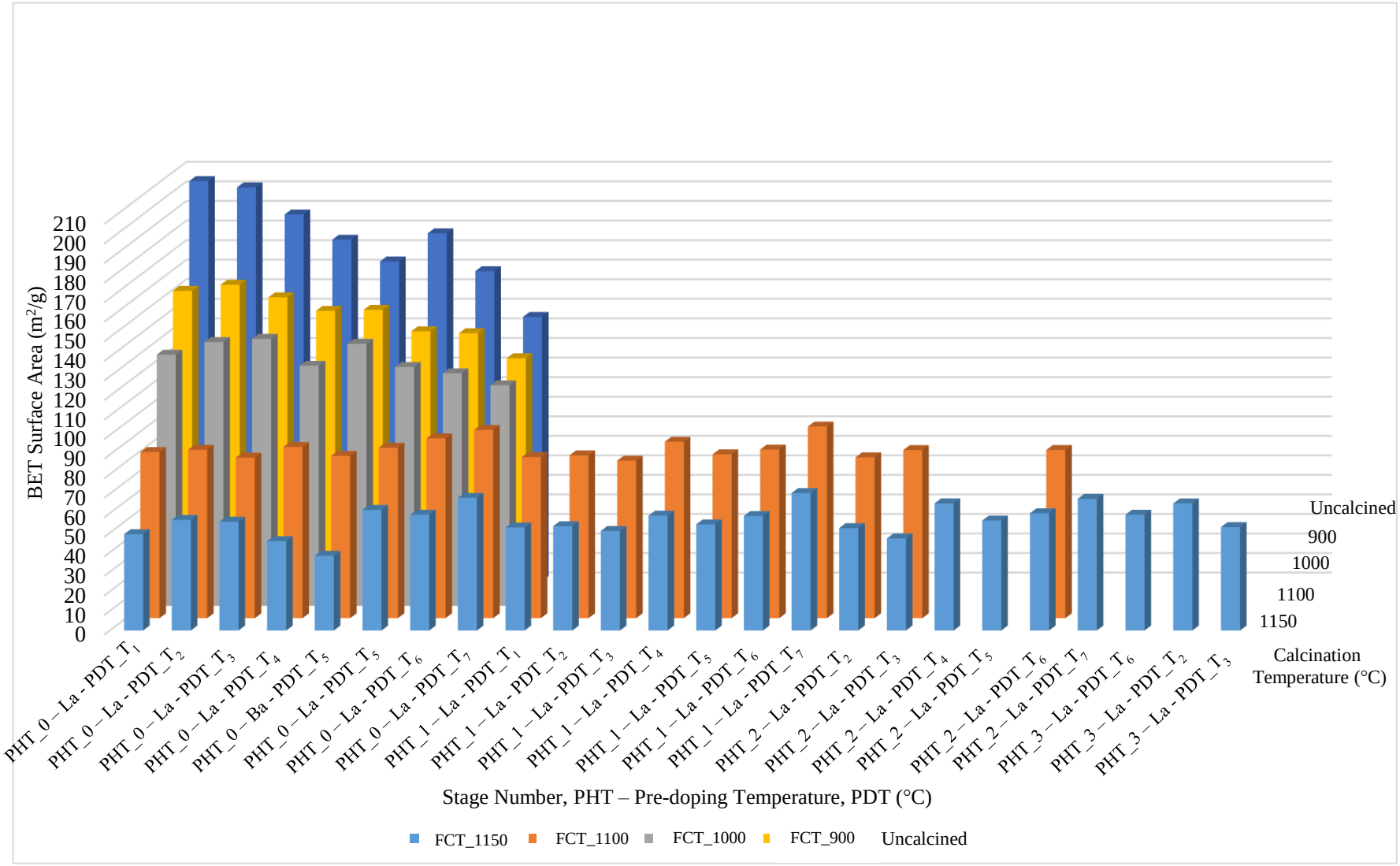

Figure 4.26 BET Surface Areas (m^2/g) of pH_1 Samples with Respect to Stage Number, Final Calcination Temperature (°C) and PDT (°C).

In Figure 4.27, circle sizes represent the BET surface areas of pH_1 samples with respect to stage number and PDT (°C). To disambiguate, the stage numbers are represented as real stage number +1 in MATLAB figures. Stage number 1 basically indicates 0-stage samples. Although the circles are nested, at high calcination temperatures, like FCT_1100 and FCT_1150 the increase in size for high pre-doping temperatures (PDT) is remarkable, revealing high thermal stability of samples prepared through high PDT application.

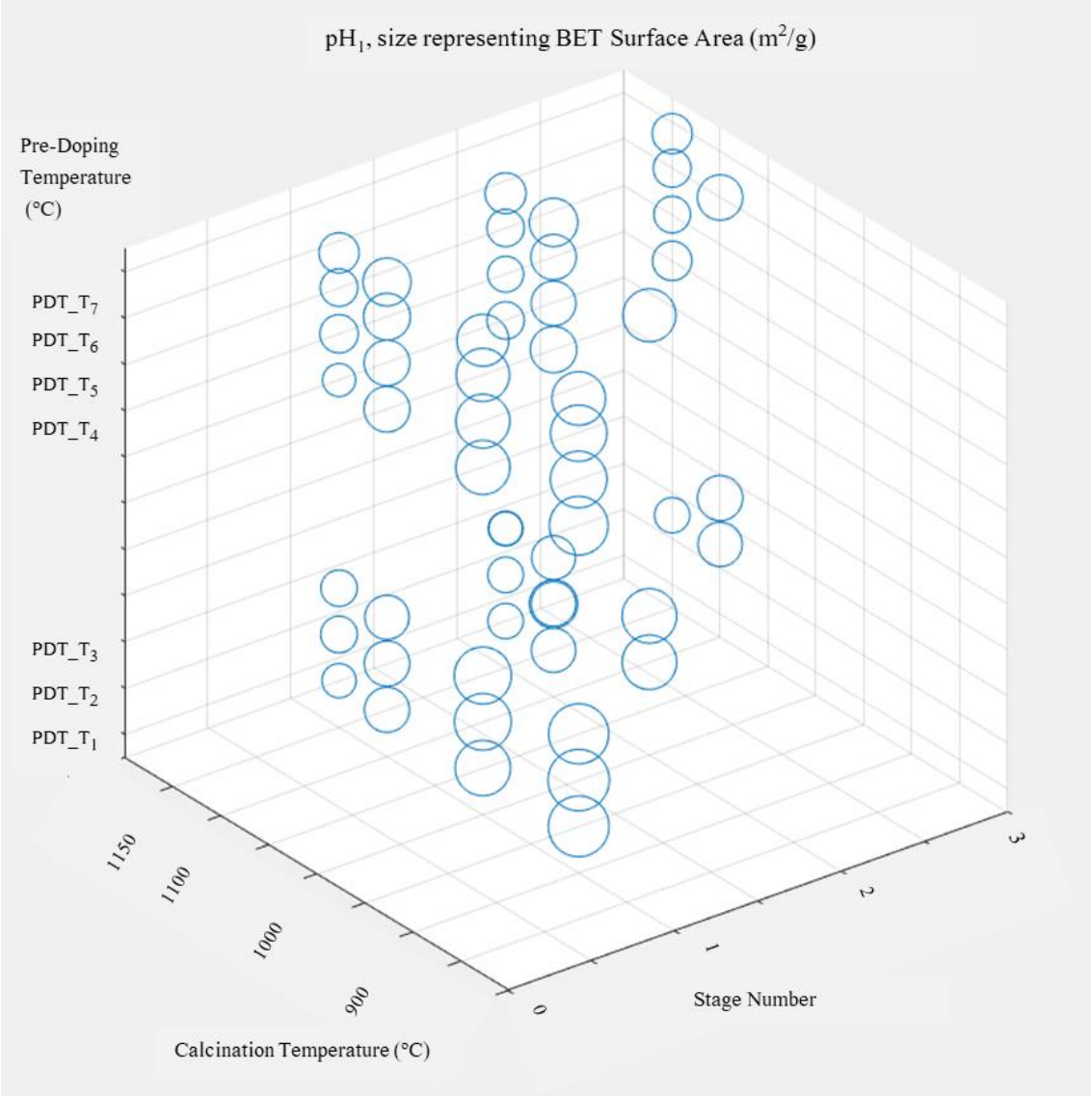

Figure 4.27 Circle Size Represent BET Surface Areas (m^2/g) of pH_1 Samples with Respect to Stage Number, Calcination Temperature (°C) and PDT (°C).

In Figure 4.28, the results are observed in the perspective of pre-doping temperature and final calcination temperature. Circle sizes represent the BET surface areas of pH_1 samples with respect to final calcination temperature (°C) and PDT (°C). The increase in size at high pre-doping temperatures (PDT), such as PDT_T_6 and PDT_T_7, for high calcination temperatures is remarkable.

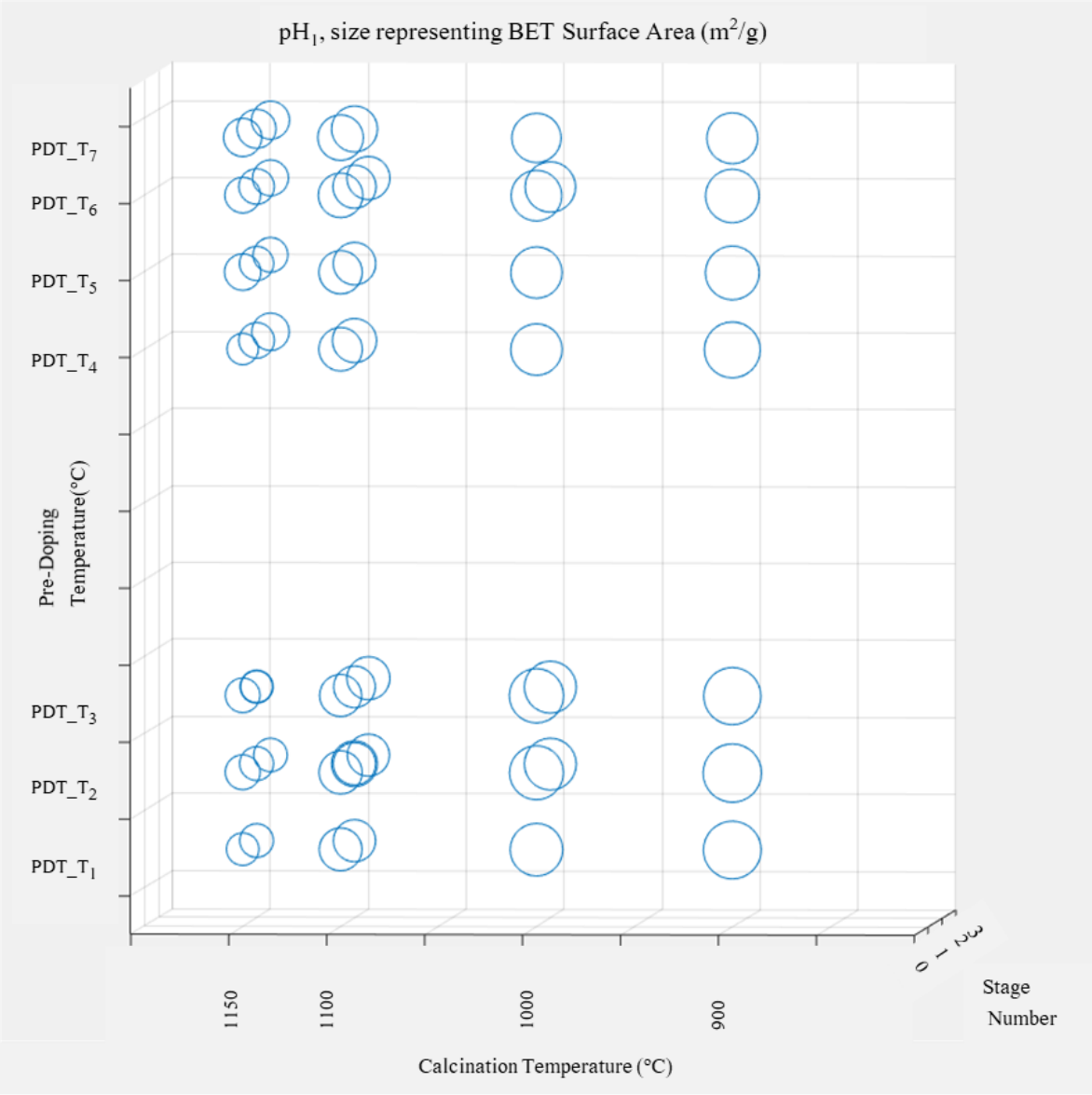

Figure 4.28 Circle Size Represent BET Surface Areas (m^2/g) of pH_1 Samples with Respect to Final Calcination Temperature (°C) and PDT (°C).

In Figure 4.29, the results are observed in the perspective of pre-doping temperature and stage number. Circle sizes represent the BET surface areas of pH_1 samples with respect to pre-calcination heat treatment stage numbers and pre-doping temperature (°C). The increase in stage number results in decrease in surface area, apart from the sample with pre-doping temperature of PDT_T_7.

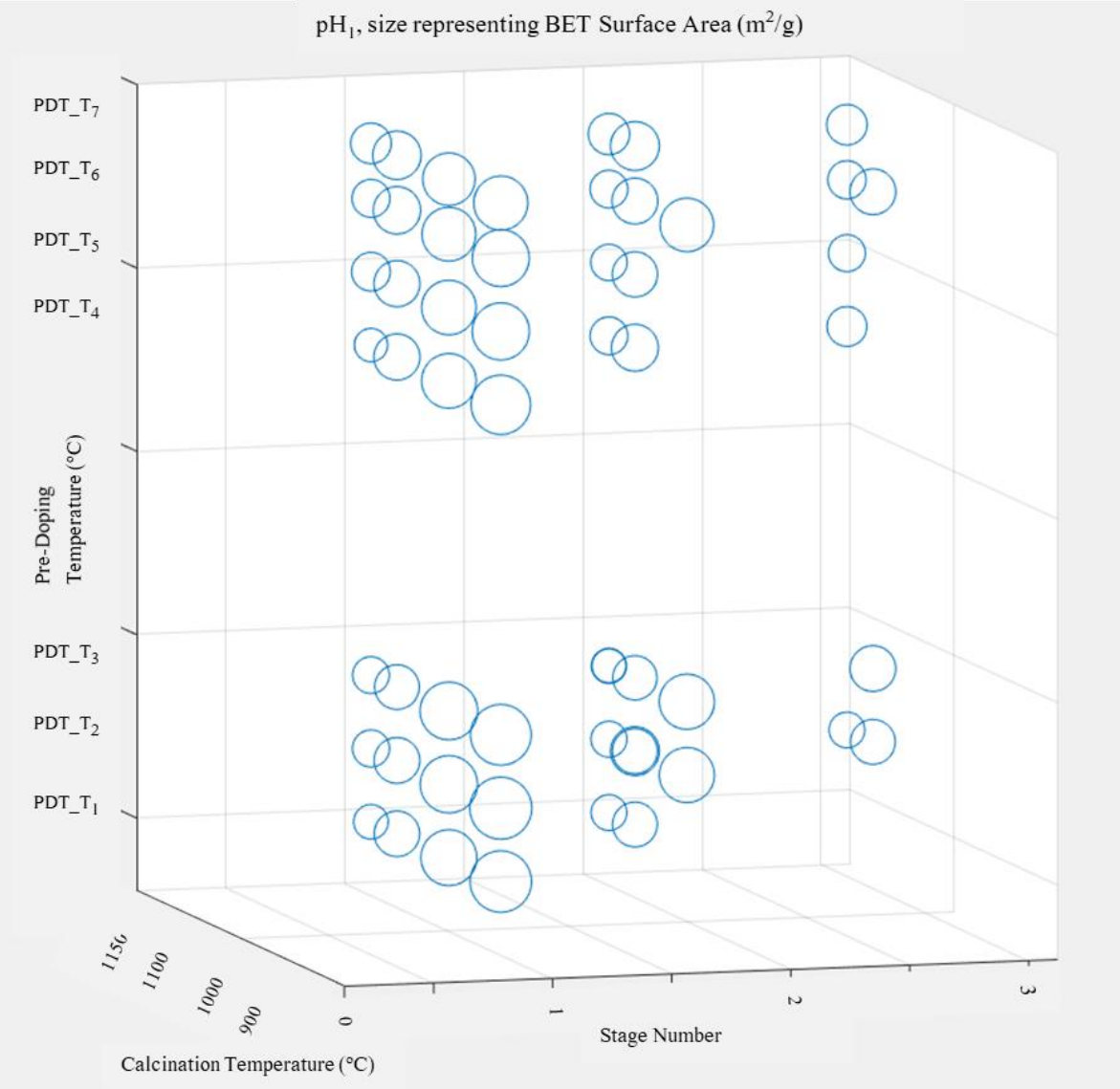

Figure 4.29 Circle Size Represent BET Surface Areas (m^2/g) of pH_1 Samples with Respect to Stage Number and PDT (°C).

In Figure 4.30, circle sizes represent the BET surface areas of pH_2 samples with respect to stage number and PDT (°C). In this figure, the sizes of the circles are approximate. The samples with pH_2 are affected less from increasing calcination temperature than the samples with pH_1, indicating the relatively higher thermal stability of the samples prepared through using pH_2.

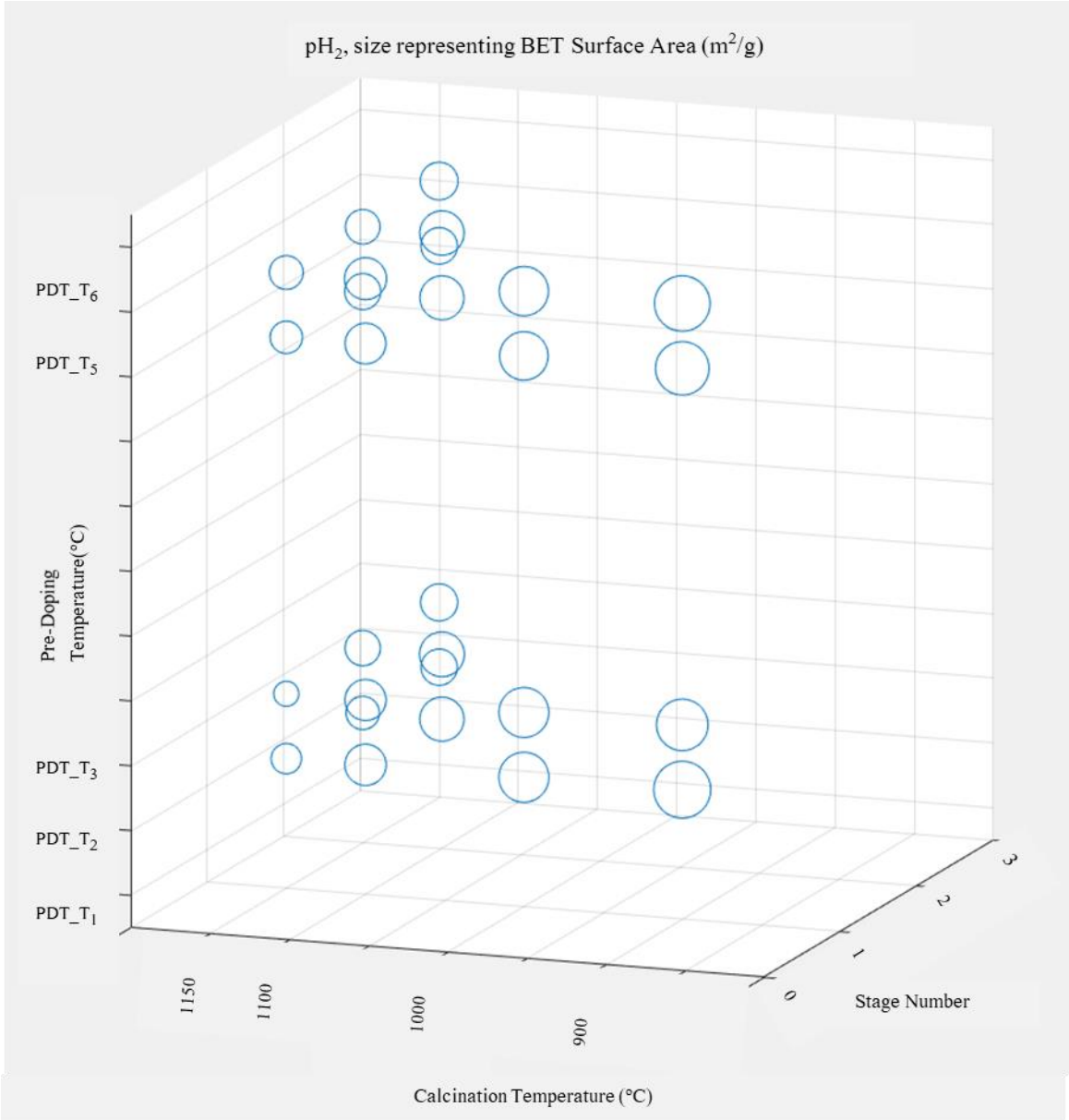

Figure 4.30 Circle Size Represent BET Surface Areas (m^2/g) of pH_2 Samples with Respect to Stage Number, Final Calcination Temperature (°C) and PDT (°C).

In Figure 4.31, circle sizes represent the BET surface areas of pH_2 samples with respect to calcination temperature (°C) and PDT (°C). Although the sizes of the circles are approximate, at calcination temperature of FCT_1150 and FCT_1100, the samples with pre-doping temperatures of PDT_T_5 and PDT_T_6 have slightly bigger sizes, therefore, surface area measurements indicate relatively higher thermal stabilities of PDT_T_5 and PDT_T_6 samples.

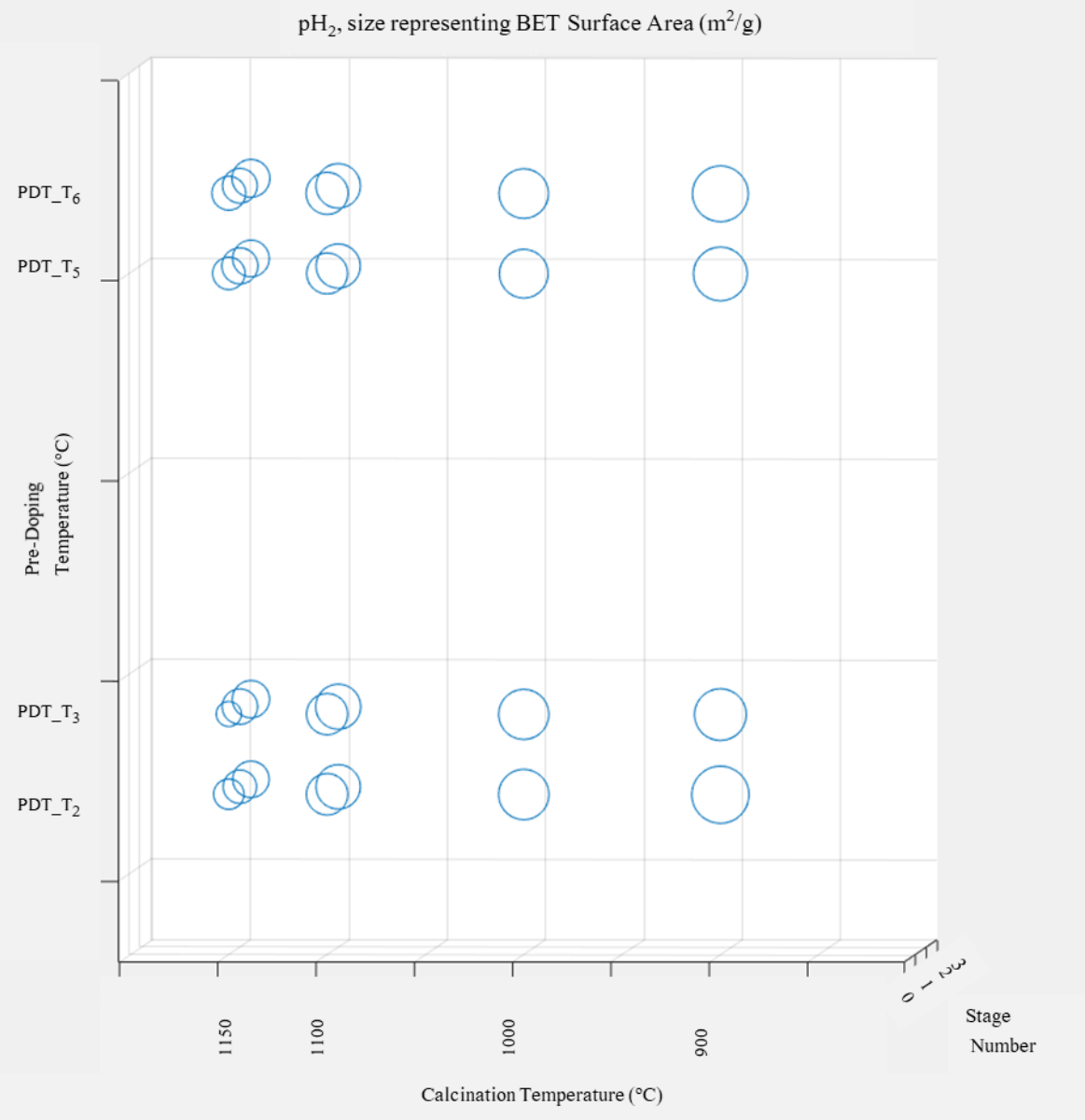

Figure 4.31 Circle Size Represent BET Surface Areas (m^2/g) of pH_2 Samples with Respect to Final Calcination Temperature (°C) and PDT (°C).

In Figure 4.32, circle sizes represent the BET surface areas of pH_2 samples with respect to stage number and pre-doping temperature (°C). In this figure, the increase in surface area with increasing stage number is obvious. 2-stage samples calcined at FCT_1150, have the largest surface area, revealing their enhanced thermal stability.

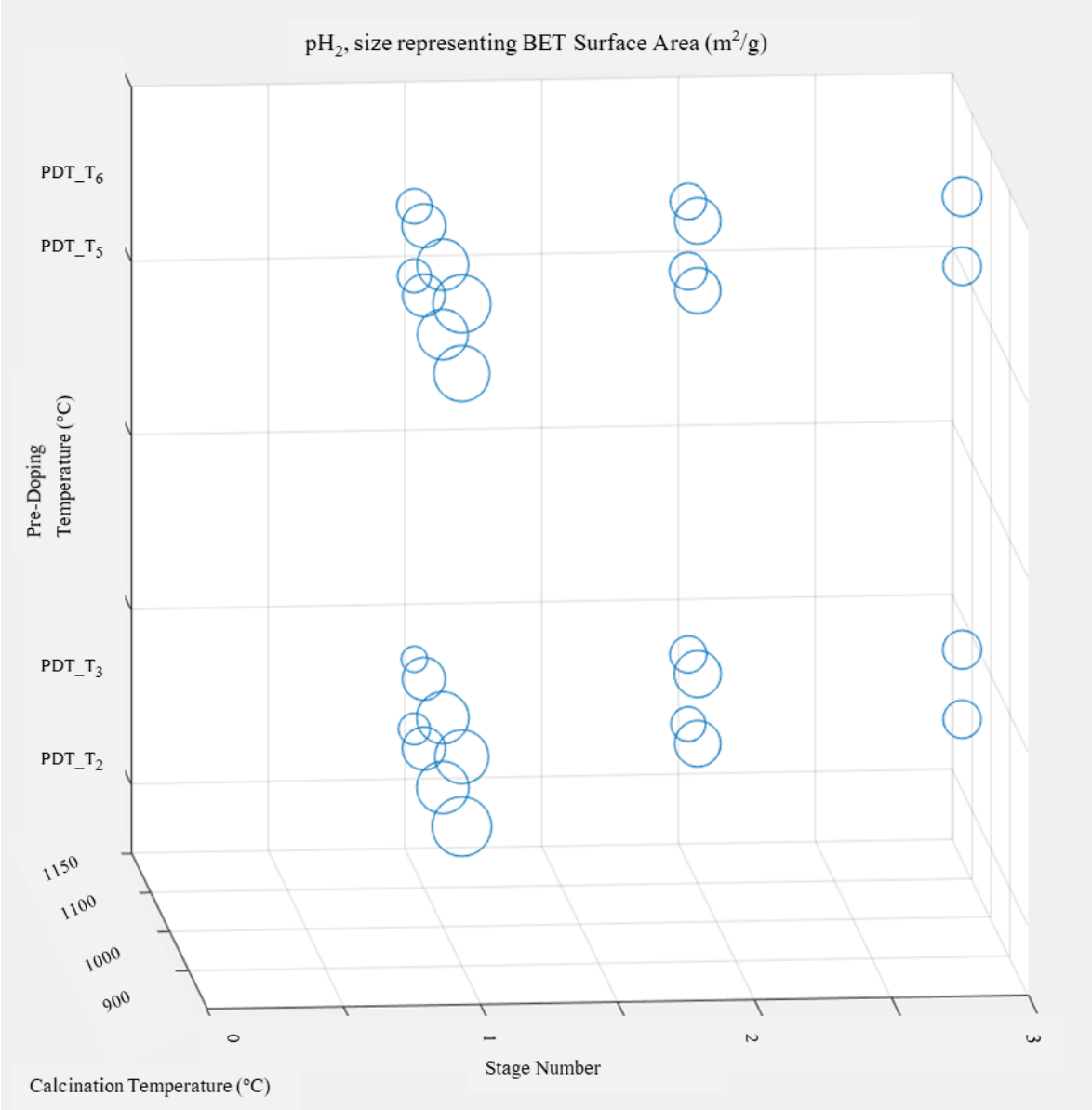

Figure 4.32 Circle Size Represent BET Surface Areas (m^2/g) of pH_2 Samples with Respect to Stage Number and PDT (°C).

5. CONCLUSIONS

5.1. Conclusions

In the present study, the aim was to enhance the thermal stability of commercial γ-Al_2O_3 samples, via doping with stabilizer(s), including -but not limited to- La, Ba, through using various preparation and pre-treatment methods/parameters.

Experimental studies were performed to characterize the support material and to assess the outcomes after exposing the samples to different types of preparation and pre-treatment methods/parameters.

In order to achieve thermal stability, the phase change of Al_2O_3 to its lower-TSA forms should be shifted to higher temperatures. Since γ-Al_2O_3 is a form of alumina with one of the highest surface areas (≈ 220 m^2/g) and it is easy to access, it was chosen as starting support material to be enhanced.

Pre-doping temperature treatment has a positive impact on increasing the stability of alumina. Especially the samples treated before doping at relatively high temperatures have higher BET surface area at high calcination temperatures and even at cumulative temperature exposures upon doping (before calcination) for 2+2+2 hours. 1%La/Al_2O_3 with pre-doping temperature of PDT_T_7 exposed to final calcination at FCT_1150 for 2 hours has the highest BET surface area, 70 m^2/g, throughout this study.

The effect of metal doping type was investigated mainly for Barium and Lanthanum. Even though Ba-doped samples have higher BET surface areas upon 900 ^oC and 1000 ^oC (i.e., FCT_900 and FCT_1000) calcination for 2 hours; for higher calcination temperatures, 1100 ^oC and 1150 ^oC (i.e., FCT_1100 and FCT_1150) for the same duration, La-doped samples have higher BET surface area, therefore have better thermal stability.

The effect of vacuum pressure applied during impregnation and drying temperature is ambiguous. Even though some samples show an increase in stability, no clear correlation was determined.

Long term water contact of alumina samples was investigated because it might led to structural changes. The starting material was Boehmite and by providing -OH bonds the material may have been shift to other forms of alumina, for instance Gibbsite. However, Raman spectroscopy displayed distinguishable peaks at 3399 cm^{-l}, 3484 cm^{-l} in Figures 4.5-4.7, and around 3540 cm^{-1} and the spectra's observed are compatible with Bayerite formation.

Apart from drying temperature, drying methodology was also investigated. For uncalcined samples, the samples treated with ultrasonic mixing and direct liquid N_2 contact had remarkably high surface areas, 230.00 m^2/g and 232.71 m^2/g respectively. Ultrasonic mixing is known to lead considerable changes in surface morphology due to sonochemical effects, however, in terms of pore size distribution, pore width variation is high and has an undesirable pore size distribution. Direct liquid N_2 contact may cause water in the pores of alumina to freeze too fast and cause more cracks due to the expansion of water when it freezes. Te samples prepared with direct liquid N_2 contact has better pore size distributions.

The results revealed that combined use of pH regulation during impregnation and post heat treatments upon doping significantly have a stabilizing effect on the structure of alumina exposed to high calcination temperatures. As an example, BET surface area of 1%La/Al_2O_3, with pre-doping temperature of PDT_T_6 exposed to 2-stage heat treatment for 2+2 hours and calcination at 1150 ^oC for 2 hours, is 60.0136 m^2/g when it was prepared with pH_1 precursor solution. The same sample prepared with pH_2 precursor solution has BET surface area of 68.2673 m^2/g.

To sum up, our reference γ-Al_2O_3 has 214.82 m^2/g BET surface area and after final calcination at 1150 ^oC for 2 hours it decreased down to 8.81 m^2/g. On the other hand, through application of optimum pre-doping heat treatment, metal doping and pre-heating cycles determined within the ranges used in this study for thermal stabilization, the BET surface

area of the sample upon calcination at 1150 ^{o}C for 2 h measured as 70.36 m^2/g, which shows nearly 8-fold increase in TSA compared to that of the reference sample.

5.2. Recommendations

The following recommendations may improve the results obtained in future experimental studies.

- The metal loading can be varied and the impregnation may be applied stagewise.

- The temperature of water in ultrasonic mixing tank during impregnation changes with time. In future work, it may be stabilized such as to eliminate the effect of possible parameter changes.

- Other pH levels may be tested for the precursor solution used in impregnation.

- Both ultrasonic mixing during impregnation and direct liquid N_2 contact for drying have an increasing effect on surface area. Ultrasonic mixing and direct liquid N_2 contact for drying can be combined.

REFERENCES

Alphonse, P. and Faure, B., 2014. Thermal stabilization of alumina modified by lanthanum. Microporous and Mesoporous Materials, 196, pp.191-198.

Andersson, J. (2005). Controlling the formation and stability of alumina phases. Linköping: Linköpings universitet.

Arai, H. and Machida, M. (1996). Thermal stabilization of catalyst supports and their application to high-temperature catalytic combustion. *Applied Catalysis A: General*, 138(2), pp.161-176.

Argyle, M. and Bartholomew, C., 2015. Heterogeneous Catalyst Deactivation and Regeneration: A Review. *Catalysts*, 5(1), pp.145-269.

Baranak, M., 2014. *Development of Alternative Fischer-Tropsch Catalysts for Conversion of Synthesis Gas into Liquid Fuels*. Ph.D. Istanbul Technical University, Graduate School of Science Engineering and Technology.

Belekar, R. and Dhoble, S. (2018). Activated Alumina Granules with nanoscale porosity for water defluoridation. *Nano-Structures & Nano-Objects*, 16, pp.322-328.

Carrier, X., Marceau, E., Lambert, J. and Che, M., 2007. Transformations of γ-alumina in aqueous suspensions 1. Alumina chemical weathering studied as a function of pH. Journal of Colloid and Interface Science, 308(2), pp.429-437.

Cesteros, Y., Salagre, P., Medina, F. and Sueiras, J., 1999. Several Factors Affecting Faster Rates of Gibbsite Formation. *Chemistry of Materials*, 11(1), pp.123-129.

Cho, S., Seo, Y., Song, K., Jeong, N. and Kang, S. (2001). Surfactant-mediated synthesis of metal substituted hexaaluminate from alumina sol. *Applied Catalysis B: Environmental*, 30(3-4), pp.351-357.

Daza, C., Moreno, S. and Molina, R., 2012. Ce - promoted catalyst from hydrotalcites for CO2 reforming of methane: calcination temperature effect. *Química Nova*, 35(7), pp.1325-1328.

Deraz, N., 2018. The comparative jurisprudence of catalysts preparation methods: I. precipitation and impregnation methods. *Journal of Industrial Environmental Chemistry*, 2(1), pp.19-21.

Disdale, W., *An Experimental and Computational Investigation of the Time Dependency of Automotive Catalyst Deactivation*. Ph.D. Thesis, Coventry University, 2007.

Gao, J., Jia, C., Li, J., Gu, F., Xu, G., Zhong, Z. and Su, F., 2012. Nickel Catalysts Supported on Barium Hexaaluminate for Enhanced CO Methanation. *Industrial & Engineering Chemistry Research*, 51(31), pp.10345-10353.

Guo, Y., Zhou, L. and Kameyama, H., 2011. Thermal and hydrothermal stability of a metal monolithic anodic alumina support for steam reforming of methane. *Chemical Engineering Journal*, 168(1), pp.341-350.

Fokin, P., Peretyagin, P. and Smirnov, A. (2017). Effect of drying methods of Al2O3-GO powder mixture on the properties and microstructure of sintered composites obtained by spark plasma sintering. *MATEC Web of Conferences*, 129, p.02027.

Forzatti, P. and Lietti, L. (1999). Catalyst deactivation. *Catalysis Today*, 52(2-3), pp.165-181.

Huang, W., Liu, G., Li, X., Qi, T., Zhou, Q. and Peng, Z., 2020. Structural variation in improving thermal stability of transition alumina with La dopant. *Journal of Alloys and Compounds*, 824, p.153905.

İşli, A., Aksoylu, A. and Önsan, Z., 1997. The Effect of Lanthanum and Barium Additives on theThermal Stabilization of-Al2O3. *Turkish Journal of Chemistry*, 22(3), pp.253 - 260.

Jokar, S., Parvasi, P. and Basile, A., 2018. The evaluation of methane mixed reforming reaction in an industrial membrane reformer for hydrogen production. *International Journal of Hydrogen Energy*, 43(32), pp.15321-15329.

Labalme, V., Garbowski, E., Guilhaume, N. and Primet, M. (1996). Modifications of Pt/alumina combustion catalysts by barium addition II. Properties of aged catalysts. *Applied Catalysis A: General*, 138(1), pp.93-108.

Lamouri, S., Hamidouche, M., Bouaouadja, N., Belhouchet, H., Garnier, V., Fantozzi, G. and Trelkat, J., 2017. Control of the γ-alumina to α-alumina phase transformation for an optimized alumina densification. *Boletín de la Sociedad Española de Cerámica y Vidrio*, 56(2), pp.47-54.

Levy, R. M., and Bauer, D. J. (1967). The effect of foreign ions on the stability of activated alumina. *Journal of Catalysis*, 9(1), pp.76-86.

Mizushima, Y. and Hori, M. (1993). Preparation of heat-resistant alumina aerogels. *Journal of Materials Research*, 8(11), pp.2993-2999.

Maraeva, E., Moshnikov, V. and Groshev, P., 2018. The analyses of the parameters of microporous structure in metal-oxide nanomaterials by comparative sorption methods. *Journal of Physics: Conference Series*, 1038, p.012052.

Nasrallah M, D., 2018. Sintering process and catalysis. *International Journal of Nanomaterials, Nanotechnology and Nanomedicine*, pp.001-003.

Ozawa, M., Kimura, M. and Isogai, A. (1990). Thermal stability and characterization of γ-Al2O3 modified with rare earths. *Journal of the Less Common Metals*, 162(2), pp.297-308.

Paranjpe, K. (2017). Alpha, Beta and Gamma Alumina as a catalyst -A Review. *The Pharma Journal*, 6(11), pp.236-238.

Pearson, A. (2003). Aluminum Oxide (Alumina), Activated. Kirk-Othmer *Encyclopedia of Chemical Technology*.

Pijolat, M., Dauzat, M. and Soustelle, M., 1992. Influence of water vapour and additives on the surface area stability of γ-Al2O3. *Solid State Ionics*, 50(1-2), pp.31-39.

Rabia, A., Ibrahim, A. and Zulkepli, N. (2018). Activated alumina preparation and characterization: The review on recent advancement. *E3S Web of Conferences*, 34, p.02049.

Rahmani, S., Meshkani, F. and Rezaei, M., 2018. Preparation of Ni-M (M: La, Co, Ce, and Fe) catalysts supported on mesoporous nanocrystalline γ-Al2O3 for CO2 methanation. *Environmental Progress & Sustainable Energy*, 38(1), pp.118-126.

Santos, P., Santos, H. and Toledo, S., 2000. Standard transition aluminas. Electron microscopy studies. *Materials Research*, 3(4), pp.104-114.

Sharma, S. and Ghoshal, S., 2015. Hydrogen the future transportation fuel: From production to applications. *Renewable and Sustainable Energy Reviews*, 43, pp.1151-1158.

Shtyka, O., Zakrzewski, M., Ciesielski, R., Kedziora, A., Dubkov, S., Ryazanov, R., Szynkowska, M. and Maniecki, T., 2020. Efficient removal of the carbon deposits formed during the mixed methane reforming over Ni/Al2O3. *Korean Journal of Chemical Engineering*, 37(2), pp.209-215.

Shohaimi, N., Jaafar, J., Bakar, W. (2012). A chemical technique for total acid number reduction in crude oil. In: *Universiti Malaysia Terengganu 11th International Annual Symposium on Sustainability Science and Management*. Chemistry Department, Faculty of Science, Universiti Teknologi Malaysia.

Simon, C., Bredesen, R., Grøndal, H., Hustoft, A. and Tangstad, E. (1995). Synthesis and characterization of Al2O3 catalyst carriers by sol-gel. *Journal of Materials Science*, 30(21), pp.5554-5560.

Stumpf, H., Russell, A., Newsome, J. and Tucker, C., 1950. Thermal Transformations of Aluminas and Alumina Hydrates - Reaction with 44% Technical Acid. *Industrial & Engineering Chemistry*, 42(7), pp.1398-1403.

Thevenin, P., Pocóroba, E., Pettersson, L. and Järås, S. (2001). Deactivation of Pd-based combustion catalysts supported on modified alumina. *Catalyst Deactivation 2001, Proceedings of the 9th International Symposium*, pp.189-196.

Tian, M., Wang, X., and Zhang, T. (2016). Hexaaluminates: a review of the structure, synthesis and catalytic performance. *Catalysis Science & Technology*, 6(7), pp.1984-2004.

Trimm, D. and Stanislaus, A. (1986). The control of pore size in alumina catalyst supports: A review. *Applied Catalysis*, 21(2), pp.215-238.

Trueba, M. and Trasatti, S. (2005). γ-Alumina as a Support for Catalysts: A Review of Fundamental Aspects. *European Journal of Inorganic Chemistry*, 2005(17), pp.3393-3403.

Valenzuela-Muñiz, A., 2012. *ABC'S of Electrochemistry Series Materials Characterization Techniques: Surface Area and Pore Size Distribution.* Ohio University, Center for Electrochemical Engineering Research.

Wefers, K. and Misra, C. (1987). *Oxides and Hydroxides of Aluminum.* Alcoa Laboratories, Aluminum Company of America, Pittsburgh, p.47.

Wei, J., Bischoff, K., Chakraborty, A., Denn, M., Peppas, N., Seinfeld, J., Stephanopoulos, G. and Ying, J., 2001. *Advances In Chemical Engineering*. San Diego: Academic Press [Imprint].

Yao, D., Yang, H., Chen, H. and Williams, P., 2018. Co-precipitation, impregnation and so-gel preparation of Ni catalysts for pyrolysis-catalytic steam reforming of waste plastics. *Applied Catalysis B: Environmental*, 239, pp.565-577.

Zarur, A., Hwu, H. and Ying, J. (2000). Reverse Microemulsion-Mediated Synthesis and Structural Evolution of Barium Hexaaluminate Nanoparticles. *Langmuir*, 16(7), pp.3042-3049.

Zhang, G., Liu, J., Xu, Y. and Sun, Y., 2018. A review of CH4CO2 reforming to synthesis gas over Ni-based catalysts in recent years (2010–2017). *International Journal of Hydrogen Energy*, 43(32), pp.15030-15054.

Zhang, J., Li, H., Guo, J. and Hu, F., 2015. Raman Scattering Modification Induced by Structural Change in Alumina Polymorphs. *Chinese Physics Letters*, 32(12), p.126801.

Zou, H. and Ge, X., Shen, J. (2003). Surface acidity and basicity of γ-Al2O3 doped with K+ and La3+ and calcined at elevated temperatures. *Thermochimica Acta*, 397(1-2), pp.81-86.

APPENDIX A: RESULTS OF BET SURFACE AREAS FOR ALL SAMPLES

Table A.1. Data of BET Surface Areas of Alumina Types.

Alumina Types	**BET Surface Area (m^2/g)**
Al_2O_3 High SA 1-8 pellet (Gamma)	217.05
Al_2O_3 High SA pellet (Gamma)	214.82
Al_2O_3 Low Si pellet	0.57
Al_2O_3-SiO_2 13-Percent Low SA pellet	-0.03

Table A.2. Data of BET Surface Areas of Alumina Phases Calcinated at Different Temperatures.

	BET Surface Area (m^2/g)	
Calcination T (°C)	**δ-Al_2O_3**	**γ-Al_2O_3**
TCT_T_1	133.34	159.70
TCT_T_2	97.42	116.71
TCT_T_3	10.84	42.81
TCT_T_4	9.79	8.81

All samples in Table A.3, A.4, A.5, and A.6, are consists of Aluminum Oxide as support material, with mesh size of 10-18. The samples were dehumidified at 150°C for 2 hours. The impregnation method is incipient to wetness, doping percentage is 1%, and the doping time is 1.5 hours.

Table A.3. Data of BET Surface Areas for the Samples with PDT of PDT _T_5 and PDT_T_2 for Lanthanum Doping and PDT _T_5 for Barium Doping.

PDT (ºC)	**Doping Material**	**pH**	**Stage Number PHT_#**	**Calcination Temperature FCT (°C)**	**Calcination time (h)**	**BET Surface Area (m^2/g)**
PDT_T_5	Lanthanum	pH_1		Uncalcined	-	177.87
				900	2	134.17
				1000		122.23
				1100		87.24
				1150		61.74
			1	1100		83.87
			2	1150		56.30
			1	1150		54.31
PDT_T_5	Barium	pH_1	0	Uncalcined	-	163.51
				900	2	145.09
				1000		134.07
				1100		83.04
				1150		38.26
			1	1150		34.74
PDT_T_2	-	-	0	Uncalcined	-	189.69
	Lanthanum	pH_1		Uncalcined	-	201.33
				900	2	157.91
				1000		134.95
				1100		86.19
				1150		56.64
			1	1000		124.69
			2	1100		82.34
			3	1150		65.03
			1	1100		83.32
			1	1100	1	97.89
			2	1150	2	52.44
			1	1150		53.39

Table A.4. Data of BET Surface Areas for the Samples with PDT of PDT _T_3, PDT _T_4 and PDT _T_1.

PDT (ºC)	**Doping Material**	**pH**	**Stage Number PHT_#**	**Calcination Temperature FCT (°C)**	**Calcination time (h)**	**BET Surface Area (m^2/g)**
PDT_T_3	-	-	0	Uncalcined	-	177.30
	Lanthanum	pH_1		Uncalcined	-	187.49
				900	2	151.47
				1000		136.63
				1100		82.17
				1150		55.71
			1	1000		125.05
			2	1100		86.04
			3	1150		52.93
			1*	1150		47.13
			1	1100		80.61
			1	1150		50.97
PDT_T_4	-	-	0	Uncalcined	-	159.24
	Lanthanum	pH_1		Uncalcined	-	174.62
				900	2	144.58
				1000		122.85
				1100		87.65
				1150		45.75
			1	1150		58.80
			1	1100		90.31
			2	1150		65.10
PDT_T_1	-	-	0	Uncalcined	-	192.46
	Lanthanum	pH_1		Uncalcined	-	204.59
				900	2	154.81
				1000		128.50
				1100		85.05
				1150		49.32
			1	1150		52.74
				1100		82.44

The asterisk implies 1000 ºC post heat treatments upon doping for 2 hours.

Table A.5. Data of BET Surface Areas for the Samples with PDT of PDT_T_6 and PDT_T_7 for pH_1 and PDT _T_2 for pH_2.

PDT (ºC)	**Doping Material**	**pH**	**Stage Number PHT_#**	**Calcination Temperature FCT (°C)**	**Calcination time (h)**	**BET Surface Area (m^2/g)**
PDT_T_6	-	-	0	-	-	150.35
	Lanthanum	pH_1		Uncalcined	-	158.53
				900	2	133.20
				1000		118.99
				1100		92.05
				1150		59.23
			1	1000		117.73
			2	1100		86.09
			3	1150		59.29
			1	1100		86.32
			2	1150		60.01
			1	1150		58.61
PDT_T_7	Lanthanum	pH_1	0	Uncalcined	-	138.28
				Uncalcined	-	135.19
				900	2	120.40
				1000		112.85
				1100		96.35
				1150		67.90
			1	1100		98.09
			2	1150		67.39
			1	1150		70.36
PDT_T_2	Lanthanum	pH_2	0	Uncalcined	-	191.32
				900	2	154.70
				1000		119.89
				1100		81.54
				1150		43.99
			1	1150		53.01
			1	1100		93.27
			2	1150		63.24

Table A.6. Data of BET Surface Areas of for the Samples with PDT of PDT_T_5, PDT_T_6, and PDT_T_3 for pH_2.

PDT (ºC)	**Doping Material**	**pH**	**Stage Number PHT_#**	**Calcination Temperature FCT (°C)**	**Calcination time (h)**	**BET Surface Area (m^2/g)**
PDT_T_5	Lanthanum	pH_2	0	Uncalcined	-	156.94
				900	2	136.96
				1000		112.38
				1100		79.56
				1150		50.07
			1	1150		62.02
			1	1100		92.55
			2	1150		64.01
PDT_T_6	Lanthanum	pH_2	0	Uncalcined	-	170.92
				900	2	147.35
				1000		116.16
				1100		84.14
				1150		54.59
			1	1150		57.45
			1	1100		93.80
			2	1150		68.27
PDT_T_3	Lanthanum	pH_2	0	Uncalcined	-	192.34
				900	2	127.01
				1000		119.28
				1100		80.85
				1150		30.13
			1	1150		59.72
			1	1100		96.26
			2	1150		65.98

Table A.7. Data of BET Surface Areas of for 2%Pt/Al_2O_3 Calcinated at 1000 for 2 hours with Respect to Drying Temperatures (^oC) and Vacuum Pressures (bar) During Impregnation.

Doping Material	**Wet Sample at SATP Time (h)**	**Vacuum Pressure (bar)**	**Drying T (°C)**	**Drying Time (h)**	**BET Surface Area (m^2/g)**
Platinum	-	Vac_{1}	40	21	118.14
Platinum	-	Vac_{1}	110	21	116.02
Platinum	12	Vac_{1}	40	21	116.62
Platinum	12	Vac_{1}	110	21	127.93
Platinum	-	Vac_{2}	40	21	130.21
Platinum	-	Vac_{2}	110	21	123.27
Platinum	12	Vac_{2}	40	21	119.76
Platinum	12	Vac_{2}	110	21	128.71
Platinum	-	Vac_{3}	40	21	114.11
Platinum	-	Vac_{3}	110	21	121.27
Platinum	12	Vac_{3}	40	21	121.89
Platinum	12	Vac_{3}	110	21	115.46

Table A.8. Data of BET Surface Areas of for Alumina with Respect to Different Drying Methods.

Drying Methods	**BET Surface Area (m^2/g)**
1-2 mm gamma alumina	216.63
12 h ultrasonic mixing SAPT + 21 h oven at 110^oC	221.18
12 h ultrasonic mixing SAPT + 21 h oven at 40^oC	230.00
12 h SAPT + Directly poured into Liquid N_2 + 21 h oven at 40^oC	232.71
12 h SAPT + Placed into Liquid N_2 with a flask + 21 h oven at 40^oC	226.93
12 h SAPT + 20 h at the freezing section of the refrigerator + 21 h oven at 40^oC	212.86
12 h SAPT + 21 h oven at 40^oC	224.31
12 h SAPT + drying at SAPT for 92 h + 21 h oven at 40^oC	220.51

APPEDIX B: MATLAB CODE

```
[x1,txt1] = xlsread('gulten','pH1')
[x2,txt2] = xlsread('gulten','pH2')

varNames1 = txt1(1, 1:5);
varNames2 = txt2(1, 1:5);

x2(isnan(x2))=0;
x1(isnan(x1))=0;

data1 = array2table(x1)
data1.Properties.VariableNames = varNames1

data2 = array2table(x2)
data2.Properties.VariableNames = varNames2


figure(1)

scatter3((data1.StageNumber+1),   data1.CalcinationTemperature,   data1.PDT,
data1.BETSurfaceArea*7)


xlim([0 3]) %xlimit
 ylim([900 1150]) %ylimit
 zlim([PDT_T1 PDT_T7]) %zl?m?t


xlabel('Stage Number')
ylabel('Calcination Temperature (°C)')
zlabel('PDT (°C)')

title('pH1, size representing BET Surface Area (m^2/g)')



figure(2)

scatter3((data2.StageNumber+1),   data2.CalcinationTemperature,   data2.PDT,
data2.BETSurfaceArea*7)



xlim([0 3]) %xlimit
ylim([900 1150]) %ylimit
 zlim([PDT_T1 PDT_T7])  %zl?m?t


xlabel('Stage Number')
```

```
ylabel('Calcination Temperature (°C)')
zlabel('PDT (°C)')
title('pH2, size representing BET Surface Area (m^2/g)')
```

APPEDIX C: DATA SHEET OF MATLAB CODE

Table C.1. Data Sheet of MATLAB Code for pH_2.

CalcinationTemperature	PDT	StageNumber	BETSurfaceArea	pH
900	PDT_T_2	0	154.6978	pH_2
1000	PDT_T_2	0	119.8916	pH_2
1100	PDT_T_2	0	81.5387	pH_2
1150	PDT_T_2	0	43.9913	pH_2
1150	PDT_T_2	1	53.0079	pH_2
1100	PDT_T_2	1	93.2709	pH_2
1150	PDT_T_2	2	63.2363	pH_2
900	PDT_T_5	0	136.9618	pH_2
1000	PDT_T_5	0	112.376	pH_2
1100	PDT_T_5	0	79.5633	pH_2
1150	PDT_T_5	0	50.0679	pH_2
1150	PDT_T_5	1	62.021	pH_2
1100	PDT_T_5	1	92.5501	pH_2
1150	PDT_T_5	2	64.0144	pH_2
900	PDT_T_6	0	147.3526	pH_2
1000	PDT_T_6	0	116.1557	pH_2
1100	PDT_T_6	0	84.1355	pH_2
1150	PDT_T_6	0	54.5938	pH_2
1150	PDT_T_6	1	57.4545	pH_2
1100	PDT_T_6	1	93.8024	pH_2
1150	PDT_T_6	2	68.2673	pH_2
900	PDT_T_3	0	127.0136	pH_2
1000	PDT_T_3	0	119.2801	pH_2
1100	PDT_T_3	0	80.8501	pH_2
1150	PDT_T_3	0	30.1256	pH_2
1150	PDT_T_3	1	59.7196	pH_2
1100	PDT_T_3	1	96.2624	pH_2
1150	PDT_T_3	2	65.9826	pH_2

Table C.2. Data Sheet of MATLAB Code for pH_1 for PDT of PDT_T_5, PDT_T_2, and PDT_T_3.

CalcinationTemperature	PDT	StageNumber	BETSurfaceArea	pH
900	PDT_T_5	0	134.1671	pH_1
1000	PDT_T_5	0	122.2268	pH_1
1100	PDT_T_5	0	87.2358	pH_1
1150	PDT_T_5	0	61.7443	pH_1
1100	PDT_T_5	1	83.866	pH_1
1150	PDT_T_5	2	56.302	pH_1
1150	PDT_T_5	1	54.3057	pH_1
900	PDT_T_2	0	157.9081	pH_1
1000	PDT_T_2	0	134.9458	pH_1
1100	PDT_T_2	0	86.1907	pH_1
1150	PDT_T_2	0	56.6379	pH_1
1000	PDT_T_2	1	124.6903	pH_1
1100	PDT_T_2	2	82.3369	pH_1
1150	PDT_T_2	3	65.0275	pH_1
1100	PDT_T_2	1	83.3204	pH_1
1100	PDT_T_2	1	97.8879	pH_1
1150	PDT_T_2	2	52.4367	pH_1
1150	PDT_T_2	1	53.3902	pH_1
900	PDT_T_3	0	151.4738	pH_1
1000	PDT_T_3	0	136.6321	pH_1
1100	PDT_T_3	0	82.169	pH_1
1150	PDT_T_3	0	55.7114	pH_1
1000	PDT_T_3	1	125.0517	pH_1
1100	PDT_T_3	2	86.043	pH_1
1150	PDT_T_3	3	52.9266	pH_1
1150	PDT_T_3	1	47.1252	pH_1
1100	PDT_T_3	1	80.6143	pH_1
1150	PDT_T_3	1	50.9726	pH_1

Table C.3. Data Sheet of MATLAB Code for pH_1 for PDT of PDT_T_4, PDT_T_1, PDT_T_6, and PDT_T_7.

CalcinationTemperature	PDT	StageNumber	BETSurfaceArea	pH
900	PDT_T_4	0	144.5787	pH_1
1000	PDT_T_4	0	122.8473	pH_1
1100	PDT_T_4	0	87.647	pH_1
1150	PDT_T_4	0	45.7503	pH_1
1150	PDT_T_4	1	58.8015	pH_1
1100	PDT_T_4	1	90.311	pH_1
1150	PDT_T_4	2	65.1018	pH_1
900	PDT_T_1	0	154.8128	pH_1
1000	PDT_T_1	0	128.4981	pH_1
1100	PDT_T_1	0	85.0546	pH_1
1150	PDT_T_1	0	49.3179	pH_1
1150	PDT_T_1	1	52.7419	pH_1
1100	PDT_T_1	1	82.4407	pH_1
900	PDT_T_6	0	133.1978	pH_1
1000	PDT_T_6	0	118.9946	pH_1
1100	PDT_T_6	0	92.0453	pH_1
1150	PDT_T_6	0	59.2283	pH_1
1000	PDT_T_6	1	117.7274	pH_1
1150	PDT_T_6	2	86.094	pH_1
1150	PDT_T_6	3	59.2874	pH_1
1100	PDT_T_6	1	86.3171	pH_1
1150	PDT_T_6	2	60.0136	pH_1
1150	PDT_T_6	1	58.6129	pH_1
900	PDT_T_7	0	120.4034	pH_1
1000	PDT_T_7	0	112.8541	pH_1
1100	PDT_T_7	0	96.3513	pH_1
1150	PDT_T_7	0	67.8962	pH_1
1100	PDT_T_7	1	98.0943	pH_1
1150	PDT_T_7	2	67.3903	pH_1
1150	PDT_T_7	1	70.36	pH_1